AD NUMBER

**AD886615**

LIMITATION CHANGES

TO:

**Approved for public release; distribution is unlimited.**

FROM:

**Distribution authorized to DoD only; Administrative/Operational Use; AUG 1974. Other requests shall be referred to Space and Missile Systems Organization, Attn: RNSE, Norton AFB, CA 92409.**

AUTHORITY

**SAMSO ltr, 7 Apr 1978**

PHILCO-FORD CORPORATION PUBLICATION NO. U-4950

# TECHNICAL REPORT
# ADVANCED PENETRATION PROBLEMS PROGRAM
# MEAN FLOW MEASUREMENTS IN A HYPERSONIC TURBULENT BOUNDARY LAYER

Prepared by:

A. J. Laderman and A. Demetriades

Philco-Ford Corporation
Aeronutronic Division
Newport Beach, California

Monitored by:

Space and Missile Systems Organization
Air Force Systems Command
Norton Air Force Base, California

Under Contract

F04701-70-C-0130

Sponsored by:

Advanced Research Projects Agency
Department of Defense
ARPA Order No. 888

August 1971

PHILCO-FORD CORP PUB. NO. U-4950

# TECHNICAL REPORT

# MEAN FLOW MEASUREMENTS IN A HYPERSONIC TURBULENT BOUNDARY LAYER

Prepared by:

A. J. Laderman

and

A. Demetriades

August 1971

## FOREWORD

This report is the eleventh in a series describing research in re-entry phenomenology performed by Philco-Ford Corporation as part of the Advanced Penetration Problems (APP) project. The work described herein was sponsored by the U. S. Air Force and the Advanced Research Projects Agency and monitored by the Space And Missile Systems Organization, USAF, under Contract No. F04701-70-C-0130 Modification P0004.

Previous technical reports in this series have presented the turbulence structure in flow fields representative of those encountered in re-entry flight. Such experiments have included compressible axi-symmetric and two-dimensional wakes and highly heated plasma jets in which the electron behavior was measured together with the gasdynamical turbulence. New techniques and devices were introduced to overcome the rigors of high-speed, high-temperature flows and the greatly increased complexities of compressible turbulence. The present report deals with the mean flow from a hypersonic turbulent boundary layer experiment. Analog hot-wire anemometer signals from the same experiment have been stored on magnetic tape, and a detailed profile of the turbulent flow in that boundary layer will be analyzed and presented in a forthcoming report.

In addition to the support and encouragement of the agencies mentioned above, the authors wish to acknowledge the assistance of Lee Von Seggern and the expertise with which Ernest L. Doughman prepared the smallest hot-wires (0.00001" diameter) ever to be used in supersonic or hypersonic flow. The work further benefited greatly from previous work done in the same wind-tunnel by Dr. John Laufer of the University of Southern California and Dr. Harry Ashkenas of the Jet Propulsion Laboratory (NASA) and their coworkers.

## ABSTRACT

An experimental investigation was carried out to determine the structure of the turbulent boundary layer on the wall of the Jet Propulsion Laboratory Hypersonic Wind Tunnel at a free-stream Mach number of 9.37. Profiles of flow properties were obtained from pitot pressure, static pressure, and total temperature surveys made through the 6 inch thick boundary layer at a station 160 inches from the nozzle throat. Tests were conducted primarily for the following conditions: unit free-stream Reynolds number of 127,000 per inch, corresponding to a Reynolds number based on momentum thickness of 36,800, and a wall to free-stream total temperature ratio of 0.385. A cursory examination of the boundary layer was also made at a unit stream Reynolds number of 67,000. The static pressure measurements, although indicating negligible streamwise variation, revealed the existence of a significant pressure gradient normal to the wall, with the pressure at the wall approximately 45% greater than its free-stream value. The data indicate that the profile of total temperature ratio versus velocity ratio agrees with the linear Crocco theory in the sub-layer region, but in the outer portion of the boundary layer, closely follows the quadratic relation which has been observed to characterize nozzle wall measurements. The data also indicate that the sub-layer is 0.05 to 0.10 inches thick which corresponds to only several percent of the total boundary layer thickness. Correlation of the velocity profile with the conventional incompressible profile shows poor agreement in the sub-layer and wall-of-the-wake regions, with the latter attributed primarily to the pressure gradient normal to the wall. However, the experimental skin friction coefficient agrees with the value predicted by the Van Driest theory within several percent. Finally, the total temperature profile determined from a hot-wire anemometer traverse through the boundary layer is in good agreement with the thermocouple measurements.

CONTENTS

## ILLUSTRATIONS

## ILLUSTRATIONS - (Continued)

## LIST OF SYMBOLS

| | | |
|---|---|---|
| $A,B,C$ | - | arbitrary constants |
| $A_i$ | - | coefficients in the hot-wire $Nu_c$-$Re_o$ correlation |
| $B_i$ | - | coefficients in the hot-wire $\eta$-$Re_o$ correlation |
| $C_i$ | - | coefficients in the static pressure probe viscous interaction correlation |
| $d$ | - | diameter |
| $i$ | - | current |
| $k$ | - | thermal conductivity |
| $k_1,k_2$ | - | parameters in the Van Driest velocity transformation |
| $M$ | - | Mach number |
| $Nu$ | - | Nusselt number |
| $P$ | - | pressure |
| $P_t$ | - | pitot pressure |
| $P_{t2}$ | - | pitot pressure measured at mid-point of instrumentation rake |
| $P_{t1},P_{t3}$ | - | pitot pressure measured at outboard positions of instrumentation rake |
| $q$ | - | heat transfer rate |
| $R$ | - | hot-wire resistance |
| $R_r$ | - | hot-wire resistance at reference temperature ($0^oC$) |
| $Re$ | - | Reynolds number |
| $Re_o$ | - | Reynolds number based on hot-wire diameter and stagnation temperature |
| $Re_o'$ | - | Unit stream Reynolds number based on stagnation temperature |
| $Re_\theta$ | - | Reynolds number based on momentum thickness |
| $T$ | - | temperature |
| $T_m$ | - | measured total temperature |

## LIST OF SYMBOLS - (Continued)

| | | |
|---|---|---|
| $\bar{T}$ | - | non-dimensional total temperature ratio = $(T_o - T_w)/(T_{oe} - T_w)$ |
| $u$ | - | velocity |
| $u_\tau$ | - | friction velocity = $(\tau_w/\rho_w)^{\frac{1}{2}}$ |
| $u^*$ | - | generalized or transformed velocity |
| $u^+$ | - | $u^*/u_\tau$ |
| $W$ | - | Cole's Wake Function |
| $X$ | - | axial distance from nozzle throat |
| $Y$ | - | distance from wall |
| $Y^*$ | - | generalized or transformed distance from the wall |
| $Y^+$ | - | $Y^* u_\tau/\nu_w$ |
| $\alpha_r$ | - | hot-wire temperature coefficient of resistivity $^oC^{-1}$ |
| $\delta$ | - | boundary layer thickness |
| $\delta^*$ | - | boundary layer displacement thickness |
| $\epsilon$ | - | convergence criteria for mean flow calculations |
| $\eta$ | - | recovery factor |
| $\gamma$ | - | ratio of specific heats |
| $\mu$ | - | viscosity |
| $\nu$ | - | kinematic viscosity |
| $\tilde{\pi}$ | - | parameter characterizing strength of the wake component of the boundary layer |
| $\rho$ | - | density |
| $\tau$ | - | shear stress |
| $\theta$ | - | boundary layer momentum thickness |
| $\theta^*$ | - | boundary layer energy thickness |
| $\chi$ | - | viscous interaction parameter |

## LIST OF SYMBOLS - (Continued)

### SUBSCRIPTS

| | | |
|---|---|---|
| aw | - | adiabatic or recovery |
| e | - | edge of boundary layer |
| i | - | inviscid |
| m | - | measured |
| o | - | stagnation |
| s | - | static |
| w | - | wall |
| ∞ | - | free-stream |

# SECTION I

# INTRODUCTION

## 1.1 PURPOSE

The hypersonic turbulent boundary layer has not been studied to the degree commensurate with its importance in reentry phenomenology. This is especially true for the turbulence characteristics of such a layer which, following Kistler's studies at Mach 4.5 (Reference 1), have received only sporadic attention. And yet, a complete study of the hypersonic layer, especially of its turbulence, would fulfill several urgent needs. It would, for example, narrow or end current speculations about the "eddy viscosity" and thus improve boundary-layer theories. As another example, it would provide a valid statistical model for electromagnetic scattering calculations which presently utilize extrapolations from data obtained at very low flow speeds.

The ultimate objective of the present work has been to provide high-resolution profiles of turbulent fluctuations in boundary layer at hypersonic speeds. A secondary objective has been to record on magnetic tape all analog data from which foreseeable questions about various features of the turbulent boundary layer may be answered without repeating the experiment. Such a magnetic-tape "library" of the sensor signals has been already collected. The mean (average) signals necessary to describe the mean-flow properties have been reduced and are presented in this report. The mean flow properties are needed to reduce the turbulence data and separate them into contributions from the various turbulence modes. Analysis of the fluctuation measurements will be presented in a subsequent report.

## 1.2 EXPERIMENT DESIGN

The following criteria were set in designing this experiment:

a. Continuous flow was required to allow the boundary conditions (e.g., wall temperature) to be well established and thus well defined; and to make the turbulence measurements possible.

b. Thick boundary layers, to increase the spatial resolution of the probes, to enable probing the sublayer and to decrease the turbulence frequencies to a manageable range.

c. Two-dimensional flow, to enable comparison with the simpler turbulent boundary layer theories.

d. Very high Reynolds numbers, to enable the layer to reach dynamic equilibrium, presumably the asymptotic form.

e. Mach numbers higher than 6, so as to approach a range of practical interest and one where turbulence was not previously studied.

f. Stagnation temperatures lower than about 1200°F to insure survival of the hot-wire anemometer.

g. No pressure gradient so that no arbitrary complexities would be introduced at the outset.

Regarding heat transfer, the practical requirement is for a cooled wall ($T_w < T_{o\infty}$) although there is also great need for an adiabatic turbulence experiment. It developed that a cooled wall was much easier to obtain; in the final tests a ratio $T_w \simeq 0.4\ T_{o\infty}$ was used. Also, because of the restricted scope of this work and the large volume of tests needed to measure the turbulence, it was decided to take very detailed data at a single streamwise and span-wise position in the flow, at a single flow condition, with only "token" measurements at other points and flow conditions.

The above criteria could be best satisfied by using a flat surface in a continuous hypersonic wind tunnel at the highest attainable pressure and temperature. To obtain turbulence, thicken the layer and equilibrate it a very long flat plate would be needed. The cost of such a plate model would be prohibitive however, and thus attention was drawn to using the sidewall boundary layer of such a tunnel.

## SECTION II

## FACILITY DESCRIPTION

The above requirements were well fulfilled by making use of the two-dimensional flexible nozzle 21-inch Hypersonic Wind-Tunnel (HWT) at the Jet Propulsion Laboratory (JPL) in Pasadena, California. This facility is described in Reference 2, and is shown in general view on Figure 1. Its proximity to Philco-Ford, flexible schedule, and low cost made this facility very attractive for this work. The flow in this tunnel is continuous, the Mach number is adjustable from 4.5 to 10.5 and the unit Reynolds number can approach 150,000 per inch ($1.8 \times 10^6 ft^{-1}$). The Reynolds number $R_\delta$ based on layer thickness $\delta$ were known to be of order 600,000 and $Re_\theta$ was estimated capable of reaching 20,000. Furthermore, favorable evidence of two-dimensionality, repeatability and dynamic equilibration in the sidewall boundary layer of this tunnel had already been collected by Laufer, Ashkenas and Gupta (Reference 3) under conditions satisfying the criteria of Section I; this will be discussed further in Section V.

It was decided to make these tests in the boundary layer growing over the upper wall (ceiling) of the 21-inch high x 20 inch wide tunnel test section, whose layout is seen in Figure 2, and which is a smooth internally water-cooled surface. The point of measurement is at the mid-span position (10 inches from each sidewall) and lies 160 inches downstream of the nozzle throat. The conditions selected were:

| | | |
|---|---|---|
| Mach number: | $M_\infty$ | = 9.4 (nominal) |
| Total pressure: | $P_o$ | = 3200 and 1700 cm Hg |
| Total temperature: | $T_o$ | = $1000^oF$ |
| Reynolds number: | Re | = 127,000 per inch ; $P_o$ = 3200 cm Hg |
| | | = 67,000 per inch ; $P_o$ = 1700 cm Hg |

Although most of the tests were performed at $P_o$ = 3200 cm Hg, a single boundary layer traverse, with measurements made at nine points ranging from 1 to 5 inches from the wall, was also carried out at $P_o$ = 1700 cm Hg.

During operation of the Wind Tunnel, pressure and temperature data are collected automatically using the JPL Wind Tunnel Data Acquisition System, a computer controlled recording device. Analog signals are conditioned at the test site and then transmitted to a central acquisition area where they are digitized and stored in the computer memory. The data can be sent back to the site for printout by a line printer and display on a visual monitoring channel.

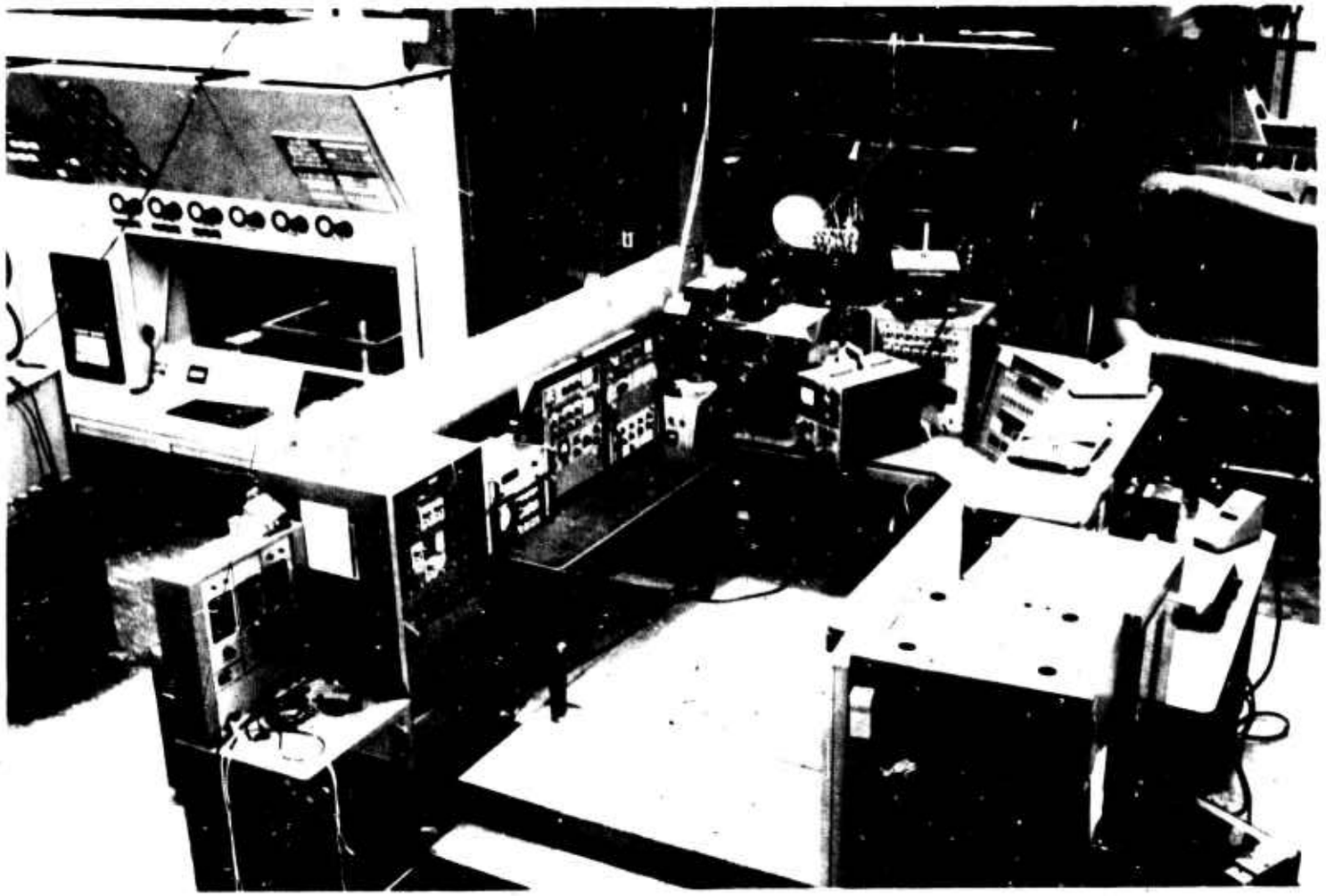

FIGURE 1. VIEW OF JPL HYPERSONIC WIND TUNNEL SHOWING DATA ACQUISITION STATION

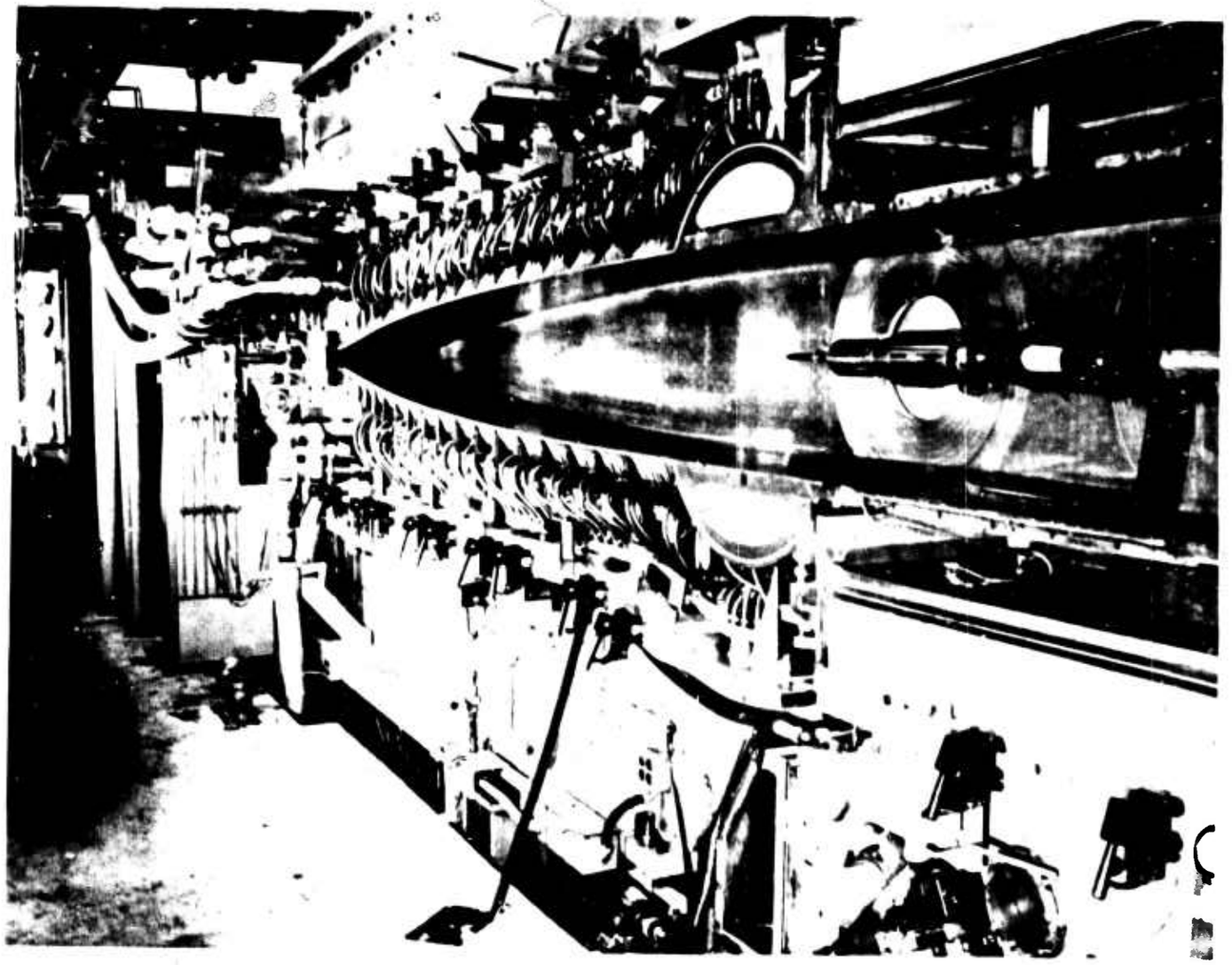

FIGURE 2. VIEW OF JPL HYPERSONIC WIND TUNNEL SHOWING NOZZLE AND TEST SECTION

## SECTION III

## DIAGNOSTIC PROBES AND PROCEDURES

The local mean flow properties were found by combining readings taken with a pitot probe, a static pressure probe and a total-temperature probe. Basically these readings, when used with aerodynamic formulas such as the ideal gas law and the Rayleigh pitot relation, yield the local flow velocity, density, longitudinal velocity, etc. Once these are known, non-dimensional quantities, integral properties and some "wall" effects can be computed.

The diagnostic probes were mounted on an instrumentation "rake" shown in Figure 3, with their sensing tips lying on a straight line normal to the flow and parallel to the ceiling. The two outboard and the center probe positions were occupied by 1/8 inch diameter pitot tubes, with the two intermediate positions occupied by a total-temperature probe and the hot-wire anemometer. The probes were separated by a distance of 3 inches. As shown in Figure 4, the static pressure tube is attached under the rake, below the center pitot probe, with its sensing orifices vertically separated from the other probes by 5/16 inch.

To improve the resolution of the pitot survey near the wall, several tests were performed with a miniature probe fitted to the tip of one of the outboard pitot tubes. The miniature probe was comprised of a flattened tube with an opening 0.008 inches high and 0.060 inches wide. In order to approach the wall without interference the tube was bent S-shaped so that its opening was vertically offset from the remaining probes. The hot-wire anemometer was designed in a similar fashion. Figure 4 shows an end view of the rake, as seen by the approaching flow, indicating the various offsets which had to be accounted for during data reduction.

The rake was suspended on an actuator mechanism by which the distance Y between the wall and the probes could be fixed with a precision of 0.001". During the tunnel run Y could be changed continuously at arbitrary speed for a maximum stroke of 8 inches. Data were taken only after the rake had been at the desired Y position for several minutes, so as to allow the probe readings to equilibrate. During operation of the tunnel, a difficulty arose in determining the Y = 0 position of the rake. Because of the pressure differential across the wall of the wind tunnel, the ceiling shifted downward approximately 0.030 inches. Although the test section was provided with viewing ports, the diameter of the port was less than the height of the test section. This prevented a horizontal line-of-sight through the test section at Y positions near the wall, and in particular, at the location of the ceiling itself. The following procedure was finally used to define the location of the ceiling during a run. With air-off the Y indication of the rake with the uppermost pitot tube immediately adjacent to the ceiling was recorded. The rake was moved away from the wall, the tunnel was turned on and as the rake was slowly moved upward, the uppermost pitot tube and the image formed by its reflection from the ceiling were observed visually until the two merged. This position of the

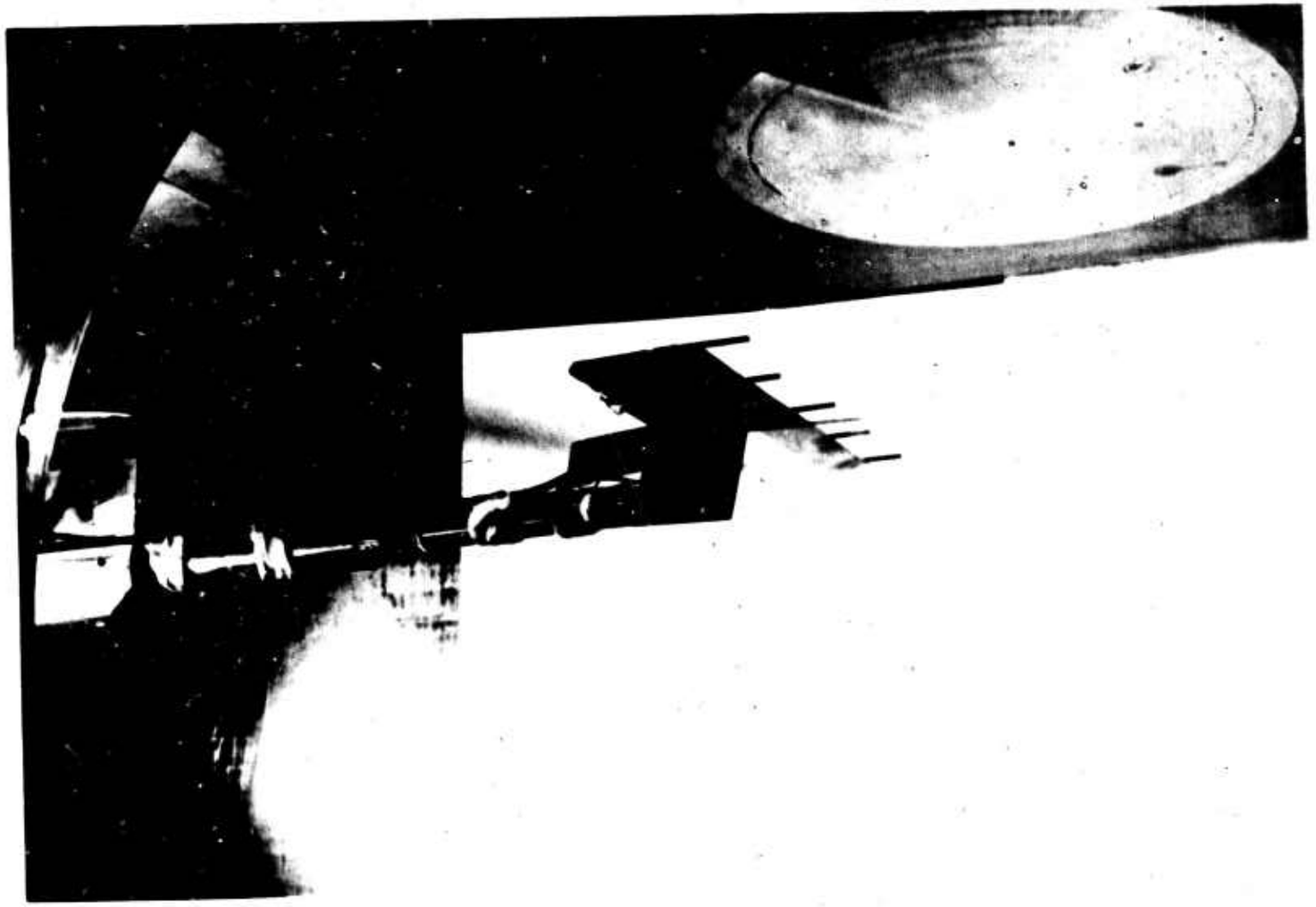

FIGURE 3. INSTRUMENTATION RAKE INSTALLED IN JPL/HWT TEST SECTION

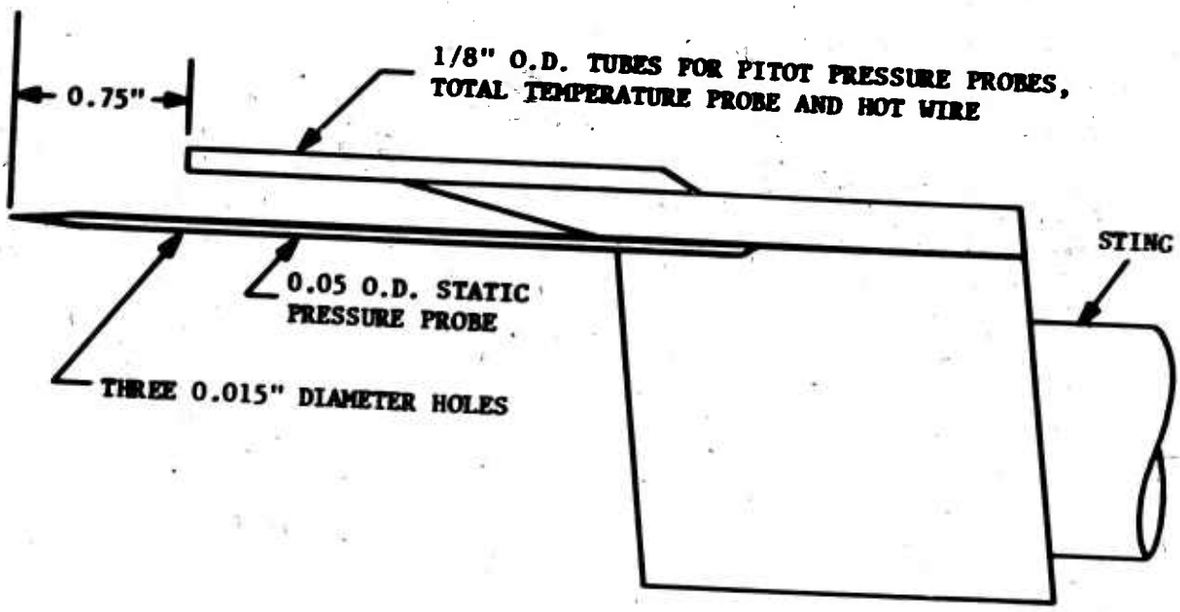


(a) SIDE VIEW OF INSTRUMENTATION RAKE

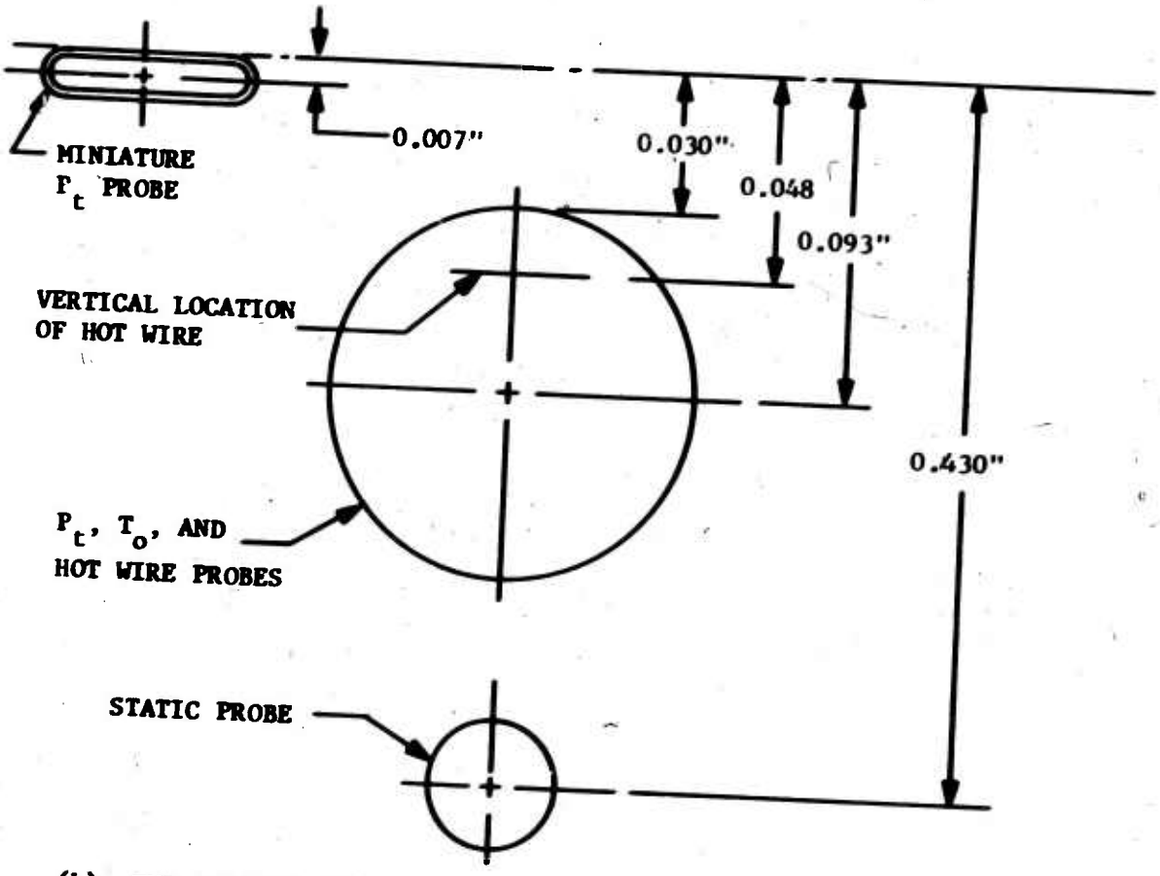


(b) END VIEW OF RAKE SHOWING VERTICAL LOCATION OF PROBES

FIGURE 4. SCHEMATIC OF INSTRUMENTATION RAKE

rake, which could be determined within 0.005 inches, was defined as Y = 0 and all Y indications were corrected by the difference between the air-on and air-off zeros.

The schematic of the data recording system is shown in Figure 5 (for clarity, the static pressure probe has been omitted). Pressure, temperature, and Y position measurements are processed by the Wind Tunnel Data Acquisition System and printed out by the JPL line printer for immediate monitoring by the test personnel. In addition, the center pitot pressure, the total temperature and the Y position data, together with the hot-wire signals, are recorded on magnetic tape to provide a permanent data file for subsequent processing.

It is clear that more diagnostic probes were available on the rake than were needed for determining the local flow conditions. The final data reduction utilized the data from the center pitot tube,* the static pressure probe (corrected for Y offset) and the total temperature probe. Although the latter is laterally offset from the other two by 3 inches, the evidence of two-dimensionality presented in Section V allowed the use of this reading without fear of error due to lateral gradient effects. The hot-wire probe, also offset by 3 inches from the center offers an independent measurement of local total temperature $T_o$ and unit Reynolds number. These were used as redundant cross-checks on $T_o$ and Reynolds number (see Section VIII). The turbulence data collected with this probe will be described in a later report.

---

* For Y distances less than 0.8 inches, data from the miniature probe was used. However, as shown later, the pressures recorded at the three pitot probe positions were in excellent agreement for distances close to the wall.

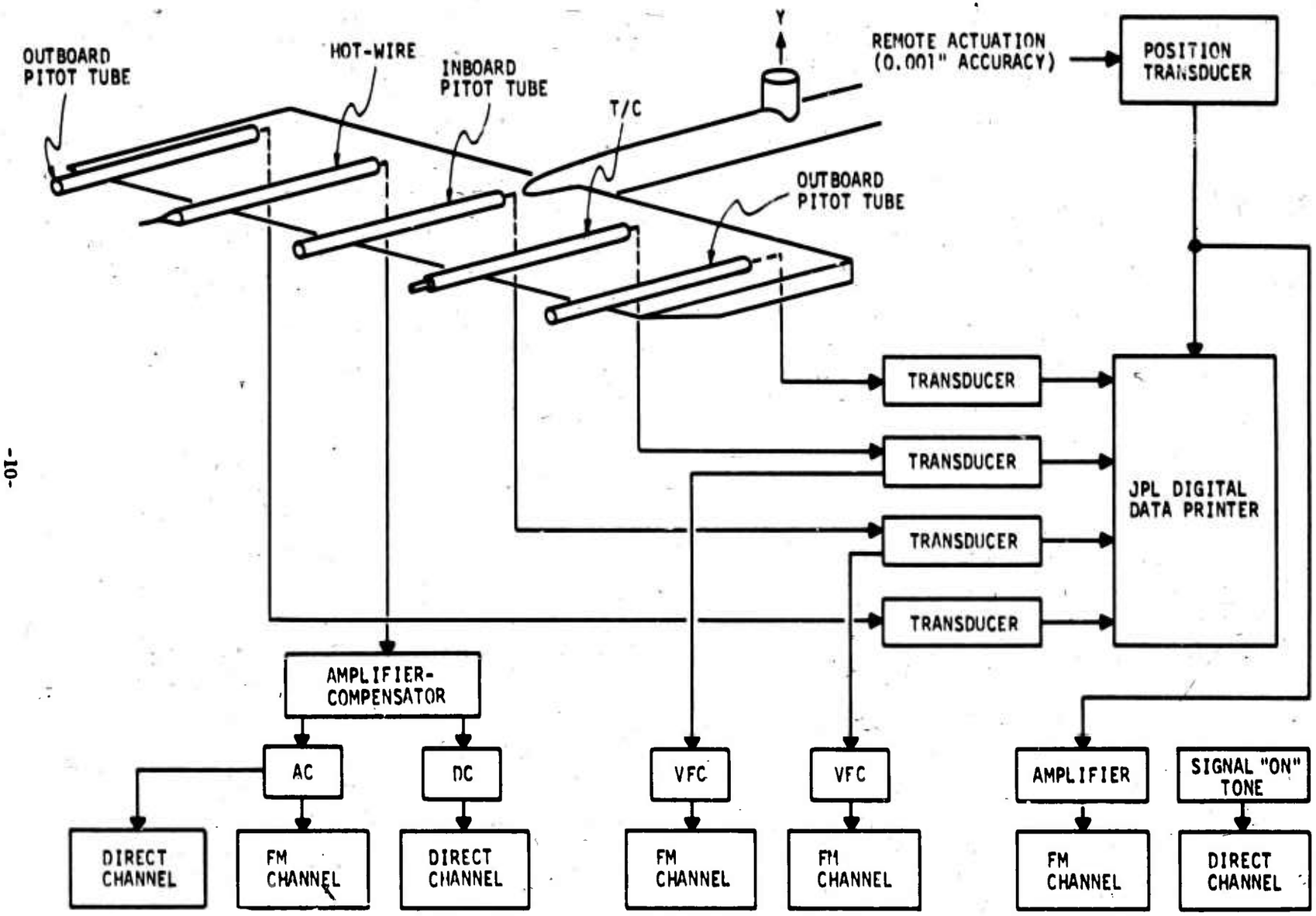


FIGURE 5. SCHEMATIC OF DATA RECORDING SYSTEM

## SECTION IV

## INSTRUMENTATION

### 4.1 PRESSURE TRANSDUCERS

Pressure measurements were made with Statham Instruments absolute pressure transducers which utilize an unbonded, fully active, strain gage bridge as the sensing element. Pitot or impact pressures were measured using model PA208TC-K transducers, with a range of 0 - 15 psia, while a model PA208TC-5 transducer, with a range of 0 - 5 psia, was used to record static pressure. Before each run the transducers were subjected to full vacuum to adjust the zero setting and then calibrated with a McLeod gage over the anticipated pressure range. A check of the zero setting was made just prior to and immediately after each run. The pitot transducers exhibited relatively stable characteristics with negligible zero point drift. The static pressure transducer, however, was initially observed to drift an amount corresponding to approximately 5-10% of the nominal measured pressure. This problem was alleviated to a large extent by mounting the transducer in a temperature controlled water-cooled housing.

The signals from the transducers were converted to digital form for visual display and printout, with the pitot pressure output appearing as 100 counts per cm Hg and the static pressure output as 200 counts/mm Hg. While the error in the pressure readings was approximately 1%, the accuracy of both measurements was dictated by non-linearity and hysteresis of the transducers which was 0.75% of full scale. This is of the same order as the value of the static pressure throughout the boundary layer and of the pitot pressure near the wall. The resolution of the transducer therefore may have contributed to the observed scatter in the static pressure data, Sections V and VI, and to the uncertainties in the velocity profile, Sections IX and X.

Both measurements were examined for corrections due to various probe effects. The static pressure measurements had to be corrected for viscous interaction effects as described in Section VI. The influence of thermal creep and vibrational degree-of-freedom effects on both the static and pitot pressures was examined and found to be negligible. In addition, viscous[4,5] and rarefaction effects[6] on the response of the pitot pressure probe were investigated. For the large pitot probe, the corrections due to these effects did not exceed 1% and were therefore ignored. For the miniature pitot probe the viscous interaction effect was more pronounced, reading an estimated maximum of 10% near the wall. However, experimental data on viscous corrections is scarce and restricted to specific probe geometries which differ considerably from the probe used in the present tests. For this reason, and since the possible error did not exceed 10%, no correction was applied and the miniature probe data was used as recorded.

## 4.2 TOTAL-TEMPERATURE PROBE

As explained previously, the total temperature probe consisted of a type J iron-constantan thermocouple. The thermocouple leads were inserted through and cemented in a 3/32 inch diameter alumina tube which was then installed in the 1/8 inch O.D. copper tube located on the instrumentation rake. The alumina body was notched and the adjacent tube wall grooved so that the thermocouple could be held in position by a spring slip inserted over the tube. The thermocouple junction was positioned 7/16 inches from the opening of the copper tube and three .031 inch diameter vent holes were drilled through the tube wall at this same location.

The signal from the thermocouple was also converted to digital form for display and printout with 80 counts corresponding to 1 mV. The accuracy of the probe measurement, however, was dictated by the precision with which the tunnel supply temperature could be controlled. During a run, the supply temperature varied typically by $\pm$ 2 to 3°C and similar variations were reflected in the measured total temperature.

The total temperature probe was calibrated in the free-stream of the HWT at Mach 9.5 and 6 and 800°K and at Mach 4 and stagnation temperatures ranging from 300 to 810°K. The high Mach number data was supplied by the JPL/USC investigators[3] while the Mach 4 data was obtained during the present study because of concern that the recovery factor of the probe might depend on Mach number and temperature. Calibration results are shown in Figure 6 where the probe recovery factor, defined as the ratio of measured temperature to actual stagnation temperature is plotted against Reynolds number based on probe diameter and stagnation temperature. It is seen that while the Mach 6 and Mach 9.5 data coincide, the Mach 4 data shows a lower recovery factor for a given Reynolds number. The Mach 4 data, however, shows no significant separation due to stagnation temperature. In order to delineate regions within the boundary layer where the calibration data would apply, the Y locations, together with the associated Mach number and stagnation temperature, corresponding to specific Reynolds numbers have been indicated in Figure 6. It is clear that the high Mach number data is applicable to the outer half of the boundary layer. In addition, the possible error introduced by the separation in the data at low Reynolds numbers is at most several percent. Furthermore, the Mach 4 data indicates a possible tendency to merge with the high Mach number data at Reynolds numbers between 100 and 1000. Consequently, it was decided to represent the probe calibrations by the single curve, determined from a least squares fit to the Mach 6 and 9.5 data shown in Figure 6.

## 4.3 HOT-WIRE ANEMOMETER

### 4.3.1 PROBE CONSTRUCTION

The anemometer probe, shown in Figure 7, consisted of a 0.00001 inch diameter Pt - 10% Rh wire mounted across the tips of two sharp-pointed prongs. The wires were mounted with sufficient slack to eliminate spurious signals due to "strain-gage" effects. For the wires used in these experiments, the aspect ratio ranged from 200 to 400.

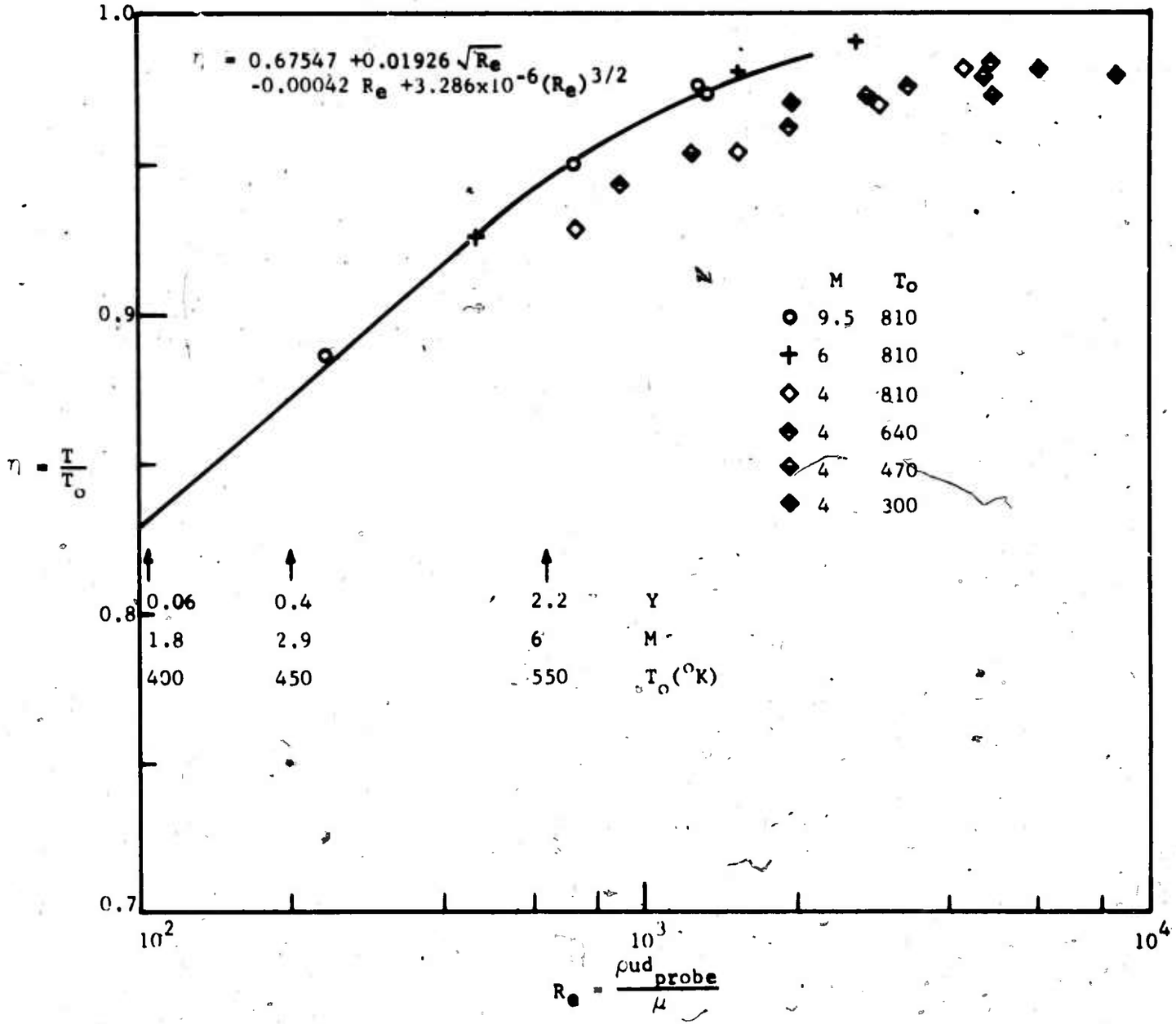


FIGURE 6. RECOVERY FACTOR CALIBRATION CURVE FOR TOTAL TEMPERATURE PROBE

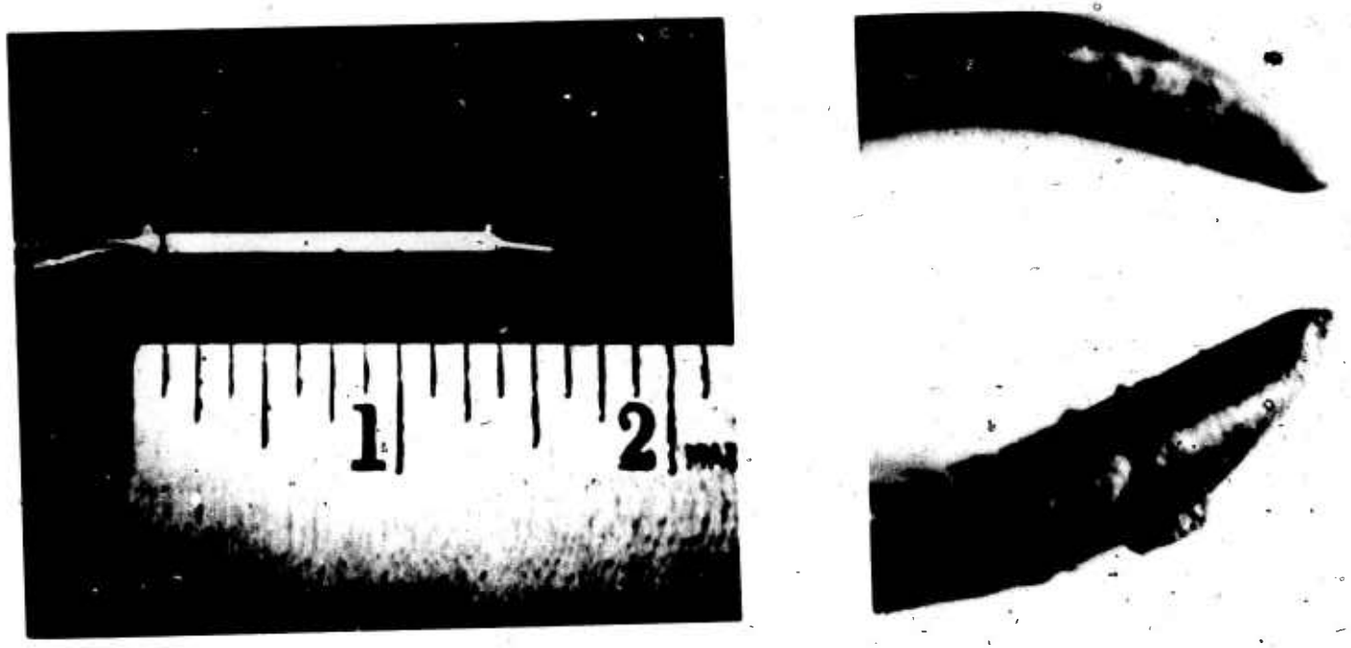




CHARACTERISTICS OF WIRES

1. MATERIAL: PT 10% RH
2. DIAMETER: 0.00001"
3. LENGTH: 0.0025 TO 0.005" (ASPECT RATIOS 250-500)
4. ATTACHMENT METHOD: GOLD PAINT
5. PROBE MATERIAL: NICKEL PRONGS BONDED IN ALUMINA TUBE. GOLD OR COPPER LEADS SOLDERED TO PRONGS
6. MEASURED TIME CONSTANTS: 15-30 MICROSECONDS
7. HEATING CURRENT RANGE: 0-1 mA

FIGURE 7. TYPICAL HOT WIRE ANEMOMETER PROBE USED IN TESTS

The probe body consisted of a 3/32 inch diameter x 1½ inches long alumina cylinder. A 1/32 inch diameter x ½ inch long alumina cylinder, used to support the hot-wire prongs, was cemented to one end of the larger cylinder at an angle of approximately 20-30 degrees. Both cylinders were provided with two holes along their length through which the hot-wire leads were inserted. The leads were 30 gage copper wire encased in high temperature fiberglass insulation. Copper was selected because of its low electrical resistance, ease of silver soldering, and bending capability without breakage. Three-mil nickel wire, used for the hot-wire prongs, were silver-soldered on one end of the copper leads. The prongs, leads, and alumina tubes were held together with Corning Class Company Pyroceram cement. Pyroceram can be used to up to 700°C, is an excellent insulator, and cures easily with an oxygen-acetylene torch, leaving a smooth glassy finish.

To assemble the probe, the 3/32 inch diameter alumina tube was first cut to length with a diamond blade saw and "V" shaped grooves were cut in both ends to provide the pyroceram cement greater bonding area. Next, the 1/32 inch diameter alumina tube was cut to 1/4 inch in length. After the nickel support wire was silver soldered to the copper wire, it was inserted through the alumina tubes. Pyroceram cement was applied, cured with a torch, with great care being exercised to keep the tips of the nickel prongs free and cleam of cement. The support wires were then prepared and adjusted for mounting the hot wire.

The technique for mounting the hot wire consists of bonding the wire on the supports with gold, which had been dissolved in a resinate and diluted with toluene. The resinate is baked away in an oven at 1000°F leaving a thin gold film approximately 5 micro-inches thick. Only one application of the gold solution is required for mounting 0.00001 inch diameter wires, although for larger wires, as many as six coats of gold are necessary for a good bond. In the process of mounting the wire, a small length of 2-mil Wollaston wire with a core of 0.00001 inch diameter Pt - 10% - Rh wire is held in a pair of tweezers. A length of about 10 mils of silver is etched off, exposing the Pt - 10% - Rh wire. The probe is held in a vise in the object plane of a 60 power stereoscopic microscope in order to observe the mounting of the wire. Next a 20 gage wire is used to apply the gold solution to the tips and along the outside length of the prongs. Then, by carefully manipulating the tweezers, the hot wire is laid along the outside of one prong, across its tip and over to the tip of, and up along the outside of the second prong. The hot-wire adheres very well to the gold solution. By wiggling the tweezers, the Pt 10% Rh wire will break where it joins the Wollaston wire. Once the hot wire is mounted, the probe is placed in an oven at about 1000°F and in two to three minutes the solution is baked away leaving a gold-bonded hot-wire.

### 4.3.2 PROBE CALIBRATION

Following the probe assembly, the temperature-resistance behavior of the wire was measured in a controlled oven over the range from 20 to 200°C. Five temperatures in this range were selected and the wire resistance, R, was recorded for eight currents. The heating due to these currents is small so that R could be expressed as a linear function of current. The

zero current resistance was obtained by extrapolation yielding a curve of R versus temperature, T. The zero temperature resistance $R_r$ and the first coefficient of resistivity, $\alpha_r$, were then found from the resistivity formula

$$R = R_r [1 + \alpha_r (T - T_r)] \tag{1}$$

where $T_r = 0^{\circ}C$.* Typical values of $\alpha_r$ ranged from $1.1 \times 10^{-3}$ to $1.8 \times 10^{-3}$ ohm/$^{\circ}$C, with the majority corresponding to $1.4 - 1.5 \times 10^{-3}$.

It was originally intended to install each wire in the Philco-Ford Mach 3 tunnel to check for "strain-gage" effects and to carry out a preliminary flow calibration prior to its use in the JPL/HWT. However, since the flow environment in the Philco-Ford tunnel is more severe than the HWT (larger dynamic pressure), wire survivability was very poor. Consequently, this phase was omitted and flow calibration of each wire was carried out in the HWT immediately prior to performing turbulence measurements. The objective of this step was to obtain the variation of the Nusselt number at zero overheat, $Nu_o$, and of the wire recovery factor, $\eta$, with Reynolds number, $Re_o$. The subscript o refers to stagnation conditions, that is,

$$Nu_o = \left[ \frac{q\, d}{T_w - T_{aw}} \frac{1}{k_o} \right]_{i = 0} \tag{2}$$

$$Re_o = \frac{\rho u d}{\mu_o} \tag{3}$$

$$\eta = \frac{T_{aw}}{T_o} \tag{4}$$

where q is the heat transfer from the wire, d is the wire diameter, $T_w$ is the wire temperature, $T_{aw}$ is the adiabatic wire temperature, $k_o$ is the thermal conductivity of air, $\rho$ and u are the local free-stream density and velocity of air respectively, and $\mu$ is the viscosity of air evaluated at $T_o$.

The calibration was performed by locating the wire in the wind tunnel free-stream where the flow conditions are well known and varying the Reynolds number by setting the tunnel total pressure at specific values between 700 and 3200 cm Hg. At each pressure the derivative $\partial R/\partial i^2$ was found from the slope of the R versus $i^2$ curve obtained by operating the wire at 8 overheat currents. The Nusselt number at zero overheat, $Nu_o$, was then given by

---

* From initial calibrations up to 500$^{\circ}$C it was found that the second coefficient of resistivity was zero. It was possible therefore to restrict subsequent calibrations to 200$^{\circ}$C, thereby facilitating the calibration process.

$$Nu_o = \frac{\alpha_r R_r}{\pi \ell k_o} \frac{R_{aw}}{\partial R/\partial i^2} \qquad (5)$$

where $\alpha_r R_r$ and $\ell$, the wire length, were obtained from the oven calibration, and $R_{aw}$ is the adiabatic resistance found by extrapolating the calibration curve to zero current. The recovery factor was computed by using $R_{aw}$ to obtain $T_{aw}$ from Eqn. (1) and $T_o$.

Typical flow calibration curves are shown in Figures 8 and 9, which also include theoretical curves for aspect ratios ranging from 100 to infinity. Because of the low Reynolds numbers it is seen that large end losses are to be expected. However, the agreement between theory and experiment is observed to be very poor, probably because the basic assumptions of the theory (e.g., straight wires, no flow interference by the prongs, etc.) are not satisfied by the actual probes.

The calibration curves shown in Figures 8 and 9 were put into the following analytical form for use in the data reduction process:

$$Nu_o = A_1 + A_2 \sqrt{Re_o} + A_3 Re_o$$

$$\text{or} \quad = B_1 + B_2 \sqrt{Re_o} + B_3 Re_o \qquad (6)$$

After the oven calibration, the wire resistance was checked daily prior to its use in the HWT to insure that the characteristics of the wire remained unchanged. Resistance changes of more than 1% forced rejection of the wire. While it would have been desirable to subject the wire to a second oven calibration following its use in the HWT, none of the wires with which turbulence data was collected survived the tunnel stop.

## 4.4 WIND TUNNEL SUPPLY CONDITIONS

The wind tunnel supply pressure, which was assumed equal to the test section freestream stagnation pressure, was measured using a Statham Instruments model PA731TC-1M-350 strain gage transducer, with a range of 0 - 1000 psia, a sensitivity of 0.01% of full scale and a linearity of 1/4% of full scale. The supply temperature was measured with a shielded Chromel-alumel thermocouple. Similar to the other measurements the signals from these instruments were digitized for visual display and printout, the pressure output appearing as one count per cm Hg and the thermocouple output as 80 counts per mV. Both instruments were located in the constant area supply chamber, 3 ft upstream of the nozzle throat and just downstream of the flow straightener.

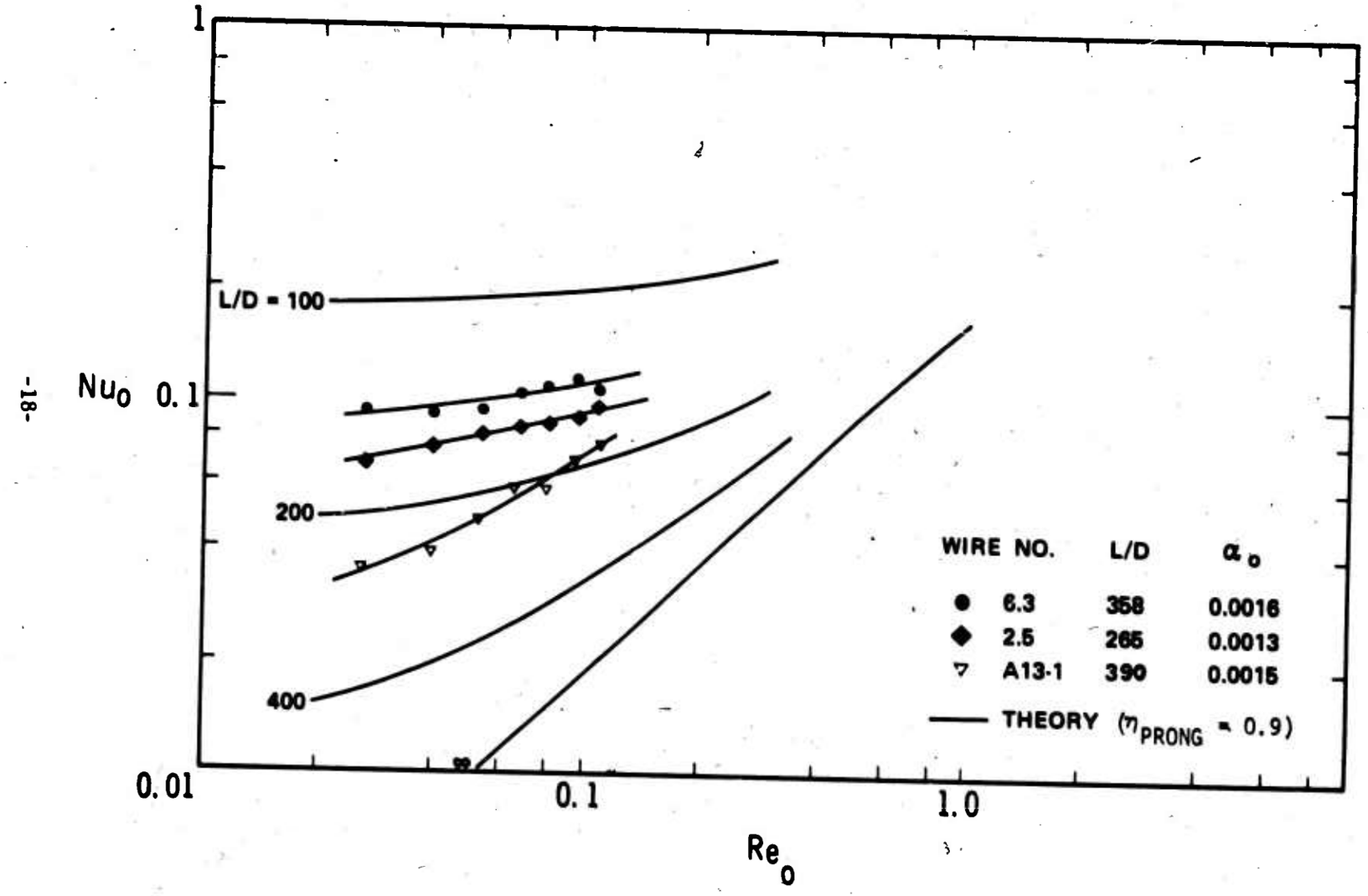


FIGURE 8. HEAT TRANSFER CHARACTERISTICS OF TYPICAL HOT WIRE PROBES

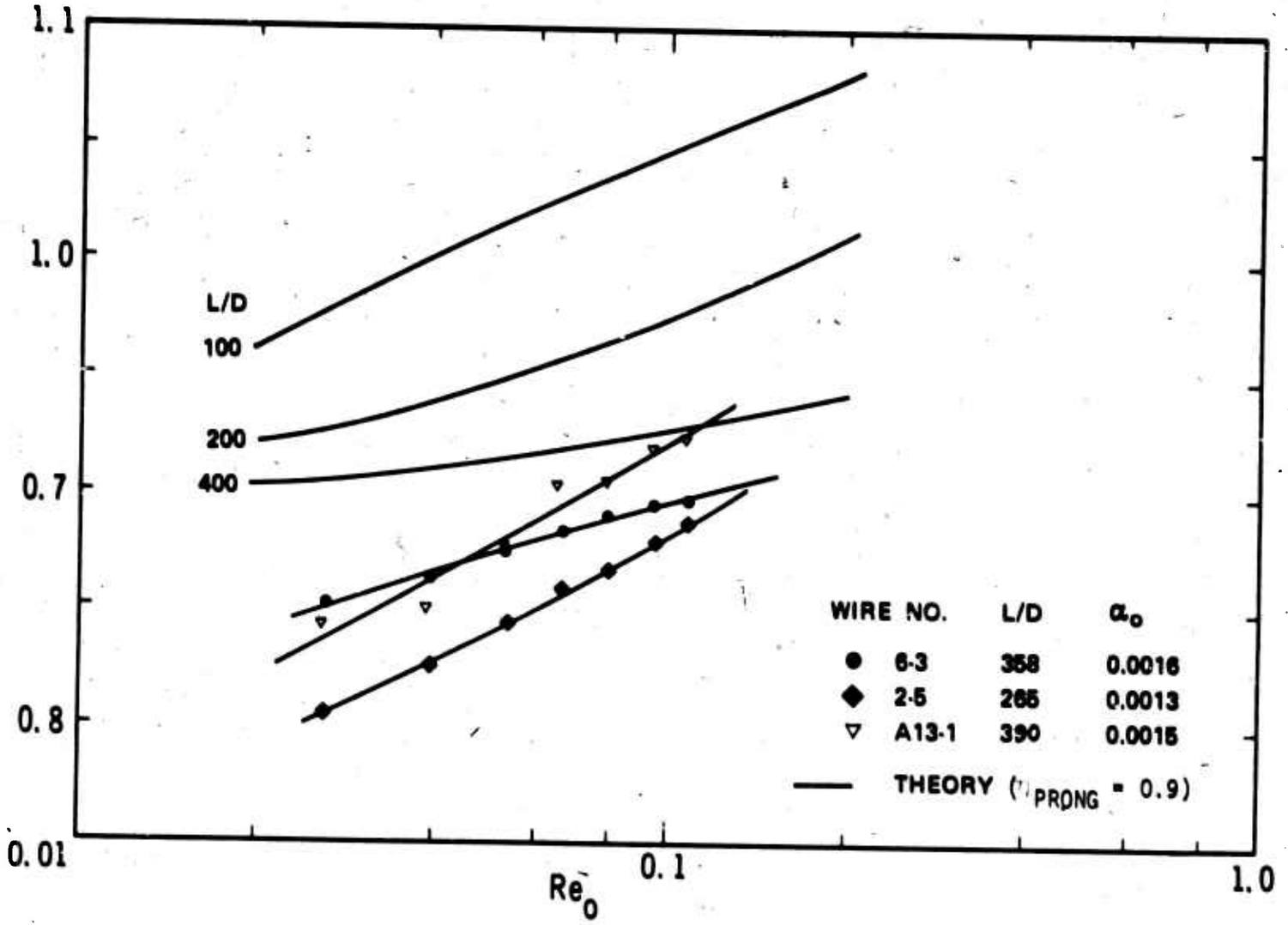


FIGURE 9. RECOVERY TEMPERATURE CHARACTERISTICS OF TYPICAL NOT WIRE PROBES

## SECTION V

## PRELIMINARY TEST RESULTS

The data described in this section have been included to demonstrate the nature of the boundary layer flow, the two-dimensionality of the boundary layer, and the reproducibility of the measurements. In addition, the mean flow properties calculated from these preliminary measurements were essential for the proper design of the hot-wire anemometer. Data is presented which was acquired over a period of six months. Most of the measurements were collected by the USC/JPL team of investigators.(3)

Figure 10 shows the pitot profiles obtained from the two outboard pitot probes at stations 112 and 160 inches from the nozzle throat. The data shown was reproduced directly from pressure traces obtained with a dual channel x-y plotter. Because of the finite size of the recording pens the $\bar{z} = -6$ pressure trace was physically offset by the amount indicated at the left-hand-side of the Figure 10 ($\Delta y \approx 0.10$ inches). Therefore the corrected trace for this transducer is obtained by translating all data points to the left by the amount $\Delta y$. In spite of this shift in the $\bar{z} = -6$ curve, the spanwise agreement in the pressure profiles at both stations is quite good, indicating that the flow can indeed be considered to be two-dimensional. Furthermore, the pressure profiles are quite similar in shape showing relatively little difference between the two measuring stations. It is inferred from this that the flow is typical of a highly developed, turbulent nozzle wall boundary layer.

The static pressure profiles measured at stations X = 112, 137, and 160 inches from the throat are shown in Figure 11. The data at X = 112 and 137 inches were obtained from single runs at these stations while the X = 160 data shows the range of measurements obtained from six runs. Also shown are the range of wall pressure measurements observed during the run made at each station. The wall measurements were made with a transducer identical to that used for the static pressure probe. Although the difference in pressure at successive stations is only slightly larger than the experimental accuracy, the data indicate a small favorable longitudinal pressure gradient of approximately - 0.005 mm Hg/inch near the wall. In the free-stream and for the wall measurements at the X = 112 and 160 inch stations, the longitudinal variation in pressure is within the scatter observed from run to run. As described in Section VI, the static probe measurements are subject to large viscous interaction corrections. The corrected data show a pressure gradient normal to the wall that is 20 times greater than the longitudinal gradient indicated above.

A further indication of the two-dimensionality of the boundary layer flow, which also demonstrates the reproducibility of the measurements, is shown in Figure 12. The envelope of measurements obtained by USC/JPL showing the small spanwise variation of pitot pressure through the boundary layer is presented, together with the results of a pitot pressure survey made six months later during the present study. The pitot profile obtained from the center probe is denoted $Pt_2$. The data indicate that spanwise variations

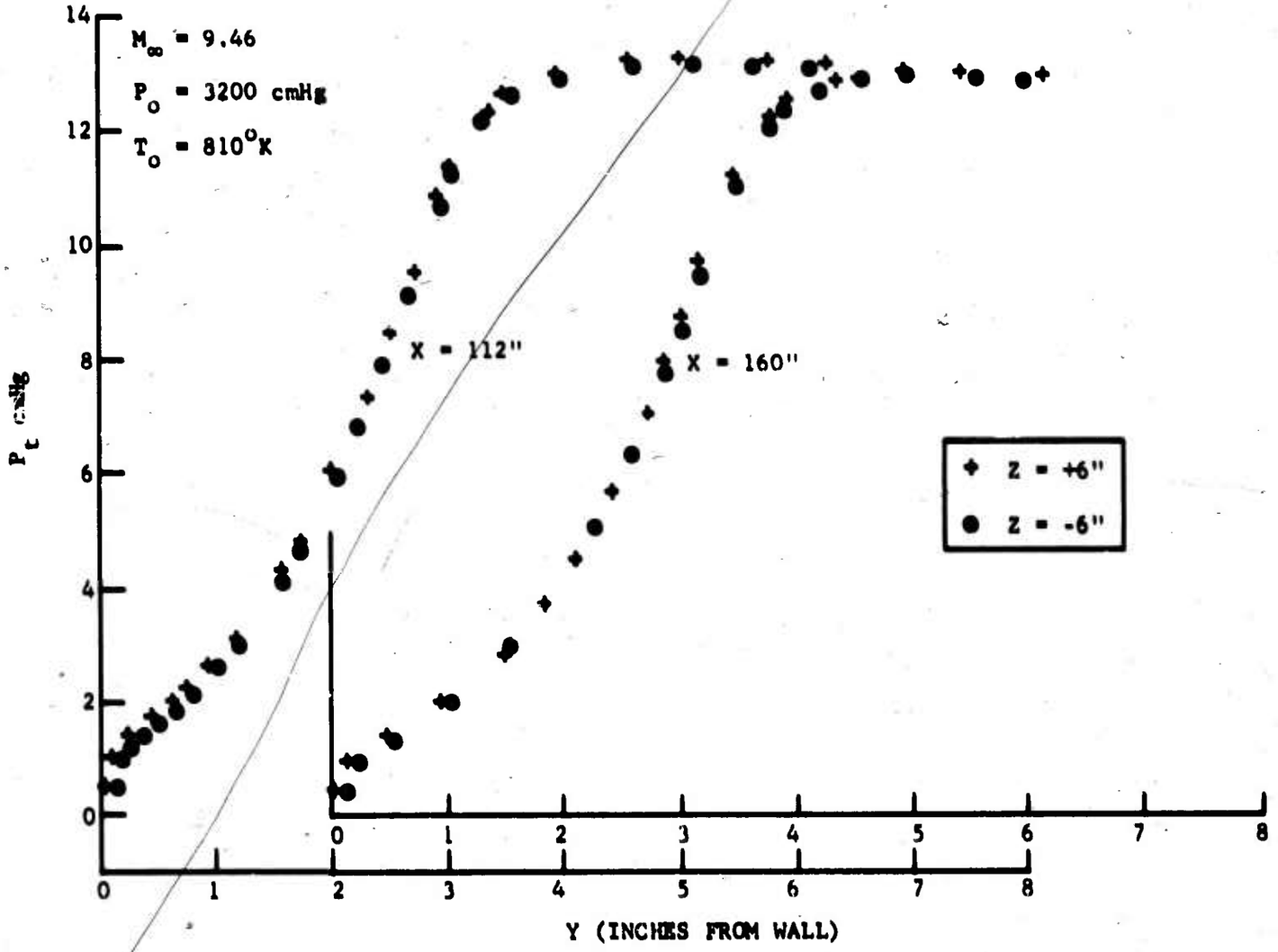


FIGURE 10. TYPICAL PITOT PRESSURE PROFILES OF MACH 9.5 BOUNDARY LAYER AT SEVERAL LONGTIUDINAL AND SPANWISE STATIONS

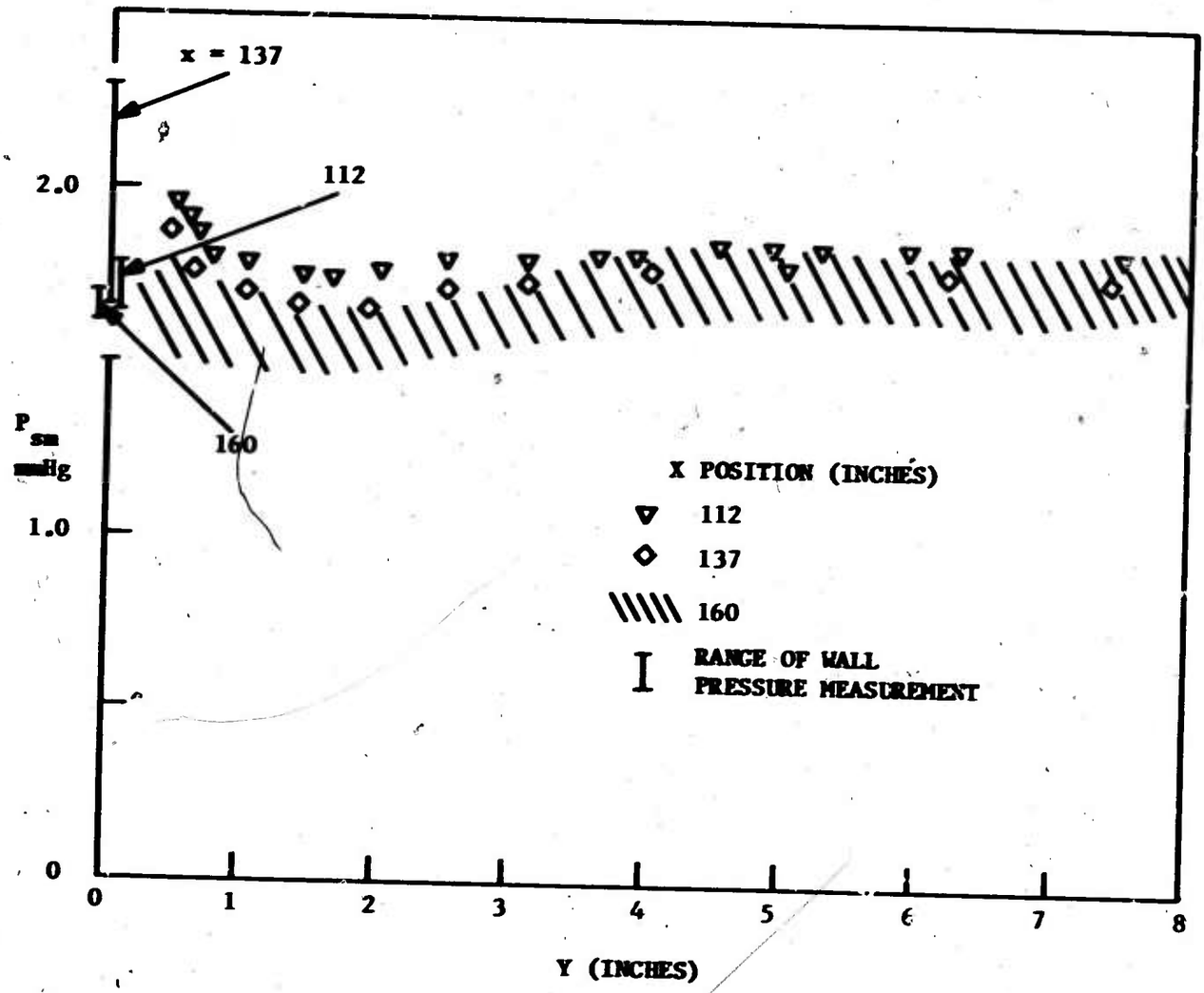


FIGURE 11. TYPICAL STATIC PRESSURE PROFILES OF MACH 9.5 BOUNDARY LAYER AT SEVERAL LONGITUDINAL STATIONS

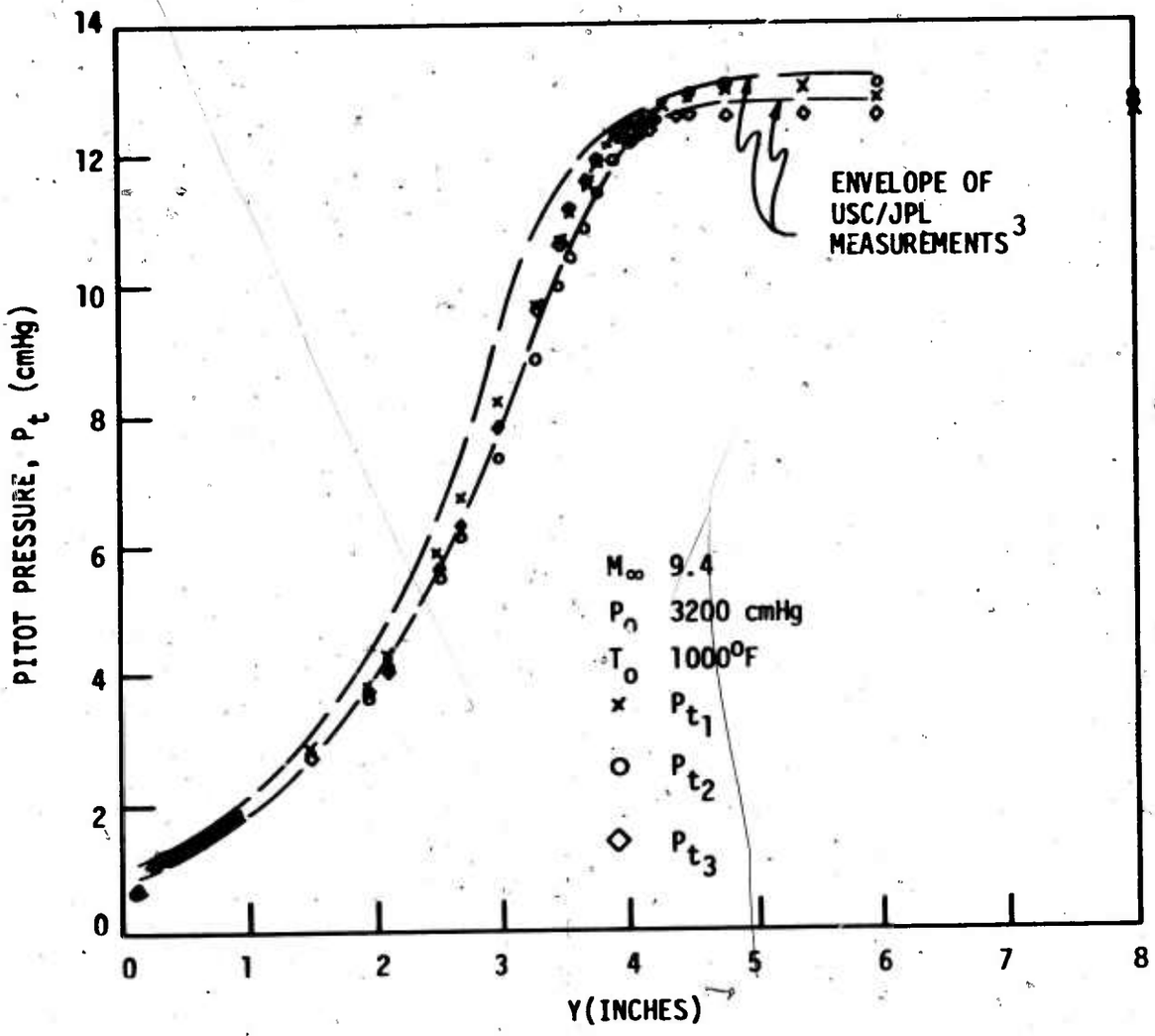


FIGURE 12. SPANWISE VARIATION OF PITOT PRESSURE PROFILES

in pressure diminish with decreasing Y and excellent agreement among the three probes readings is obtained in the immediate vicinity o. the wall.

## SECTION VI

## FINAL TEST DATA

Before discussing the method of data reduction and the final results for the mean flow profiles, the raw data is presented in order to demonstrate again the reproducibility of the measurements and, secondly, to clarify the data reduction procedure. The calculation of the mean flow properties is based on the measured pitot pressure, static pressure, and total temperature. Each of these parameters is discussed in detail in the following paragraphs.

### 6.1 PITOT PRESSURE MEASUREMENTS

Figure 13 shows the pitot profiles, denoted as $P_{t2}$, obtained with the center pitot probe during a total of five runs. Included also are the measurements obtained with the miniature probe located at one of the outboard positions. These points, denoted as $P_{t3}$, are restricted to Y distances between 0 and 1.5 inches. As shown in the insert of Figure 13, the differences between $P_{t2}$ and $P_{t3}$ are not significant and the two profiles are nearly identical for $Y > 0.5$ inches. Because of the excellent agreement between the results of different runs, the data from all runs were combined to yield a single pitot pressure profile for purposes of data reduction. Values of $P_{t3}$ were used for $0 \leq Y \leq 0.8$ inches and $P_{t2}$ data was used between $Y = 0.8$ inches and the free-stream.

### 6.2 TOTAL TEMPERATURE MEASUREMENTS

The measured total temperature profiles for three runs are shown in Figure 14 which, for comparison, also includes the data obtained by the USC/JPL team.[3] Again excellent agreement between runs is observed with differences in the data attributed primarily to variations in the supply temperature. The insert in Figure 14 shows the temperature profiles plotted to an expanded Y scale in the vicinity of the wall where again, except for several obviously erroneous points on run 10, the agreement between runs is very good.

Similar to the pitot pressure data, the data from all three runs was combined to yield a simple total temperature profile. However, since the Y position of the thermocouple did not coincide with that of the miniature pitot probe, the temperature data for $Y < 0.8$ inches was represented by the following expressions:

$$0.060 \leq Y \leq 0.275 \text{ inches}$$

$$T_m(^\circ K) = 303 + 2534\,Y - 18774\,Y^2 + 70744\,Y^3 - 127796\,Y^4 + 8896\,Y^5 \tag{7}$$

$$0.275 \leq Y \leq 0.800 \text{ inches}$$

$$T_m(^\circ K) = 460 + 45.7\,(Y - 0.275)$$

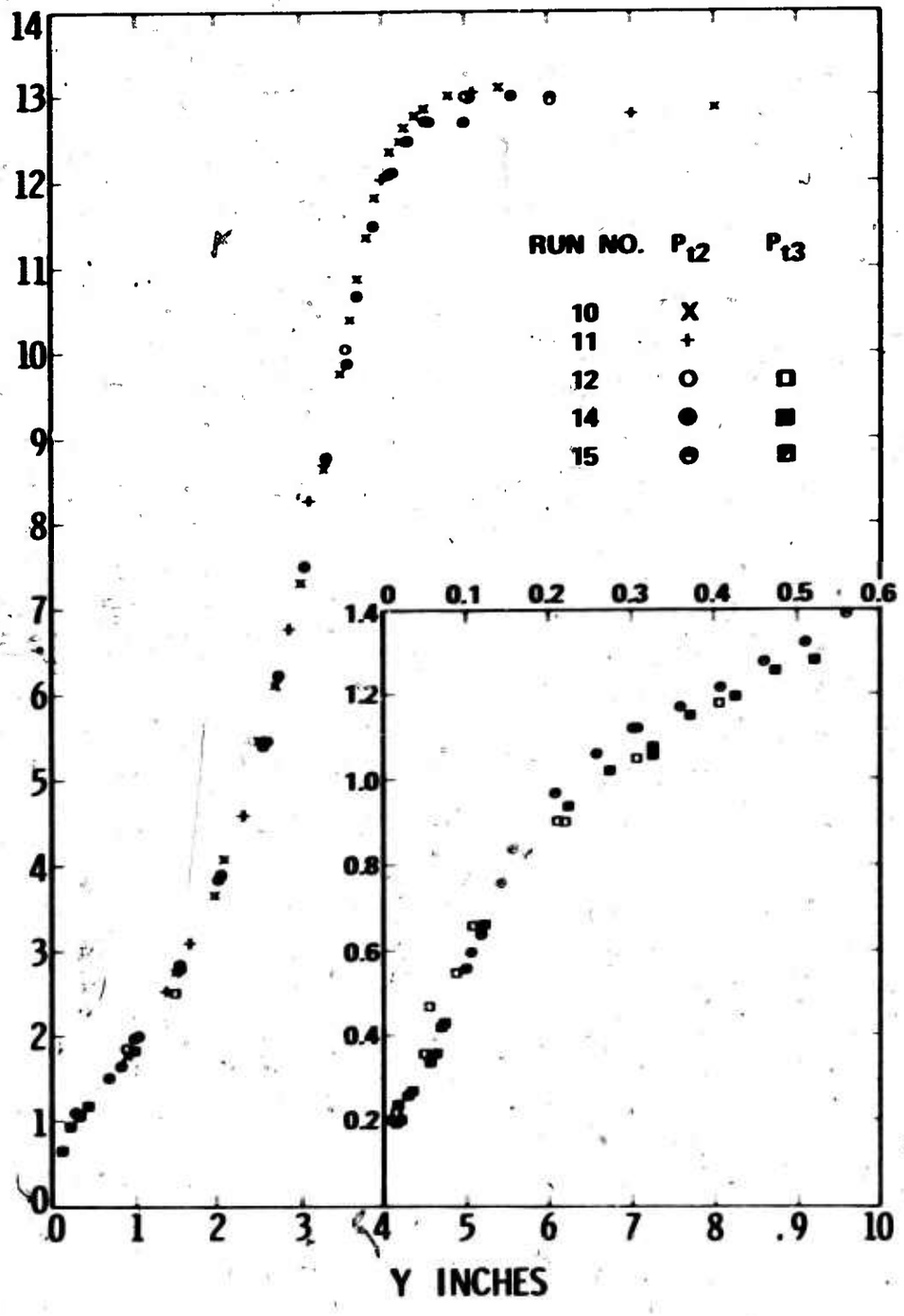


FIGURE 13. PITOT PRESSURE PROFILE USED FOR DATA REDUCTION

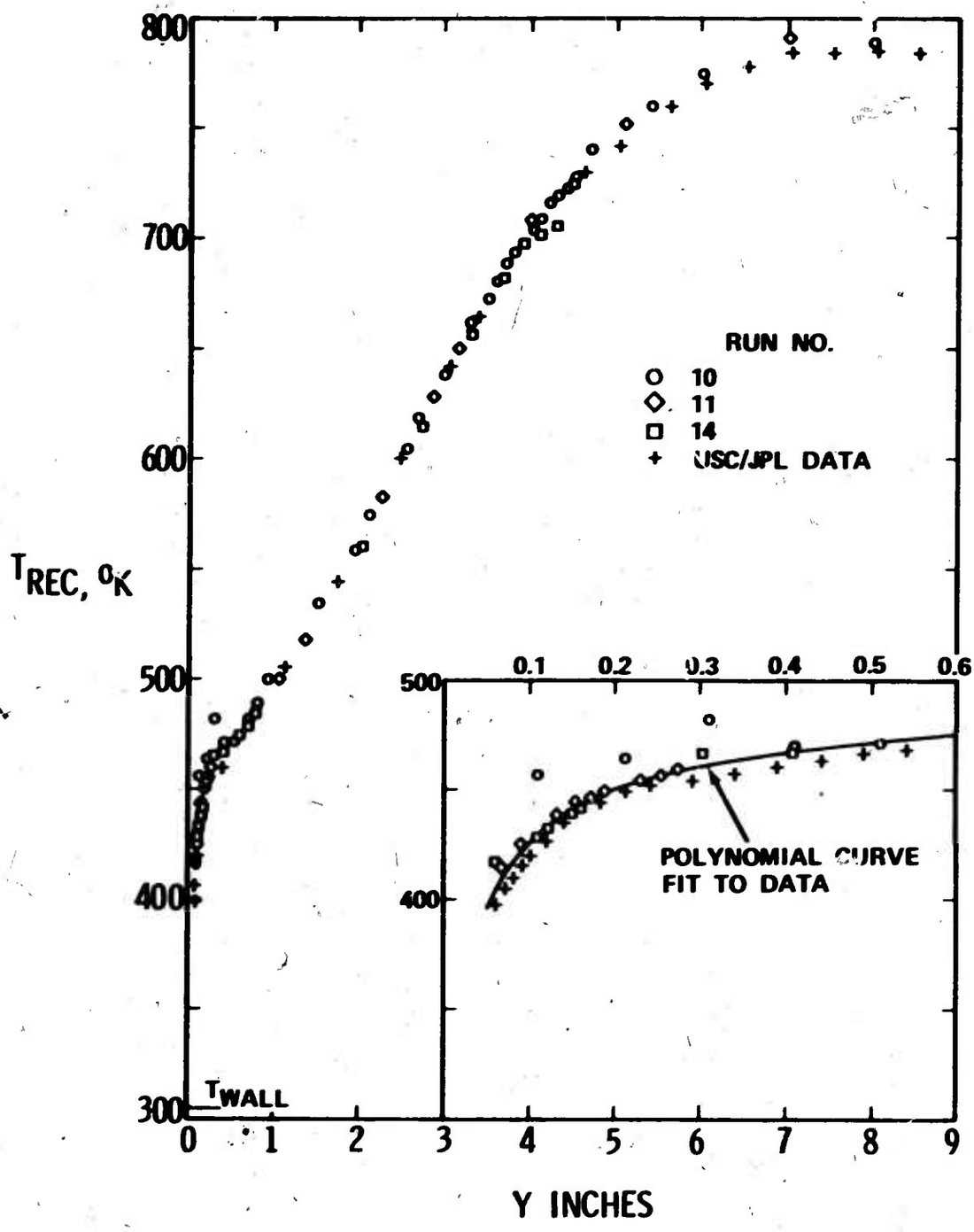


FIGURE 14. MEASURED STAGNATION TEMPERATURE PROFILE USED FOR DATA REDUCTION

The resulting curve fit is shown in Figure 14. The determination of the actual total temperature for $Y \leq 0.06$, where temperature measurements were not available, is described in Section VIII.

## 6.3 STATIC PRESSURE MEASUREMENTS

The static pressure measurements acquired from six runs are plotted as a function of Y in Figure 15. In contrast to the other data, the static pressure exhibited significant variation on a given run as well as from run to run. As shown in Figure 15, the maximum deviation in static pressure for the six tests was ± 7%, which was an order of magnitude greater then the variations in supply conditions. However, a greater precision in the static pressure measurement should not be expected since the nominal pressure was less than 1% of the range for which the transducer was designed to operate. Consequently, it was decided to represent the measured static pressure profile by the following expression, determined from a least squares fit of the data:

$$0 \leq Y \leq 5.75 \text{ inches}$$

$$P_{sm}(\text{mm Hg}) = 1.642025 - 0.197563\,Y + 0.130692\,Y^2 - 0.026982\,Y^3 + 0.002297\,Y^4 - 0.000069\,Y^5 \qquad (8)$$

$$Y > 5.75 \text{ inches}$$

$$P_{sm}(\text{mm Hg}) = 1.77$$

The resulting curve fit is shown in Figure 15.

Although the static pressure measured in the free-stream was 1.77 mm Hg, the static pressure $P_{si}$, calculated from the free-stream pitot pressure and the supply pressure, was approximately 1.1 mm Hg. The free-stream Mach numbers determined from various combinations of $P_{sm}$, $P_{si}$, $P_t$ and $P_o$ are shown below.

| PRESSURE RATIO | MACH NUMBER |
|---|---|
| $P_{sm}/P_t$ | 7.5 |
| $P_{sm}/P_o$ | 8.8 |
| $P_{si}/P_t$ (or $P_{si}/P_o$) | 9.4 |

Since the nominal Mach number corresponding to the tunnel geometry (determined from a "calibration" acquired through long term use of the tunnel) was 9.5 and since both the pitot and supply pressures are accurate within 1%, it was concluded that the actual free-stream static pressure was given by $P_{si}$. The difference between $P_{sm}$ and $P_{si}$, therefore, has been attributed to viscous interaction effects on the static pressure probe. Since the interaction effects vanish near the wall, it is seen that a significant

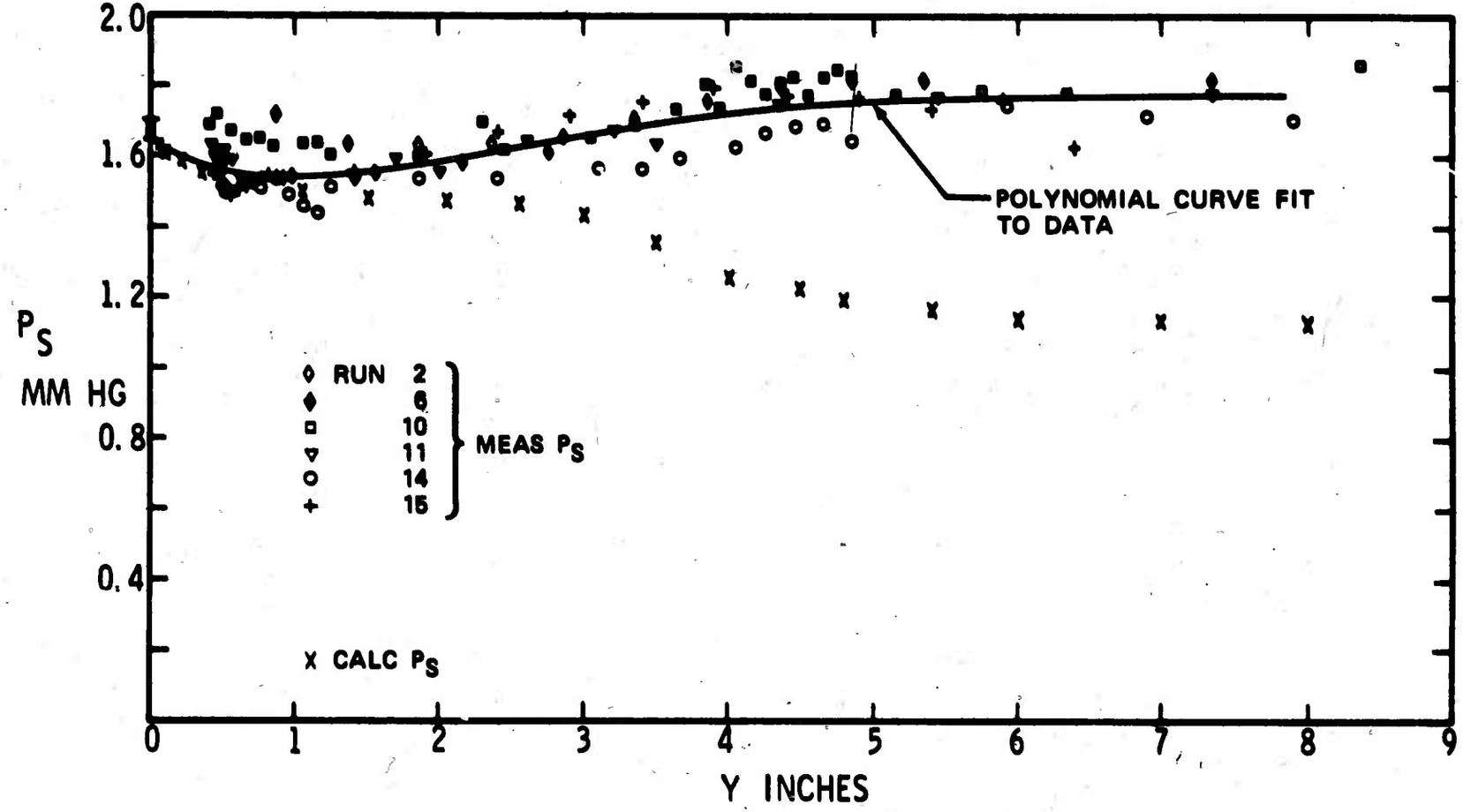


FIGURE 15. MEASURED STATIC PRESSURE PROFILE USED FOR DATA REDUCTION

pressure difference of unknown origin existed across the boundary layer. Because of the magnitude of the pressure difference (approximately 50%) it was considered necessary to account for the variation in pressure normal to the wall in the data reduction process.

Behrens,[7] using a static probe very similar in geometry to that used in the present study, developed an empirical correlation of viscous interaction effects in the form

$$P_{sm}/P_{si} = 1 + C_1\chi + C_2\chi^2$$

where:

$$\chi = M_\infty^2/(C/Re_\infty)^{\frac{1}{2}}$$

$$C = (\mu_w/\mu_\infty)(T_\infty/T_w)$$

and the Reynolds number is based on the distance between the tip of the probe and the pressure orifice, and subscripts $\infty$ and w denote free-stream and adiabatic wall conditions respectively. In our experiments the maximum value of C was found to be equal to 1.05; therefore C was set equal to unity. Behrens data was restricted to $\chi < 1.6$, which is only slightly greater than one-half the maximum value of $\chi$ in the present tests. While the results of Rogers, et al,[6] extends to larger values of $\chi$, their data, which was obtained with a large cone angle probe, fails to account for the observed pressure difference. This is in accordance with the results of Wagner and Watson[8] who found that viscous corrections diminish with increasing cone angle. Consequently, viscous corrections which cover the range of conditions encountered in the present experiments were determined by supplementing Behrens data with data acquired during calibration of: (1) the hot wire at Mach 9.5, and (2) the total temperature probe at Mach 4.

As described earlier, calibration was accomplished by locating the probe in the known free-stream flow at fixed Mach number and varying the supply pressure to change the Reynolds number. The pitot and supply pressures were used to determine the Mach number and actual static pressure as well as other flow properties. From this information and the measured static pressure, $P_{sm}/P_{si}$ and $\chi$ could be calculated. The results are shown in Figure 16, which includes also a plot of the expression

$$P_{sm}/P_{si} = 1 + 0.0457\ \chi + 0.0622\ \chi^2 \qquad (9)$$

which was fit to the data by the method of least squares.

## 6.4 1700 CM HG TEST DATA

The raw data obtained at $P_o$ = 1700 cm Hg are shown in Figure 17. The data are similar to that acquired at 3200 cm Hg, with differences between the two attributed to the increased boundary layer thickness corresponding to

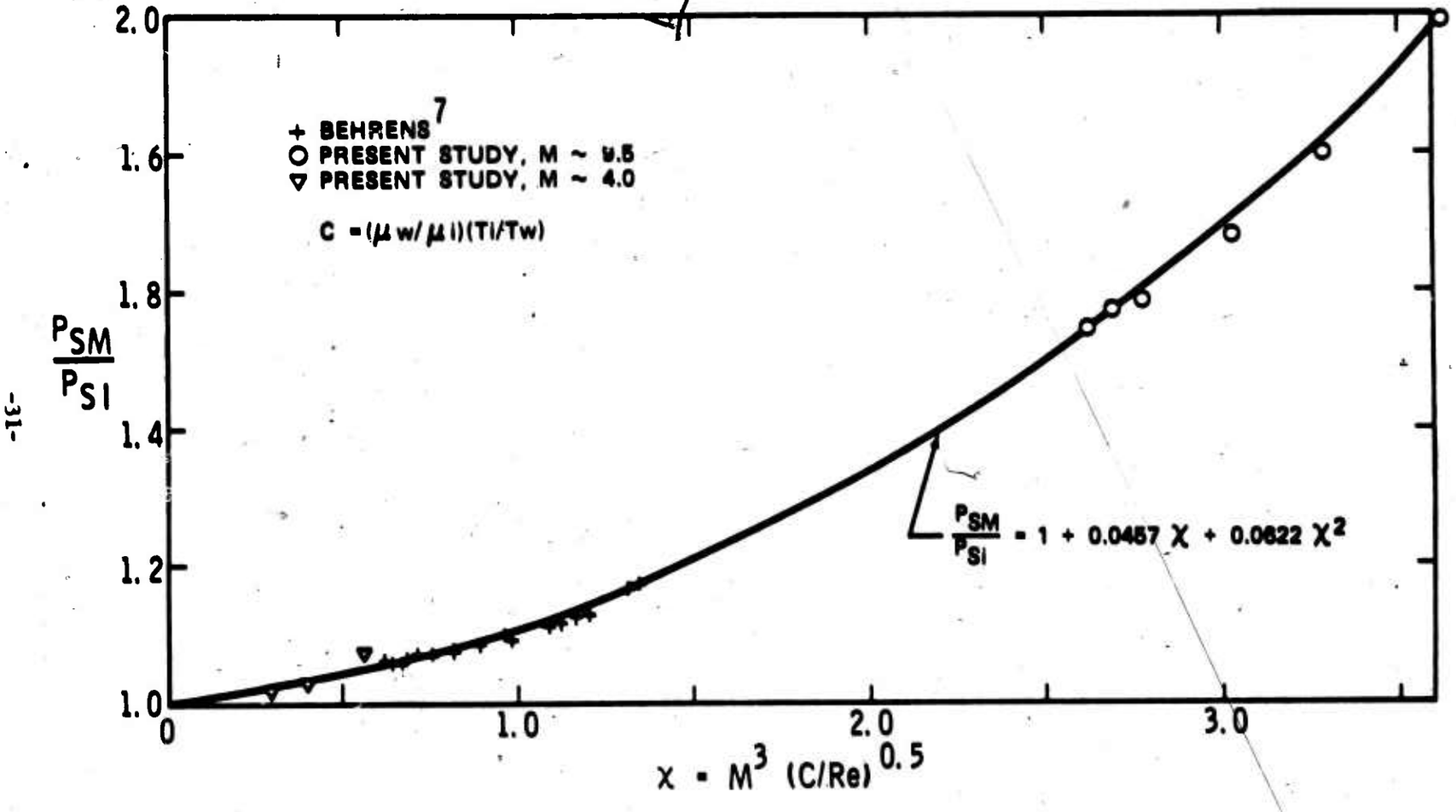


FIGURE 16. VISCOUS INTERACTION CORRECTION FOR STATIC PRESSURE PROBE

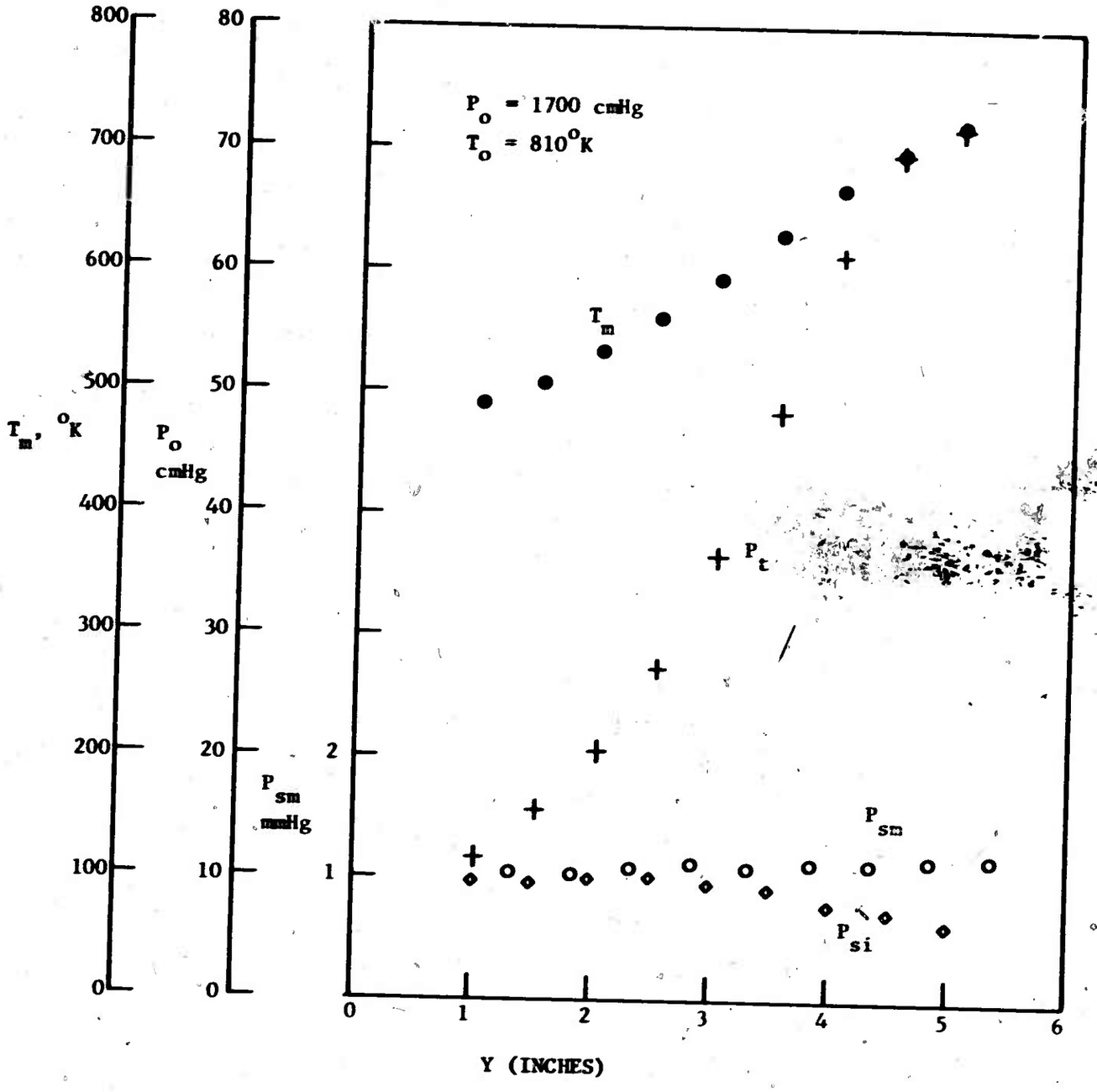


FIGURE 17. MEAN FLOW MEASUREMENTS AT $P_o$ = 1700 cmHg

the smaller Reynolds number and to the reduction in the absolute value of the supply pressure. Measurements were not made for $Y < 1.0$ inch since the Reynolds numbers near the wall are considerably less than the range over which the hot-wire anemometer was calibrated. Use of the wire in this region would have introduced large uncertainties in interpretation of the hot-wire data.

## SECTION VII

## DATA REDUCTION PROCEDURE

### 7.1 INPUT DATA

Calculation of mean flow properties were carried out at each Y position for which a measurement of the pitot pressure was made. The input data required for the calculation and the form of the data are listed below.

| INPUT QUANTITY | SYMBOL | FORM OF DATA |
|---|---|---|
| Pitot Pressure | $P_{t2}$ | Tabular, versus Y |
| Measured Total Temperature | $T_m$ | $0 \leq Y \leq 0.80$, Eqn. (7)<br>$Y > 0.80$, Tabular versus same Y as for $P_t$ |
| Measured Static Pressure | $p_{sm}$ | Eqn. (8) |
| Total Temperature Probe Recovery Factor | | Eqn. shown in Figure 9 |
| Static Pressure Probe Viscous Interaction Correction | $P_{sm}/P_{si}$ | Eqn. (9) |

As mentioned earlier, for Y less than 0.80 inches the Y position of the total temperature probe did not coincide with that of the pitot probe. Therefore, for convenience in the calculation $T_m$ was represented by Eqn.(7) for $Y \leq 0.80$. For $Y > 0.80$ inches the Y positions of the two probes were identical and $T_m$ was input to the calculations in tabular form.

### 7.2 MEAN FLOW COMPUTER PROGRAM

Calculation of the mean flow properties was programmed in Fortran for the Honeywell Model 615 Computer System. Since both the measured total temperature and static pressure had to be corrected for probe effects, the program includes iterative routines, for finding the actual value of these parameters. Referring to Figure 18, the pitot pressure and $P_{sm}$ are used to find the Mach number M and the latter two then combined to calculate the local stagnation pressure, $P_o$. The Mach number is also used with the measured total temperature to find the static stream temperature, $T_s$. With the temperatures known the corresponding viscosities are evaluated, and the Reynolds numbers based on the appropriate temperature and the characteristic probe dimension can be calculated. The Reynolds number for the static pressure probe is combined with the Mach number to find the viscous interaction parameter $\chi$ and, by means of Eqn. (9), the first order approximation to the static pressure $P_{si}$. The procedure is then repeated n times until

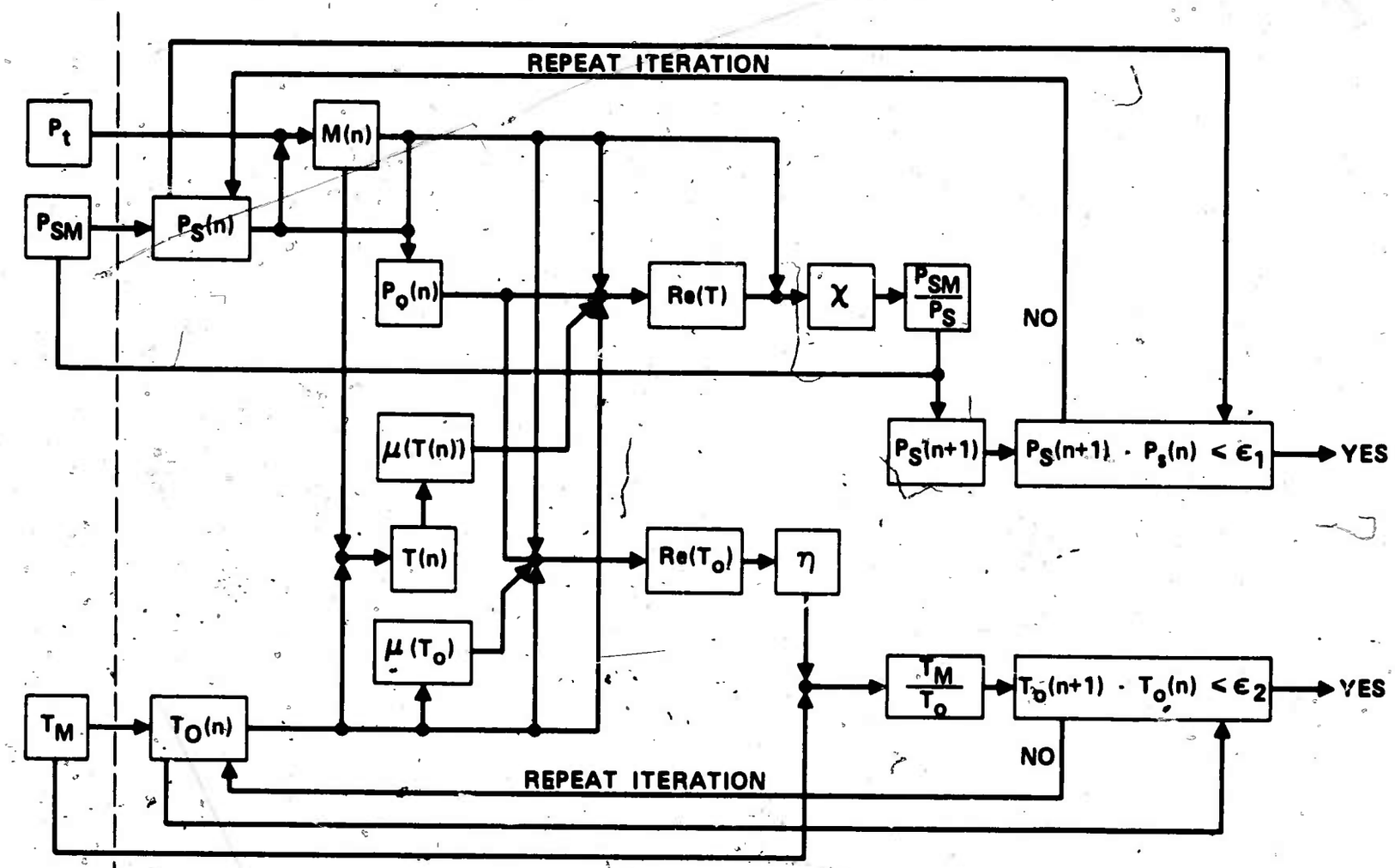


FIGURE 18. FLOW CHART FOR MEAN FLOW COMPUTER PROGRAM

the absolute value of $P_{si}(n + 1) - P_{si}(n)$ satisfies the convergence criteria $\epsilon$. Similarly the total temperature probe recovery factor, $\eta$, is found from the probe Reynolds number, yielding the first order approximation to the local total temperature, $T_o$. This calculation is also repeated until $|T_o(n + 1) - T_o(n)| < \epsilon$. In both cases the convergence parameter $\epsilon$ was 0.1%.

Results of the iterative calculation to determine $P_s$ at Y = 6.016 inches are presented in Figure 19, which indicates that 12 iterations are required to satisfy the desired convergence. Since the viscous correction is greatest near the free-stream, this example is typical of the maximum number of iterations required. Convergence of the total temperature generally occurred more rapidly, although convergence of both parameters was required before continuing the calculation procedure.

Once $T_o$ and $P_{si}$ were determined the remaining boundary layer properties were calculated, i.e., the velocity u, the density $\rho$, etc., using standard formulae for compressible flow. In addition to the local properties, several characteristic boundary layer thicknesses, including the displacement thickness $\delta^*$, and the momentum thickness, $\theta$, were determined from numerical integration across the boundary layer.

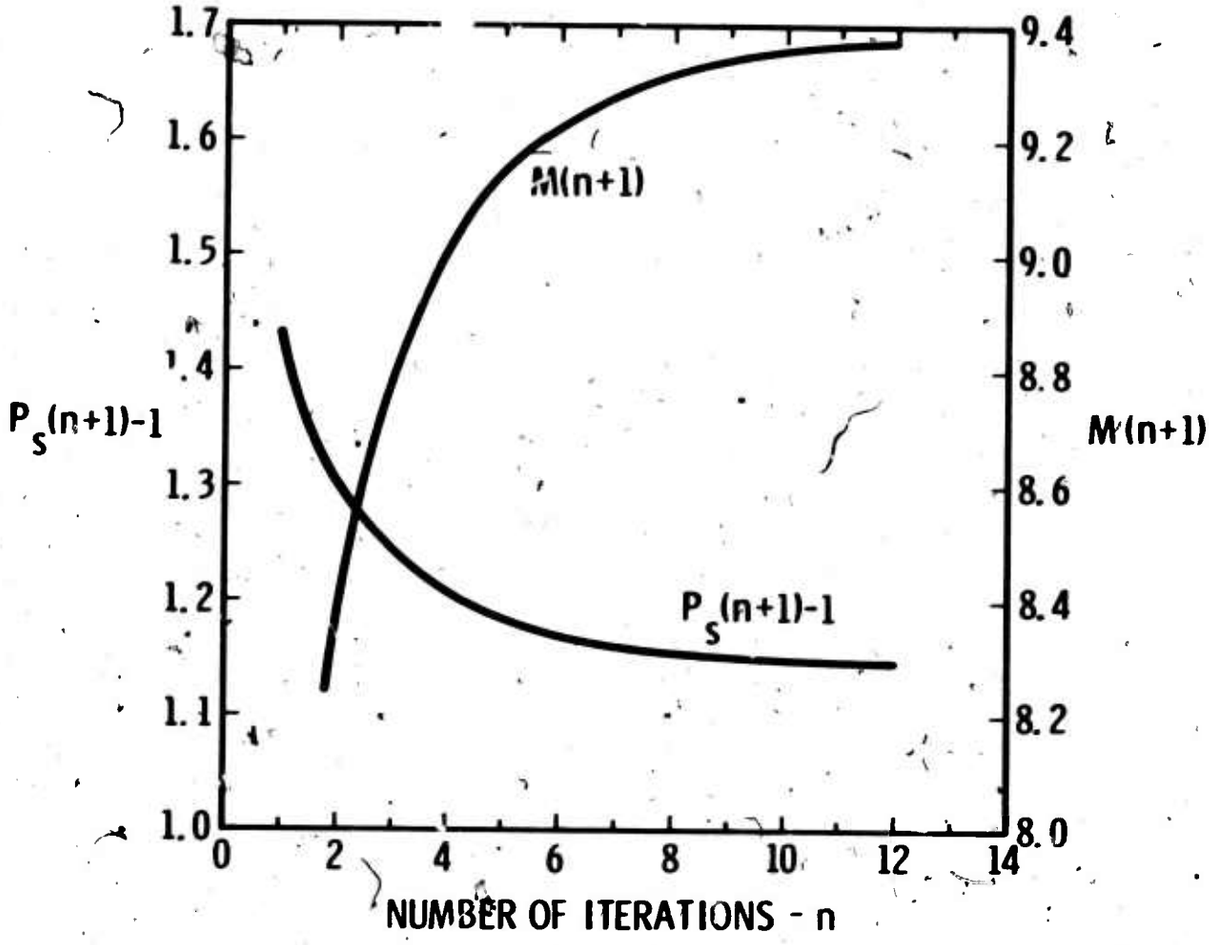


FIGURE 19. EXAMPLE OF CONVERGENCE OF ITERATIVE PROCEDURE FOR MEAN FLOW CALCULATIONS

## SECTION VIII

## RESULTS

The results of the mean flow calculations at $P_o$ = 3200 cm Hg are summarized in Table I which lists the test conditions, the characteristic boundary layers thicknesses described in Paragraph 7.2, and a tabulation of the mean flow profiles. The conventional boundary layer thickness $\delta$, which is defined as the distance from the wall where the velocity is 99% of the free-stream velocity, has been included although in the present case its significance is somewhat vague. This arises from the fact that relatively few data points were obtained for Y > 5.0 inches, thereby precluding a precise determination of the shape of the velocity versus Y curve near the edge of the boundary layer. For this reason Y, rather than Y/$\delta$, has been used in subsequent presentation of the results, even though the results have been nondimensionalized using the values of the flow properties at Y = $\delta$ as reference parameters. It should be pointed out that this represents an arbitrary, although consistent, selection of reference parameters since the velocity and thermal boundary layers are of different extent, with the latter being slightly larger. Furthermore, because of the pressure gradient normal to the wall, the fluid density actually overshoots its free-stream value within the boundary layer.

### 8.1 MEAN FLOW PROFILES

#### 8.1.1 STATIC PRESSURE PROFILE

The calculated static pressure profile is shown in Figure 15. Fiore[9] and Fischer et al[10] have also observed pressure gradients normal to the wall in hypersonic boundary layers, the former at Mach 12 in air and with the Reynolds number based on momentum thickness, $Re_{\theta}$, on the order of 1000 and the latter at Mach 21 in helium with $Re_{\theta} \approx 10{,}000$. In Fiore's case[9] the pressure gradient was smaller than observed here, with the pressure difference equal to 20% of the free-stream pressure, but was still larger than the longitudinal pressure gradient measured in his tunnel and was found to increase with increasing $Re_{\theta}$. In the experiments of Fischer et al[10] the static pressure at the wall was 40% greater than the free stream pressure, similar to our results. Fisher et al[10] also examined the results of a number of other investigators who reported an increase in measured wall pressure over the corresponding free-stream value for several gases and variety of aerodynamic bodies, including cones, wedges, and tunnel walls. They found a consistent trend of increasing wall-to-free-stream static pressure ratio with increasing Mach number which was tentatively attributed to turbulent flow effects.

#### 8.1.2 TEMPERATURE PROFILES

Figure 20 shows the ratios of local stagnation and static temperature to the stagnation temperature at the edge of the boundary layer, $T_{oe}$, (i.e., its value at Y = $\delta$) plotted against Y. The insert in Figure 20 shows the region near the wall plotted to an expanded Y scale. Since temperature

TABLE I

SUMMARY OF RESULTS

| | | | | | |
|---|---|---|---|---|---|
| $P_o$ | 3200 cm Hg | $P_{se}$ | 1.15 mm Hg | $Re_\delta$ | 36,800 |
| $T_{oe}$ | 792°K | $u_e$ | 1225 m/sec | $\delta$ | 6.01 inches |
| $T_w$ | 304°K | $M_e$ | 9.37 | $\delta^*$ | 2.29 inches |
| $T_e$ | 43°K | $Re_e$ | 127,080 | $\theta$ | .29 inches |

| No. | y(inches) | M | $u/u_e$ | $T_o/T_{oe}$ | $T/T_{oe}$ | $\rho/\rho_e$ |
|---|---|---|---|---|---|---|
| 1 | 0.010 | 0.541 | 0.161 | 0.448 | 0.424 | 0.180 |
| 2 | 0.015 | 0.541 | 0.166 | 0.477 | 0.452 | 0.170 |
| 3 | 0.015 | 0.663 | 0.201 | 0.477 | 0.438 | 0.175 |
| 4 | 0.018 | 0.760 | 0.236 | 0.493 | 0.457 | 0.168 |
| 5 | 0.022 | 0.607 | 0.189 | 0.510 | 0.475 | 0.161 |
| 6 | 0.031 | 0.842 | 0.268 | 0.545 | 0.477 | 0.160 |
| 7 | 0.037 | 0.843 | 0.276 | 0.564 | 0.504 | 0.151 |
| 8 | 0.049 | 1.130 | 0.356 | 0.591 | 0.471 | 0.163 |
| 9 | 0.054 | 1.083 | 0.347 | 0.600 | 0.486 | 0.157 |
| 10 | 0.057 | 1.354 | 0.410 | 0.605 | 0.442 | 0.176 |
| 11 | 0.063 | 1.131 | 0.363 | 0.613 | 0.488 | 0.156 |
| 12 | 0.070 | 1.260 | 0.396 | 0.616 | 0.468 | 0.163 |
| 13 | 0.075 | 1.261 | 0.398 | 0.622 | 0.472 | 0.161 |
| 14 | 0.088 | 1.497 | 0.452 | 0.625 | 0.431 | 0.176 |
| 15 | 0.110 | 1.670 | 0.490 | 0.633 | 0.406 | 0.186 |
| 16 | 0.122 | 1.672 | 0.492 | 0.639 | 0.410 | 0.184 |
| 17 | 0.172 | 1.912 | 0.537 | 0.645 | 0.373 | 0.201 |
| 18 | 0.209 | 2.004 | 0.553 | 0.649 | 0.360 | 0.207 |
| 19 | 0.219 | 2.005 | 0.554 | 0.652 | 0.361 | 0.206 |
| 20 | 0.222 | 2.055 | 0.561 | 0.650 | 0.353 | 0.211 |
| 21 | 0.273 | 2.155 | 0.579 | 0.660 | 0.342 | 0.216 |
| 22 | 0.307 | 2.193 | 0.585 | 0.661 | 0.337 | 0.219 |
| 23 | 0.322 | 2.229 | 0.590 | 0.661 | 0.331 | 0.222 |
| 24 | 0.324 | 2.206 | 0.587 | 0.662 | 0.335 | 0.220 |
| 25 | 0.370 | 2.311 | 0.601 | 0.661 | 0.320 | 0.229 |
| 26 | 0.407 | 2.347 | 0.606 | 0.663 | 0.315 | 0.232 |
| 27 | 0.422 | 2.370 | 0.609 | 0.663 | 0.312 | 0.234 |
| 28 | 0.472 | 2.438 | 0.618 | 0.665 | 0.304 | 0.239 |
| 29 | 0.521 | 2.463 | 0.622 | 0.668 | 0.302 | 0.240 |
| 30 | 0.624 | 2.592 | 0.638 | 0.671 | 0.286 | 0.251 |
| 31 | 0.722 | 2.696 | 0.650 | 0.675 | 0.275 | 0.260 |
| 32 | 0.808 | 2.869 | 0.666 | 0.675 | 0.255 | 0.279 |
| 33 | 0.815 | 2.888 | 0.671 | 0.681 | 0.255 | 0.279 |
| 34 | 0.913 | 2.999 | 0.688 | 0.696 | 0.249 | 0.285 |
| 35 | 1.064 | 3.206 | 0.701 | 0.690 | 0.225 | 0.312 |
| 36 | 1.362 | 3.584 | 0.734 | 0.709 | 0.199 | 0.353 |
| 37 | 1.515 | 3.743 | 0.753 | 0.727 | 0.191 | 0.366 |

TABLE I - (Continued)

| No. | y (inches) | M | $u/u_e$ | $T_o/T_{oe}$ | $T/T_{oe}$ | $\rho/\rho_e$ |
|---|---|---|---|---|---|---|
| 38 | 1.662 | 3.975 | 0.765 | 0.729 | 0.175 | 0.398 |
| 39 | 1.962 | 4.348 | 0.792 | 0.751 | 0.157 | 0.444 |
| 40 | 2.056 | 4.459 | 0.797 | 0.752 | 0.151 | 0.462 |
| 41 | 2.114 | 4.587 | 0.811 | 0.769 | 0.148 | 0.471 |
| 42 | 2.268 | 4.882 | 0.823 | 0.776 | 0.134 | 0.516 |
| 43 | 2.562 | 5.353 | 0.848 | 0.799 | 0.119 | 0.581 |
| 44 | 2.712 | 5.672 | 0.863 | 0.815 | 0.110 | 0.625 |
| 45 | 2.761 | 5.728 | 0.860 | 0.807 | 0.107 | 0.643 |
| 46 | 2.864 | 6.000 | 0.874 | 0.823 | 0.100 | 0.677 |
| 47 | 3.012 | 6.267 | 0.884 | 0.834 | 0.094 | 0.716 |
| 48 | 3.116 | 6.731 | 0.898 | 0.847 | 0.084 | 0.785 |
| 49 | 3.308 | 6.939 | 0.904 | 0.853 | 0.080 | 0.820 |
| 50 | 3.311 | 6.901 | 0.909 | 0.863 | 0.082 | 0.802 |
| 51 | 3.508 | 7.431 | 0.920 | 0.874 | 0.073 | 0.883 |
| 52 | 3.612 | 7.755 | 0.927 | 0.881 | 0.068 | 0.929 |
| 53 | 3.708 | 7.854 | 0.929 | 0.882 | 0.066 | 0.948 |
| 54 | 3.712 | 7.974 | 0.934 | 0.891 | 0.065 | 0.954 |
| 55 | 3.811 | 8.226 | 0.939 | 0.896 | 0.062 | 0.988 |
| 56 | 3.910 | 8.277 | 0.942 | 0.902 | 0.061 | 0.992 |
| 57 | 3.911 | 8.477 | 0.943 | 0.901 | 0.059 | 1.023 |
| 58 | 4.013 | 8.576 | 0.948 | 0.908 | 0.058 | 1.029 |
| 59 | 4.015 | 8.591 | 0.951 | 0.915 | 0.058 | 1.020 |
| 60 | 4.107 | 8.567 | 0.946 | 0.904 | 0.058 | 1.038 |
| 61 | 4.114 | 8.746 | 0.952 | 0.914 | 0.056 | 1.046 |
| 62 | 4.215 | 8.833 | 0.958 | 0.923 | 0.056 | 1.046 |
| 63 | 4.309 | 8.800 | 0.957 | 0.923 | 0.056 | 1.045 |
| 64 | 4.319 | 8.903 | 0.960 | 0.927 | 0.055 | 1.053 |
| 65 | 4.416 | 8.993 | 0.964 | 0.933 | 0.054 | 1.056 |
| 66 | 4.509 | 8.922 | 0.964 | 0.935 | 0.055 | 1.048 |
| 67 | 4.510 | 9.008 | 0.964 | 0.933 | 0.054 | 1.061 |
| 68 | 4.812 | 9.157 | 0.976 | 0.954 | 0.054 | 1.050 |
| 69 | 5.111 | 9.202 | 0.984 | 0.970 | 0.054 | 1.032 |
| 70 | 5.402 | 9.294 | 0.990 | 0.981 | 0.054 | 1.027 |
| 71 | 6.016 | 9.373 | 1.001 | 1.001 | 0.054 | 0.999 |
| 72 | 7.015 | 9.345 | 1.012 | 1.025 | 0.055 | 0.958 |
| 73 | 8.016 | 9.364 | 1.010 | 1.020 | 0.055 | 0.966 |

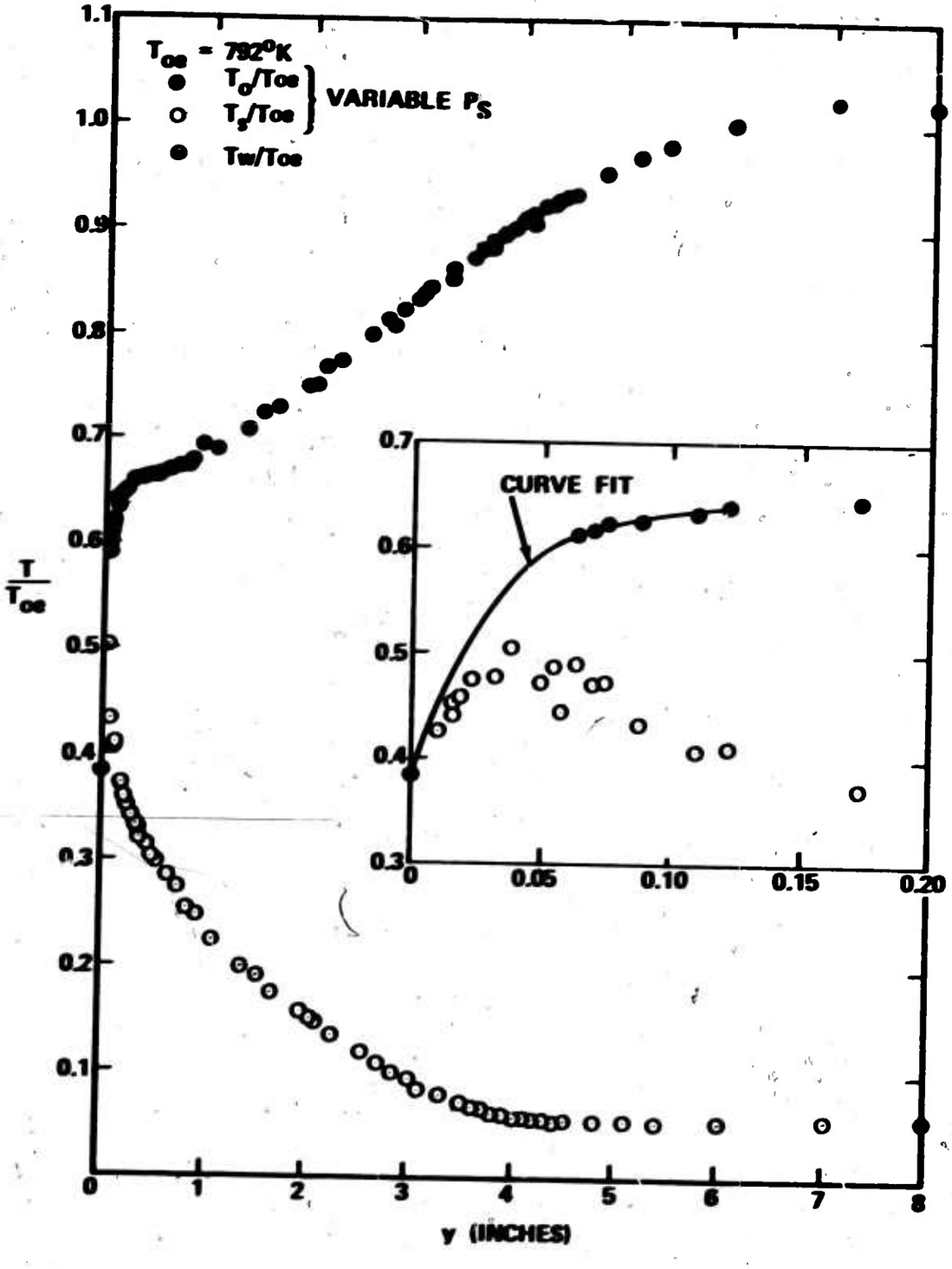


FIGURE 20. NON-DIMENSIONAL TEMPERATURE PROFILES

measurements could not be made for Y < 0.063 inches, the variation of total temperature in this region was determined by fitting a third degree polynominal curve to the data points at Y = 0 (where $T_o/T_{oe} = T_w/T_{oe}$ ) and Y = 0.063 through 0.122. Since the viscous correction to $P_{sm}$ was zero near the wall, $P_{si}$ could be determined from Eqn. (8) and the remaining flow properties evaluated explicitly. The resulting $T_s/T_{oe}$ profile shows the anticipated static temperature overshoot and indicates that the maximum static temperature occurs at Y ≈ 0.04 inches where it exceeds the wall temperature by approximately 80°K.

### 8.1.3 MACH NUMBER PROFILE

The Mach number profile is shown in Figure 21 which indicates a gradual decrease in Mach number from its free-stream value to M = 9 at Y = 4.5 inches. Between Y = 4.5 and Y = 2.5 inches, the Mach number decreases rapidly in a nearly linear fashion to M = 5, followed by a slower, but again nearly constant rate of decrease to M = 2 at Y = 0.20 inches. The sonic line occurs at approximately 0.05 inches, so that subsonic flow is restricted to a very narrow layer adjacent to the wall.

### 8.1.4 DENSITY PROFILE

The density profile, shown in Figure 22, indicates that at Y = 4.5 inches the density overshoots its free-stream value by 10%. This reflects the fact that as the wall is approached, the static pressure begins to increase over its free-stream value at Y = 6.0 inches, while the static temperature does not increase appreciably until Y = 4.0 inches. The minimum density corresponds to the static temperature overshoot and is about 25% less than its value at the wall.

### 8.1.5 VELOCITY PROFILE

The velocity profile is presented in Figure 23 which shows that over one-half the velocity change across the boundary layer occurs in the immediate neighborhood of the wall, i.e., $u/u_e$ decreases from 0.55 to zero between Y = 0.2 inches and Y = 0. This region has been plotted with an enlarged Y scale in the insert in Figure 23, where it is noted that there is no evidence of the linear variation of velocity generally attributed to the viscous sub-layer. This subject is discussed further in Section IX.

## 8.2 COMPARISON WITH HOT-WIRE DATA

The availability of the hot-wire data provides a means for partially checking the mean flow measurements. At any point in the boundary layer, the recovery temperature, $T_{aw}$, of the wire and the Nusselt number can be determined from the overheat traverse made during the turbulence measurements and, using the $Nu_o$ versus $Re_o$ calibration data shown in Figure 8, $Re_o$ can be found. Then, with $Re_o$ and $T_{aw}$ known, $T_t$ can be found from Figure 9 and the total temperature evaluated. The calculation procedure is described in Appendix A.

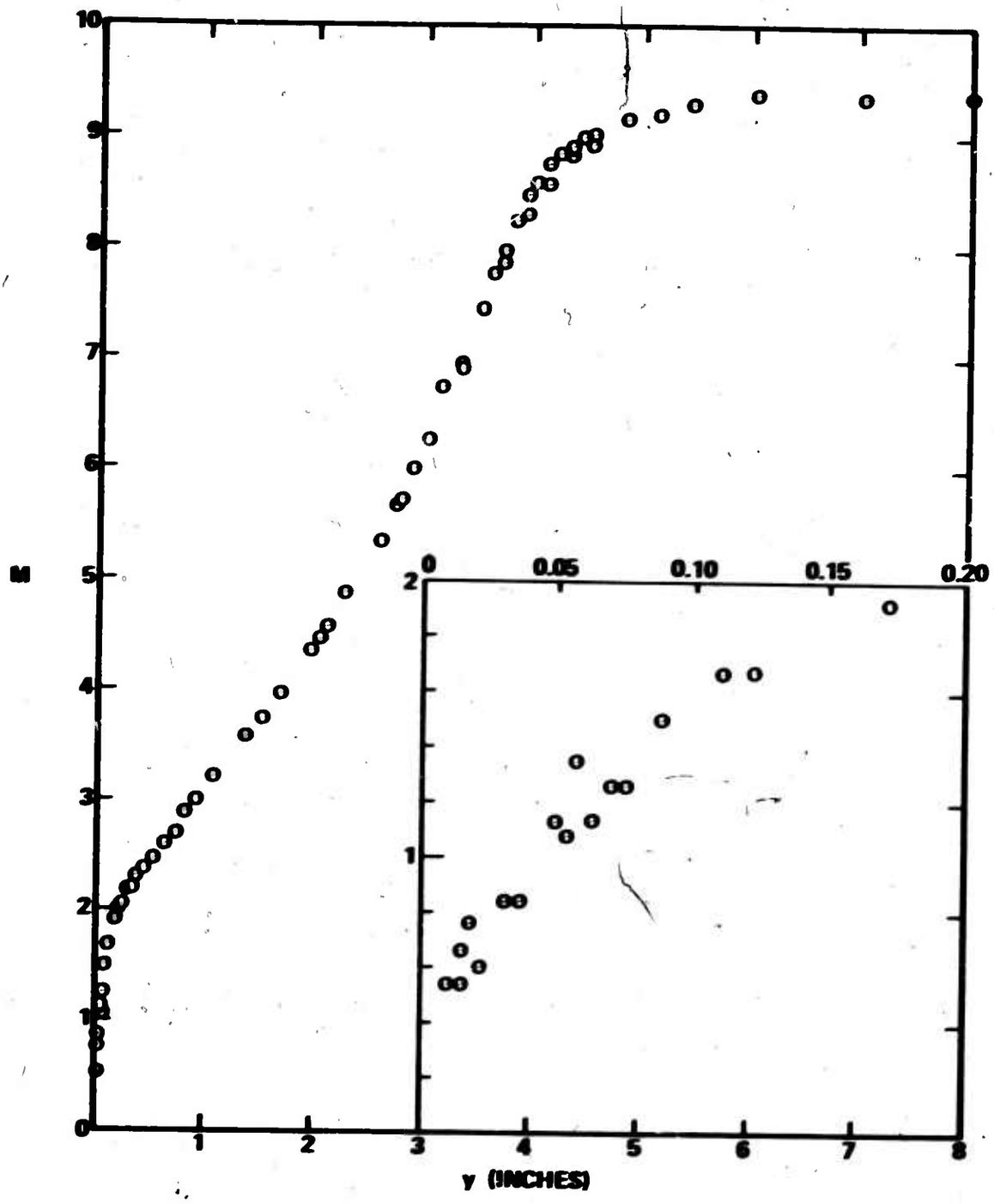


FIGURE 21. MACH NUMBER PROFILE

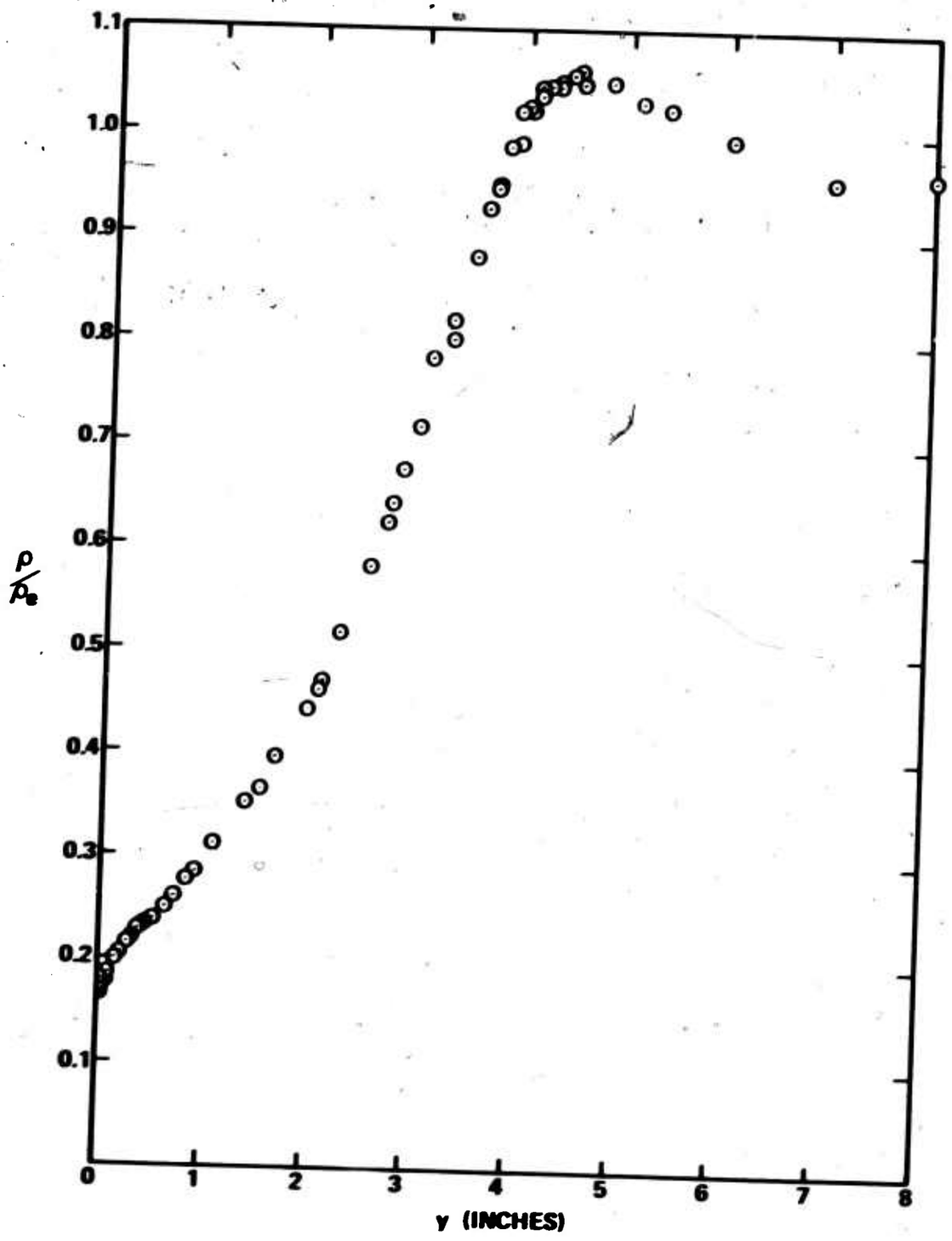


FIGURE 22. NON-DIMENSIONAL DENSITY PROFILE

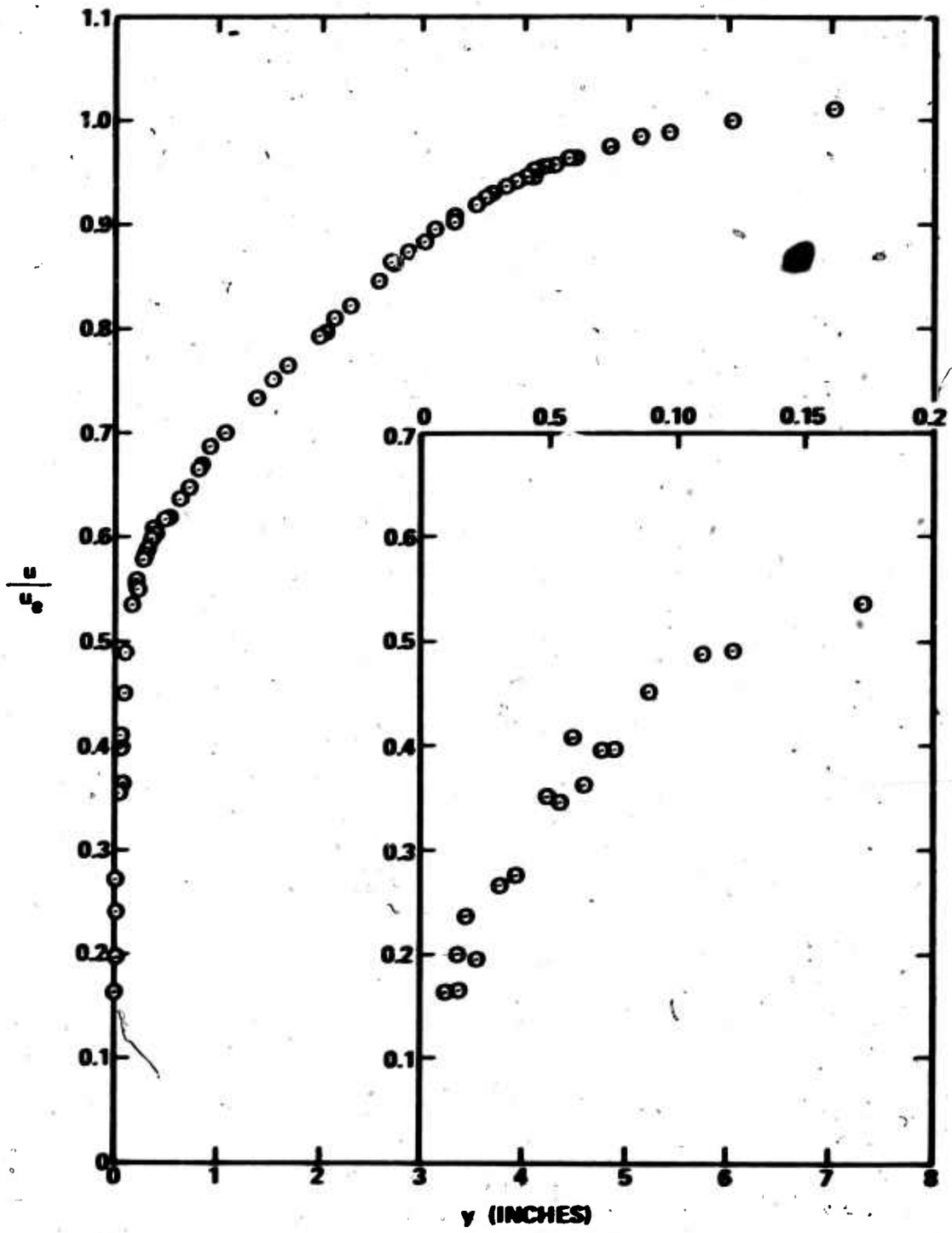


FIGURE 23. NON-DIMENSIONAL VELOCITY PROFILE

Figure 24 shows a comparison of $T_o$ profiles obtained from the hot-wire and thermocouple measurements. For wire A13-1, the agreement between the two measurements is excellent, with the hot-wire results generally no more than 5-10°C below the thermocouple data. A larger discrepancy is observed for wire 6-3, although the agreement with the thermocouple results is still encouraging. In this case, the hot wire results are about 20°C higher than those obtained from the thermocouple measurements in the outer half of the boundary layer, with the discrepancy increasing to 50°C between Y = 1 and 2 inches, then gradually diminishing as the wall is approached.

Figure 25 presents a comparison of the profiles of the unit Reynolds number per inch based on stagnation temperature, $Re_o'$. Although the shape of the curves are similar, $Re_o'$ obtained with wire A13-1 exceed those deduced from the mean flow measurements near the wall, while in the outer half of the boundary layer the converse is true. In spite of the large differences between the two results, which reach a maximum of 50%, the agreement is again encouraging. This arises from the fact that small errors in $Nu_o$ lead to errors in $Re_o'$ which are 2 to 3 times larger. This is indicated in Figure 8 which shows also the typical scatter to be expected in the determination of $Nu_o$.

The $Re_o'$ profile obtained with wire 6-3 shows much larger deviations from that deduced from the mean flow measurements, with differences as large as a factor of ten observed near the wall. This prompted a re-examination of the $Nu_o$ and $\eta$ versus $Re_o$ calibrations from which it was concluded that the data points at $Re_o$ = 0.026 and 0.11 (see Figure 8) may be in error. Consequently, new correlations were curve fit to the remaining five data points and the hot-wire data reduction was repeated. The resulting $Re_o'$ profile, Figure 25 shows much better agreement with the results obtained from both the mean flow measurements and wire A13-1. In addition, the $T_o$ profile obtained with the modified hot-wire calibration curves, presented in Figure 17, indicates slightly better agreement with the thermocouple measurements, particularly near the wall and in the region from Y = 1 to 2 inches where the difference between the two sets of results is reduced from 50 to 30-40°C.

## 8.3 TEST RESULTS AT $P_o$ = 1700 CM HG

The calculated static pressure profile is shown in Figure 17 where it can be compared to the measurements. The pressure variation is similar to that observed at $P_o$ = 3200 cm Hg although, because of the reduced Reynolds number, the viscous corrections at the outer edge of the boundary layer are slightly larger.

The static and stagnation temperature profiles and the velocity and Mach number profiles are shown in Figures 26 and 27, respectively, where, for comparison, the results at $P_o$ = 3200 cm Hg have been included. Due to the lack of data near the edge of the boundary layer, an accurate calculation of $\delta$ could not be made. However, because of the similarity in the boundary layer profiles and the known equivalence of the free-stream conditions, it was assumed that the values of $u_e$ and $T_{oe}$ at the edge of the boundary layer were identical to those at $P_o$ = 3200 cm Hg and these values were used to

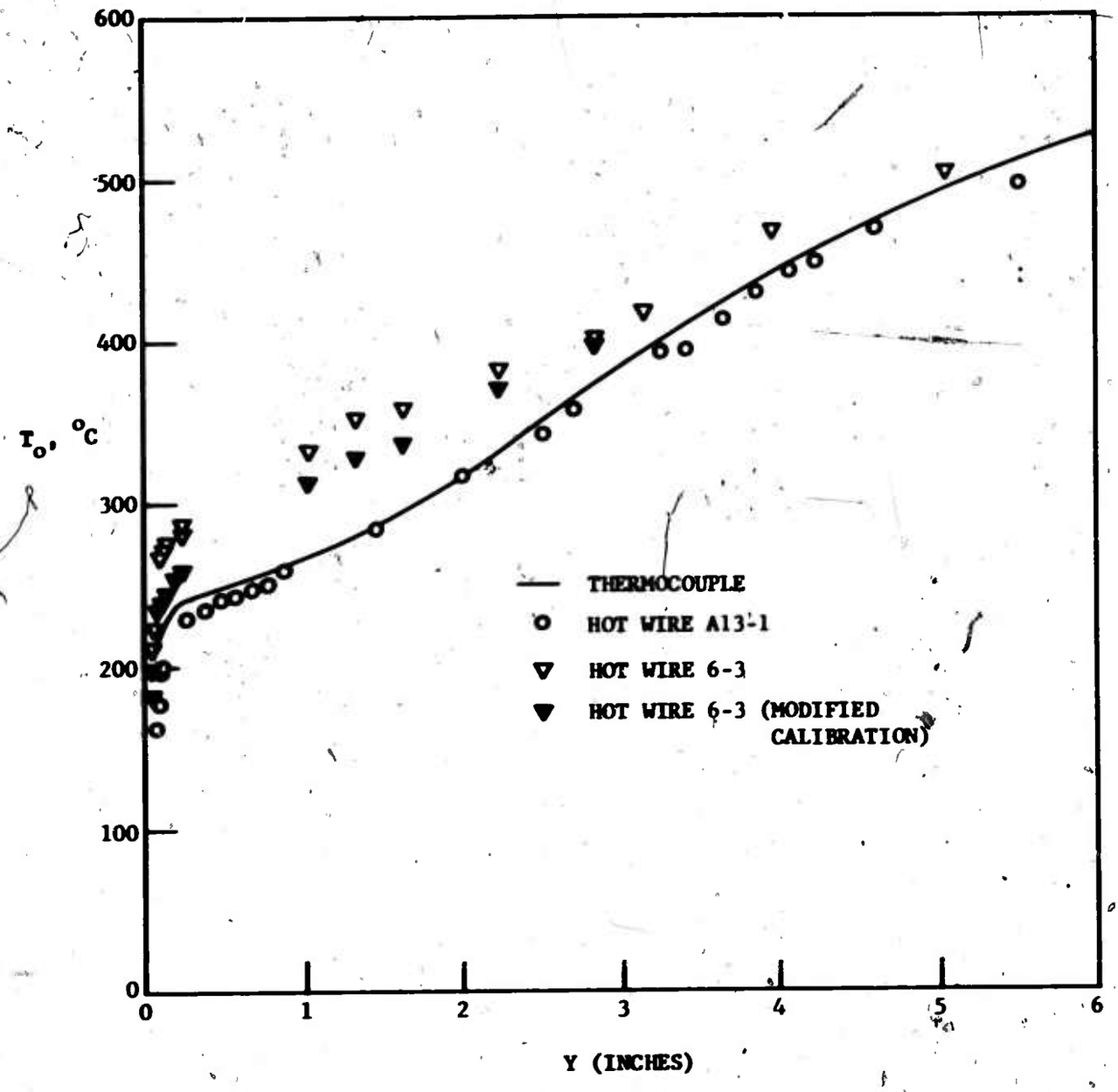


FIGURE 24. TOTAL TEMPERATURE PROFILE SHOWING COMPARISON BETWEEN THERMOCOUPLE AND HOT WIRE MEASUREMENTS

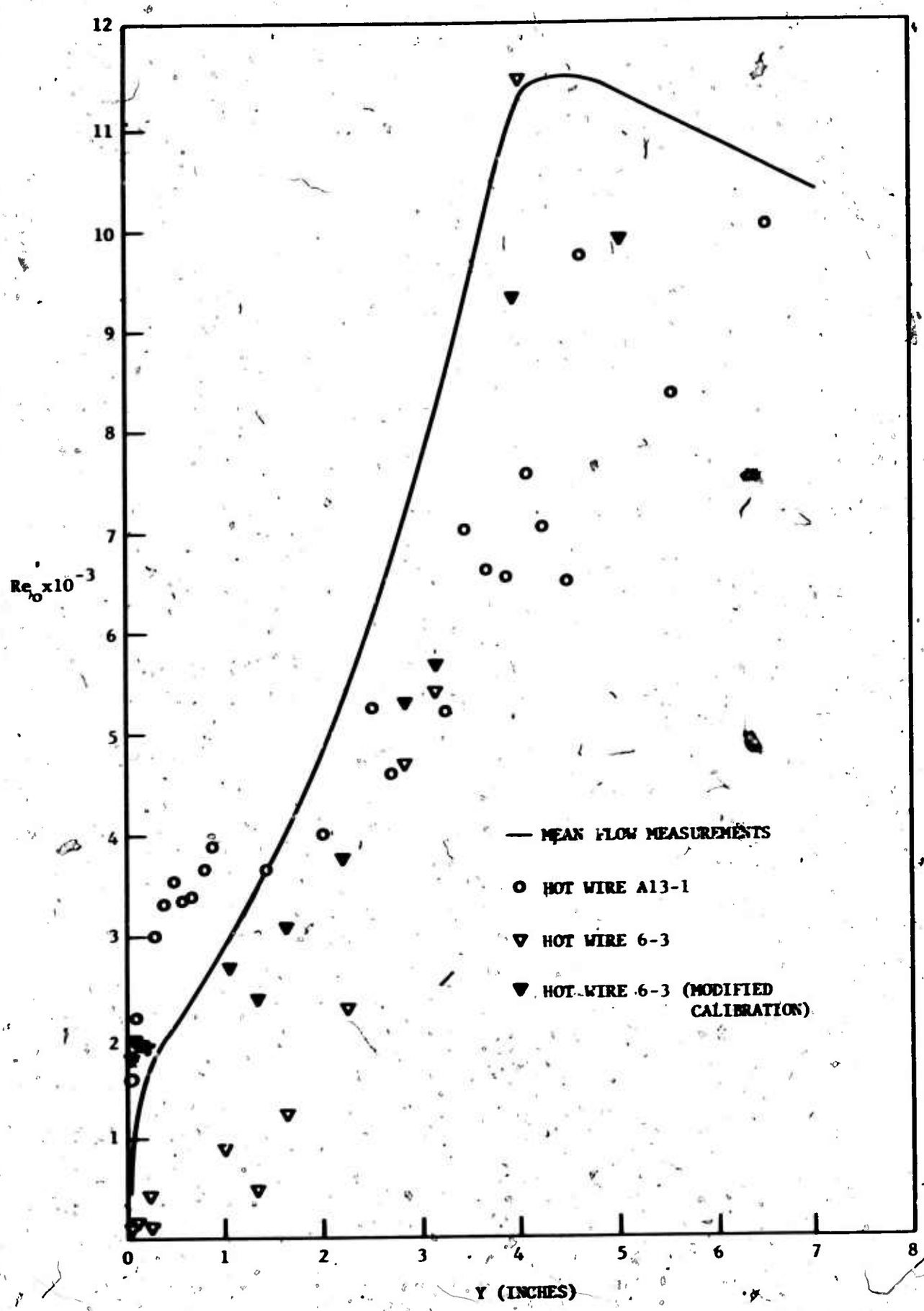


FIGURE 25. UNIT STREAM REYNOLDS NO. PROFILE SHOWING COMPARISON BETWEEN MEAN FLOW AND HOT WIRE MEASUREMENTS

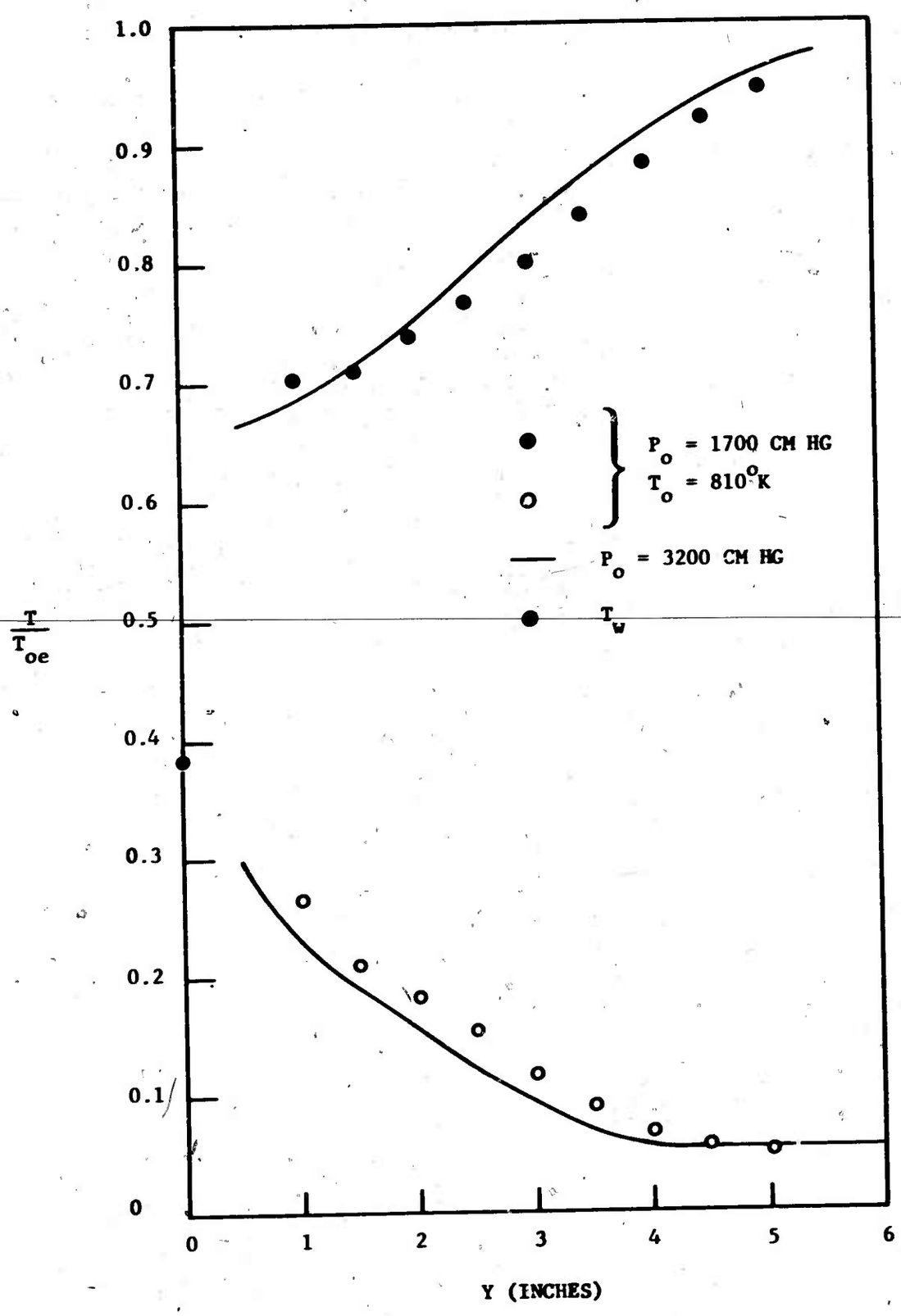


FIGURE 26. NON-DIMENSIONAL TEMPERATURE PROFILES, $P_o$ = 1700 CM HG

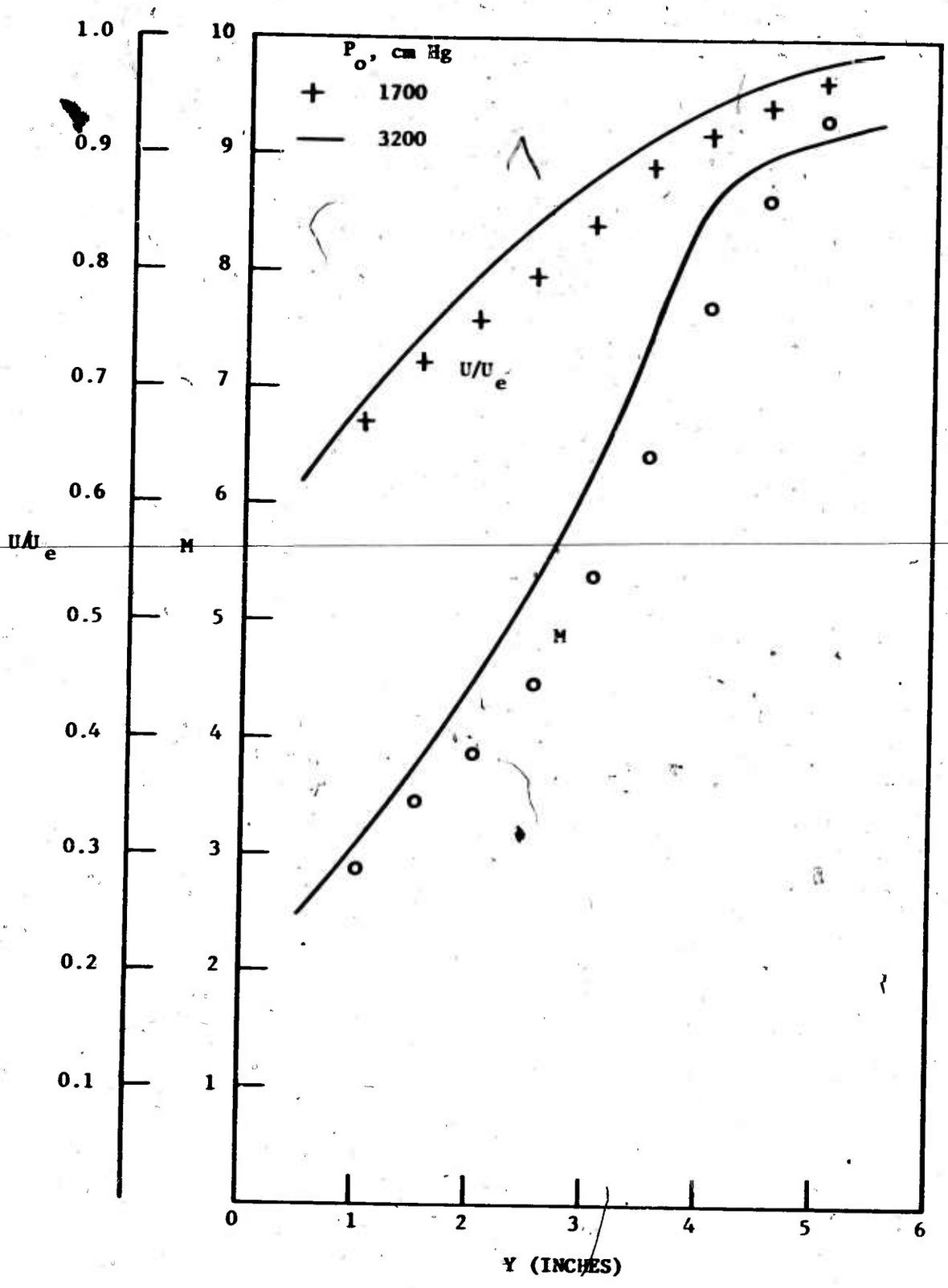


FIGURE 27. MACH NUMBER AND NON-DIMENSIONAL VELOCITY PROFILES, $P_o$ = 1700 CM HG

non-dimensionalize the $P_o$ = 1700 cm Hg data. The resulting non-dimensional profiles are in good agreement with those obtained at the higher pressures and the differences between the two could be reduced by normalizing Y with respect to a characteristic boundary layer thickness.

The lack of data also prevented a precise calculation of $Re_\delta$. To a first approximation, however, this parameter should scale as the ratio of the pressures so that for the $P_o$ = 1700 cm Hg tests, $Re_\delta \approx 20{,}000$.

## SECTION IX

## DISCUSSION OF RESULTS

### 9.1 COMPARISON WITH OTHER EXPERIMENTS

Figure 28 shows the local static temperature ratio within the boundary layer, $T/T_e$, plotted against the local velocity ratio, $u/u_e$. For comparison the Crocco relation

$$T/T_e = T_w/T_e + (1 + (\gamma-1) M_e^2/2 - T_w/T_e)\, u/u_e - (\gamma-1) M_e^2 (u/u_e)^2/2 \quad (10)$$

which is valid for arbitrary heat transfer and zero longitudinal pressure gradient, is included. While there is good agreement between experiment and theory in the sub-layer region, the data lies significantly below the Crocco relation in the outer portion of the boundary layer. This is illustrated more clearly in Figure 29, where the total enthalpy ratio, $\bar{T} = T_o - T_w/T_{oe} - T_w$, is plotted versus $u/u_e$. In these coordinates the Crocco relationship is represented by the linear function $\bar{T} = u/u_e$. Again, in the sub-layer the data agrees with the theory, while in the outer portion of the boundary layer, corresponding to the law-of-the-wake region, the data follows closely the quadratic relation $\bar{T} = (u/u_e)^2$. The interior of the boundary layer - the so-called law-of-the-wall region - is characterized by a well defined transition between the linear and quadratic behavior of the $\bar{T}$ versus $u/u_e$ relationship.

The total enthalpy profile of Figure 29 is typical of that obtained from measurements on nozzle walls. Bertram and Neal[11] and later Bushell et al[12] examined the results of numerous experiments obtained for a variety of operating conditions including Mach numbers varying from 3 to 20, $Re_\infty$ ranging from 1000 to 50,000 and $T_w/T_{oe}$ varying from 0.2 to 1.0. They found that data acquired from flat plate measurements generally followed the linear Crocco relation while the nozzle wall data approximated the quadratic law. The behavior of the nozzle wall data has been attributed by those and other investigators to the effects of the rapid expansion in the wind tunnel nozzle. They suggest that, as a consequence of the flow acceleration near the nozzle throat, the boundary layer profile distorts from the Crocco relationship and remains out of equilibrium with the local edge conditions for considerable distances downstream. For hypersonic nozzles, however, the gradients in the flow properties are concentrated immediately downstream of the throat and it seems unlikely that effects of the past history of the flow would persist for very large distances.* Figure 30 shows a plot of $\bar{T}$ versus $u/u_e$ obtained by the USC/JPL investigators[3] at X = 160 inches from the nozzle throat.* The results at the two stations, which are separated by approximately

* The shift in the transition region from $u/u_e = 0.7$ to $u/u_e = 0.5$ is due primarily to an alternate definition of the total temperature probe recovery factor used by USC/JPL in their data reduction. The data reduction process at both stations was consistent, however, and the conclusions inferred from Figure 30 concerning the streamwise variation in flow profiles and are independent of the probe calibration.

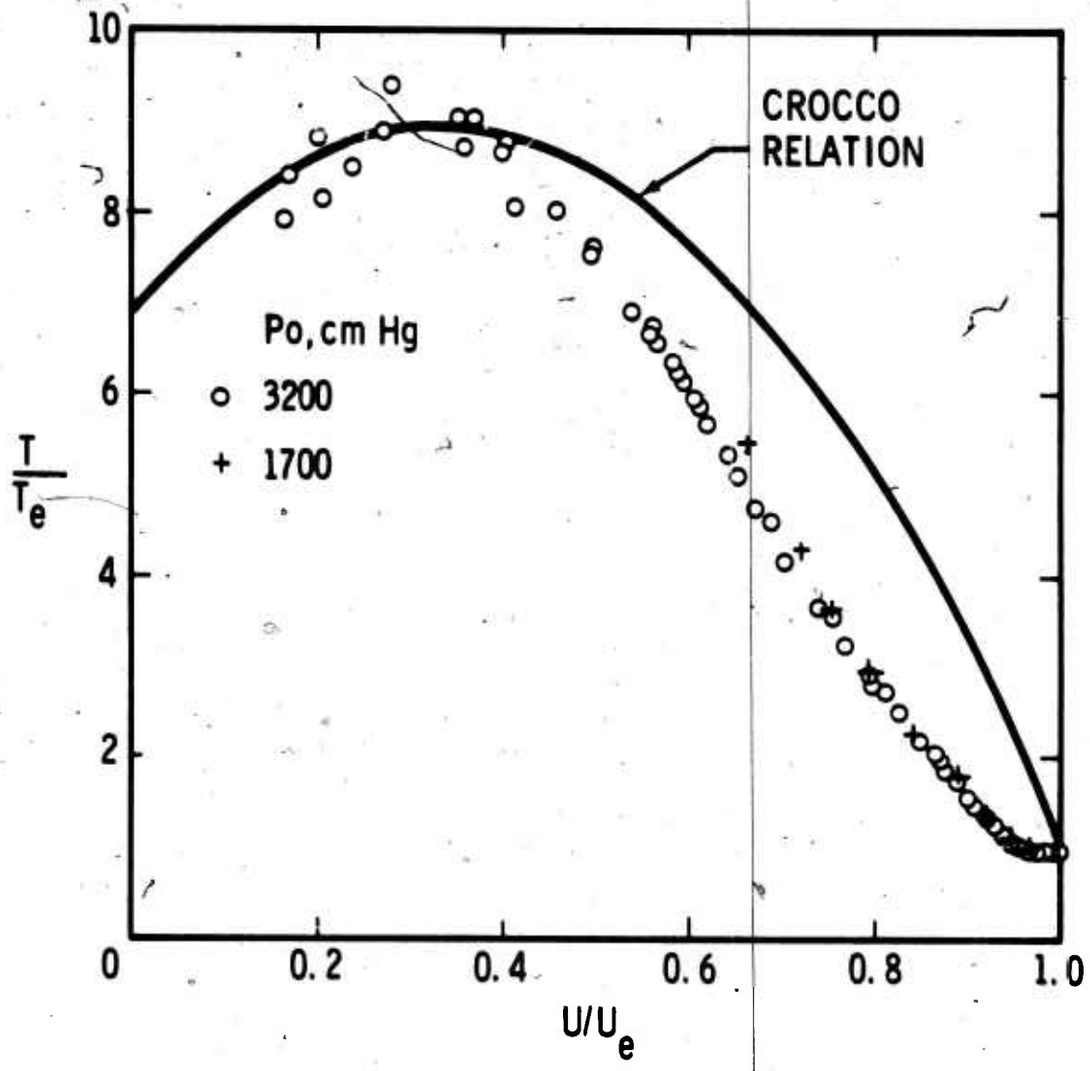


FIGURE 28. NON-DIMENSIONAL STATIC TEMPERATURE - VELOCITY PROFILE

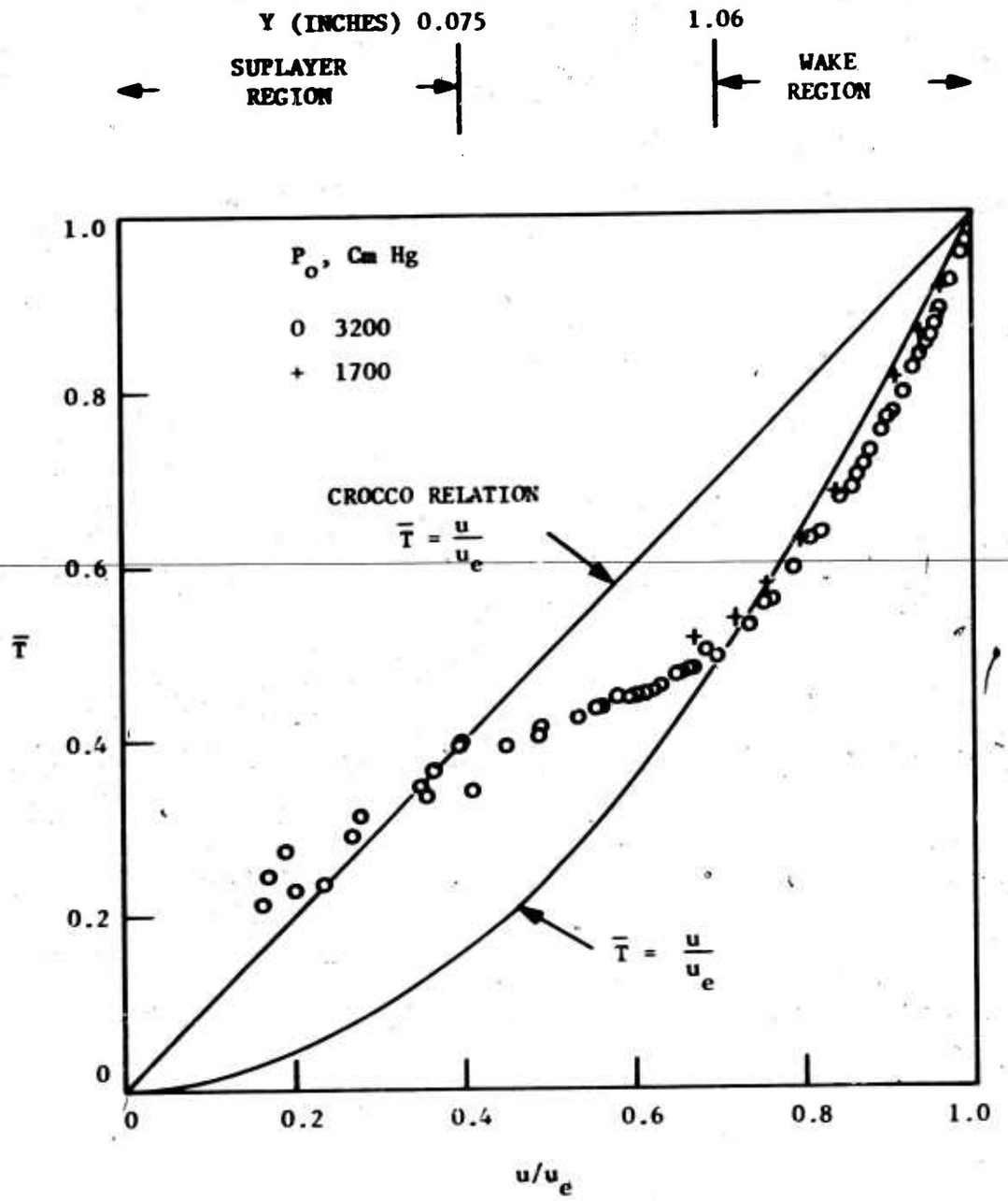


FIGURE 29. NON-DIMENSIONAL TOTAL TEMPERATURE - VELOCITY PROFILE

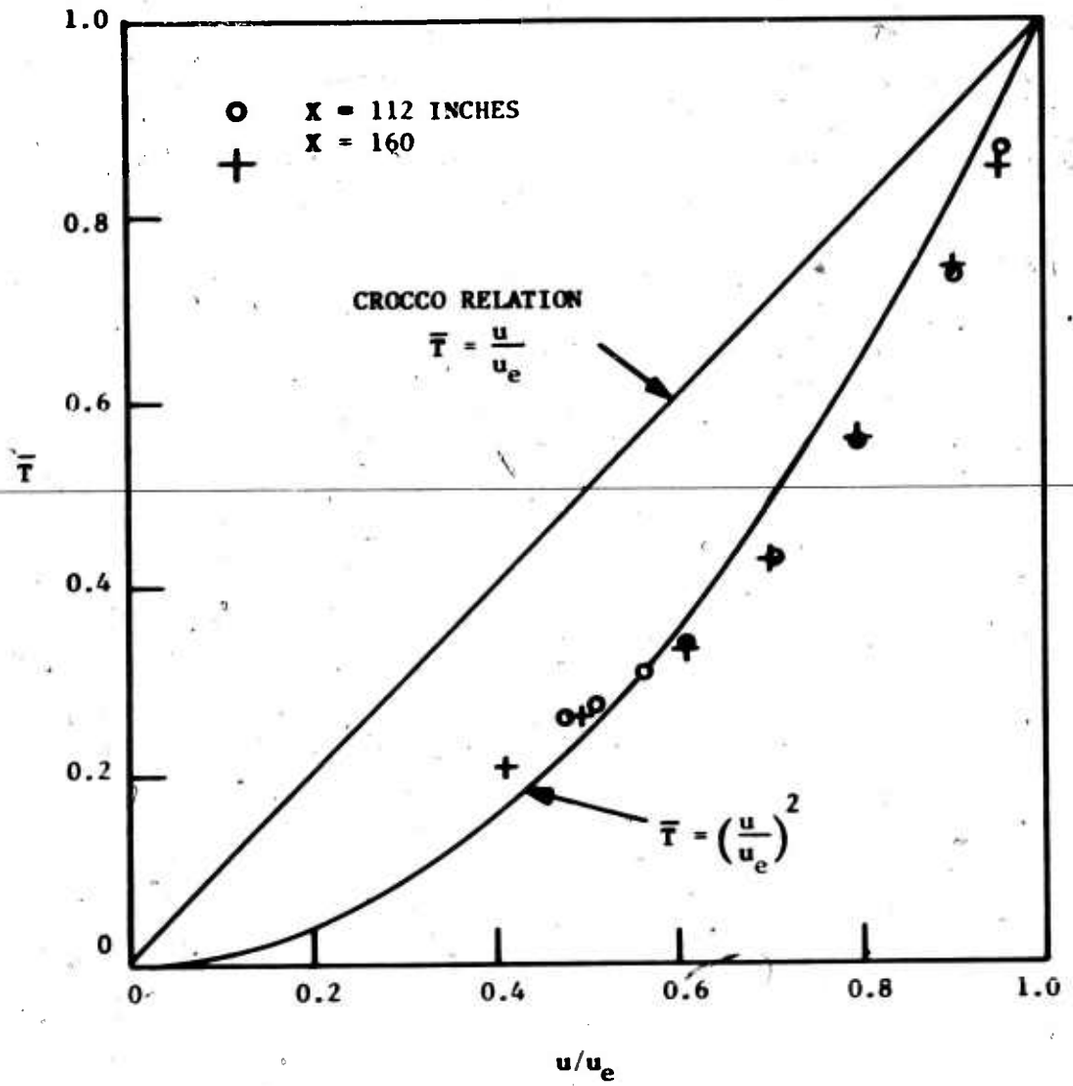


FIGURE 30. NON-DIMENSIONAL TOTAL TEMPERATURE - VELOCITY PROFILE PROVIDED BY USC/JPL[3]

eight boundary layer thicknesses, are identical within the experimental accuracy and show no evidence of relaxation from the quadratic to the linear temperature distribution. The relaxation process was investigated by Bushnell, et al,[12] who performed a numerical experiment to examine the effects of the nozzle acceleration on the boundary layer structure. Using nozzle contours for Mach 6, 8 and 19 wind tunnels for which wall measurements are available, they assumed a Crocco temperature distribution at the throat and solved the boundary layer equations to determine the resulting $\bar{T} - u/u_e$ profiles at downstream stations. Their results indicated a shift from the linear relation toward the quadratic law, particularly near the boundary layer edge, with increasing X and then a return to the linear profile, but showed no evidence of the transition region observed in Figure 29. Furthermore, their calculations predicted a more rapid relaxation to the linear distribution than observed experimentally, although at Mach 6, they found that a distance equivalent to 60 boundary layer thicknesses may be required for relaxation to occur. This may explain the lack of streamwise variation in the total temperature profile indicated in Figure 30.

Several additional comments concerning the results of Figure 29 are in order. First, Fiore's[9] measurements, which were obtained at Mach 12 and $Re_\xi \approx 1000$, show a quadratic temperature distribution in the outer portion of the boundary layer. However, in the sub-layer his results can be expressed in the form $\bar{T} = \alpha(u/u_e)$, where $\alpha \sim 0.7$, and do not indicate the transition region observed in Figure 29. In addition, Fiore's data shows no evidence of the law-of-the-wake component of the boundary layer which, because of the small $Re_\xi$, indicates that his boundary layer may not have been fully developed. Second, the results of Lee, et al,[13] who made nozzle wall measurements at Mach 5 and $Re_\xi$ ranging from 5000 to 50,000 are in accord with the general features of Figure 29. They also observed a transition from the quadratic temperature distribution in the outer portion of the boundary layer to the Crocco relation in the sub-layer. Their results indicated further that at a given station the transition region shifts closer to the wall with increasing heat transfer and $Re_\xi$. While measurements were performed at stations ranging from 48 to 94 inches from the nozzle throat (the inter-station distance is approximately 16 boundary layer thicknesses), again no evidence of streamwise relaxation was apparent.

It is clear from the preceding discussion that the present result is typical of those obtained measurements in wind tunnel wall boundary layers. The observed deviation from the Crocco total temperature distribution implies that the boundary layer is not yet in equilibrium with the local edge conditions. However, the reason for the departure from equilibrium has not yet been resolved.

## 9.2 CORRELATION OF VELOCITY PROFILE

To further demonstrate the validity of the measurements, the resulting velocity profile, Figure 23, was correlated with the "universal" incompressible profile which is conventionally represented in the form:

sub-layer;

$$u^+ = Y^+$$

law-of-the-wall;

$$u^+ = A \ln B Y^+ \qquad (11)$$

law-of-the-wake;

$$u^+ - (u_e/u_\tau) = A \ln (y/\delta) - C [2 - W(y/\delta)]$$

where

$$u^+ = u^*/u_\tau$$

$$Y^+ = Y^* u_\tau/\nu_w$$

$$u_\tau = (\tau_w/\rho_w)^{\frac{1}{2}}$$

and A and B are constants characterizing the velocity profile, C is a constant representing the strength of the wake component of the boundary layer, and W is Cole's[14] tabulated wake function. All of the variables in the above relations refer to the incompressible flow field with which the compressible boundary layer is being compared. The parameters $u^*$ and $Y^*$ denote the compressible flow properties after transformation or "stretching" to account for the density variations within the boundary layer (actually only one of these parameters is transformed; the other retains its physical identity). The friction velocity, $u_\tau$, is found either directly from the slope of the physical velocity profile at the wall, or as a consequence of the correlation procedure when it serves as an "adjustable constant" whose value is manipulated to provide the best fit of the data to the theory.

In the case of a cold wall, Walz[15] and Lee et al[13] caution against using the measured velocity profile to determine $u_\tau$ because of the temperature overshoot which occurs adjacent to the surface. They reasoned that if the shear stress is to remain constant in the sub-layer, then the velocity gradient must compensate for variations in the viscosity arising from the temperature distribution. This would lead to a nonlinear velocity profile near the wall. Since velocity measurements very close to the surface are frequently lacking or unobtainable, the actual velocity profile may be obscured by the missing information. This, in turn, could introduce large errors in determining du/dY.

In this context, Walz examined the cold wall data of Lobb et al[16] and Winkler and Cha[17] who had fit a straight line to their velocity measurements in order to determine the velocity gradient at the wall. Comparing their results to values of du/dY calculated from a similarity law he had developed for evaluating skin friction coefficients, Walz concluded that the experimentally determined slopes were too low, in some cases by as much as 50%. The effect of cooling on the sub-layer velocity profile was investigated further by Lee et al[13] who used the method of Tetervin[18] to calculate the boundary layer structure for Mach 10 and several values of $T_w/T_{aw}$, where subscript aw denotes the adiabatic wall condition. Their results showed that the curved portion of the velocity profile extended closer to the wall as $T_w/T_{aw}$ decreased, although very low wall temperatures are required for the effect to become apparent.

As mentioned in Section 8, the velocity data acquired during the present study shows no evidence of a linear profile, even though measurements were made at Y positions as close as 0.01 inches from the wall. While the results of Walz[15] and Lee et al [13] are hardly conclusive, the static temperature overshoot of the wall represents a possible cause for the distorted velocity profile. Other factors, such as poor resolution of the pitot pressure transducer near the wall and uncertainties in the Y position, were critically assessed, but again with inconclusive results. For example, in spite of the low resolution of the pitot pressure transducer, the pressure measurements were generally consistent for a given run and reproducible within 10% on successive runs. Finally it should be mentioned that the hot-wire measurements showed evidence of intermittent turbulence as close as 0.030 inches from the wall. While the hot-wire data has not yet been analyzed, this could also account for the deviation from linear velocity profile. It was decided, therefore, that the data could be assumed to provide a valid representation of the velocity distribution. However, in view of the uncertainties discussed above, it was considered inadvisable to determine du/dY from the slope of a curve fit to the experimental points.

While the present results preclude a more precise determination, the profiles shown in Figures 20 through 23 indicate that the sublayer is less than 0.10 inches thick or about 1 - 2% of the total boundary layer thickness. This is attributed primarily to the large $Re_\delta$ of the experiment. In this respect it is of interest to note that Fiore[9] reported a sublayer thickness of 15 to 30% at Mach 12 although, as indicated earlier, the $Re_\delta$ of his experiment was 30 - 40 times smaller than that of the present study. Kemp and Owens[19] also reported thick sub-layers, corresponding to as much as 40 - 50% of the total boundary layer thickness, in Helium at Mach numbers from 25 to 40. In addition, their measurements were made within the contoured section of the nozzle and, similar to Fiore's[9] observations, showed no evidence of a wake region in the outer portion of the boundary layer.

Correlation of the velocity profile was carried out using a procedure developed by Maise and McDonald[20] for adiabatic flat plates and extended by Gran[21] to include the cold wall condition. The procedure involves fitting the data to the expression for the law-of-the-wake which, following Coles[22] has been rewritten in the form:

$$u^*/u_\tau = 2.43 \ln (Y u_\tau/\nu_w) + 5.0 + 2.43 \pi W(Y/\delta) \qquad (12)$$

where $u^*$ is the generalized velocity proposed by Van Driest[23] to account for the effects of compressibility and heat transfer, i.e.,

$$u^* = \frac{u_e}{k_1} \arcsin \frac{2k_1^2(u/u_e) - k_2}{(k_2^2 + 4k_1^2)^{\frac{1}{2}}}$$

$$k_1^2 = \frac{[(\gamma-1)/2]\, M_e^2}{T_w/T_e}$$

$$k_2 = \frac{1 + [(\gamma-1)/2]\, M_e^2}{T_w/T_e} - 1$$

It should be pointed out that the Van Driest formulation assumes that the static pressure is constant in the boundary layer and that the Crocco relation, Eqn. (10), is valid, two conditions which are not met in the present experiment. This must be recognized when interpreting the results of the correlation.

Equation (12) includes three unknown constants, $u_\tau$, $\delta$, and $\tilde{\pi}$, a parameter representing the strength of the wake component of the boundary layer. By applying Eqn. (12) at the edge of the boundary layer, $\tilde{\pi}$ can be expressed in terms of $\delta$ and $u_\tau$ and the edge conditions. This reduces the number of unknown constants in Eqn. (12) to two, whose values are adjusted until the data fits the equation such that the rms error is a minimum. Data points for $Y^+ \leq 50$ and $Y > 0.9\,\delta$ are excluded since in the former case the experimental errors are usually large while in the latter case the theory deviates from the data. For convenience in the calculations Cole's wake function W is expressed as

$$W = 2 \sin^2 (\pi Y/2\delta) \qquad (13)$$

After a fit of the data is achieved, $\tilde{\pi}$ and $c_f$, the skin friction coefficient, are determined from $\delta$ and $u_\tau$.

The results of the correlations are shown in Figure 31. The value of $\tilde{\pi}$ was 1.4, slightly more than twice the value of 0.60 normally found in correlating zero pressure gradient flat plate data and typical of flows with strong adverse pressure gradients.[20] On the other hand, the skin friction coefficient was $4.6 \times 10^{-4}$, which is within several percent of the theoretical value determined from the Karman-Schoenherr incompressible formula using the $Re_\delta$ listed in Table I together with the Van Driest transformation functions and following the procedure outlined by Hopkins and Inouye.[24] Since the assumptions of the Van Driest transformation imply a specific density profile, a fictitious $Re_\delta$ can be calculated from the results of the velocity correlation. The $Re_\delta$ found in this manner was 19,100, corresponding to a 10% increase in the theoretical $c_f$, which is approximately one-half of the actual $Re_\delta$ determined from integration of the mean flow properties. This result is not surprising since Wallace[25] found that $Re_\delta$ from a quadratic temperature distribution as measured in his tests was four times larger than $Re_\delta$ from an assumed linear Crocco relation.

The rms deviation of the velocity data from the theoretical curve was 0.8%, which implies a "good fit". However, the generalized velocities for $Y^+ < 50$,

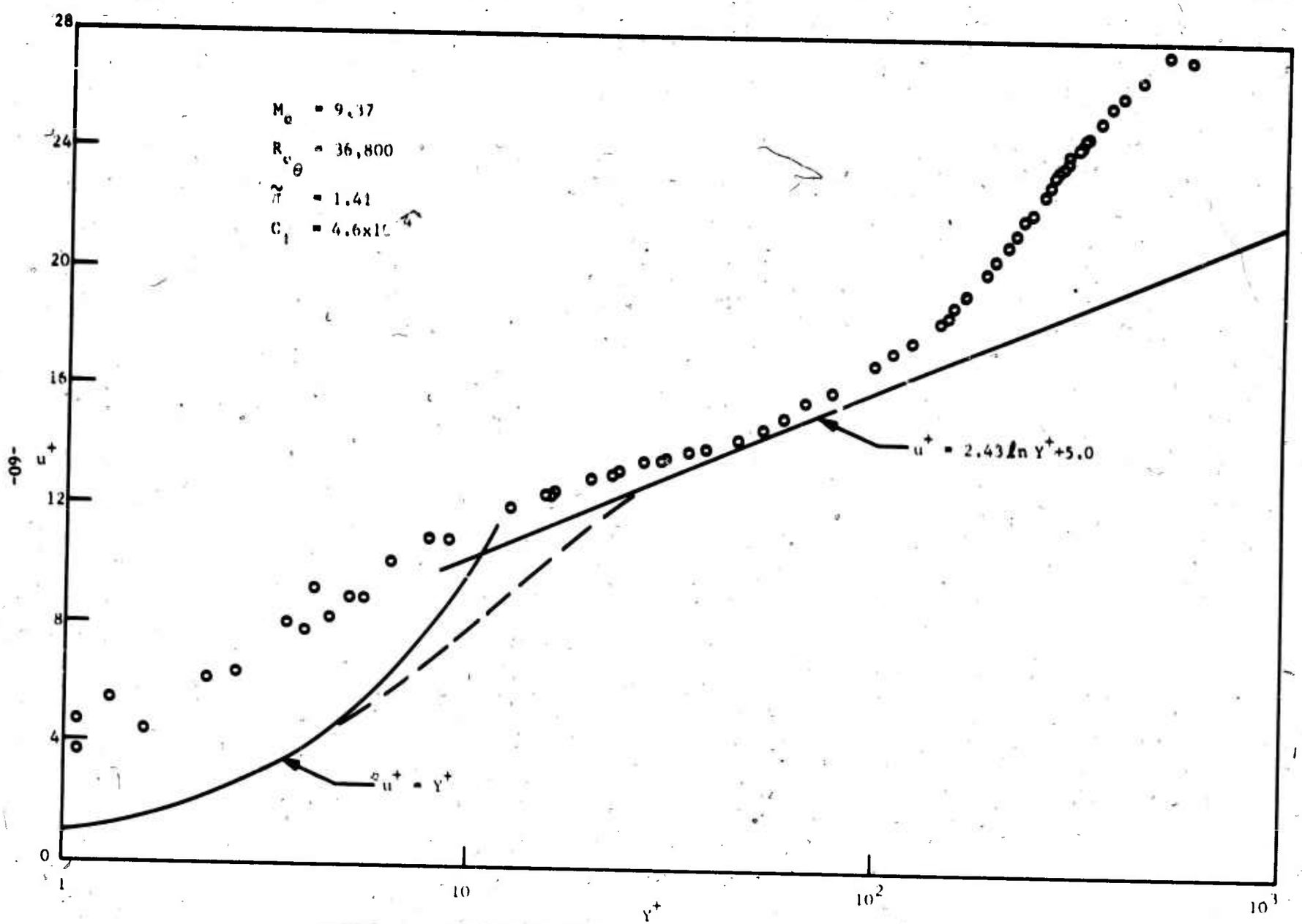


FIGURE 31. CORRELATION OF VELOCITY PROFILE IN LAW-OF-THE-WALL COORDINATES

which were excluded from data fitting process, are considerably larger than the theory reflecting the deviation from a linear profile that had been observed near the wall. While these data points could be collapsed toward the theoretical curve by increasing $u_\tau$, this would lead to a large increase in $c_f$.

In an effort to improve the correlation, the Van Driest formulation was modified by replacing the Crocco relation with the experimental observed quadratic law (the assumption of constant pressure in the boundary layer was retained).[21] The resulting curve fit was very similar to that found previously while the new values characteristic parameters were; $\pi = 1.6$, $c_f = 4.2 \times 10^{-4}$, and $Re_\theta = 27{,}000$. It appears therefore, that the anomalous value of $\pi$ and the low value of the fictitious $Re_\theta$ can be attributed primarily to the strong pressure gradient normal to the wall.

A check of the consistency of the correlation determined with the assumed Crocco relation is shown in Figure 32. While the wake function, W, was assumed to be given by Eqn. (13), W can also be calculated from Eqn. (12) after a fit of the data has been achieved. Figure 32, which shows W determined from both Eqns. (12) and (13) plotted against $Y/\delta$, indicates good agreement and justifies the assumption of Eqn. (12).

Figure 33 shows finally a plot of the velocity defect $(u_e^* - u^*)/u_\tau$ versus distance from the wall $Y/\delta$ and illustrates the effect of the wake strength parameter $\tilde{\pi}$. The correlation equation

$$(u_e^* - u^*)/u_\tau = -2.5 \ln (Y/\delta) + 1.25(2 - W) \qquad (14)$$

which is essentially Eqn. (13) written in defect form with $\tilde{\pi}$ set equal to 0.6, was shown by Maise and McDonald[20] to represent the incompressible measured profiles presented by Clauser.[26] The agreement between Eqn. (14) and the measured velocity profile, for which $\pi = 1.4$, is quite poor, although it illustrates the lack of correlation that Maise and McDonald[20] found for non-adiabatic boundary layers.

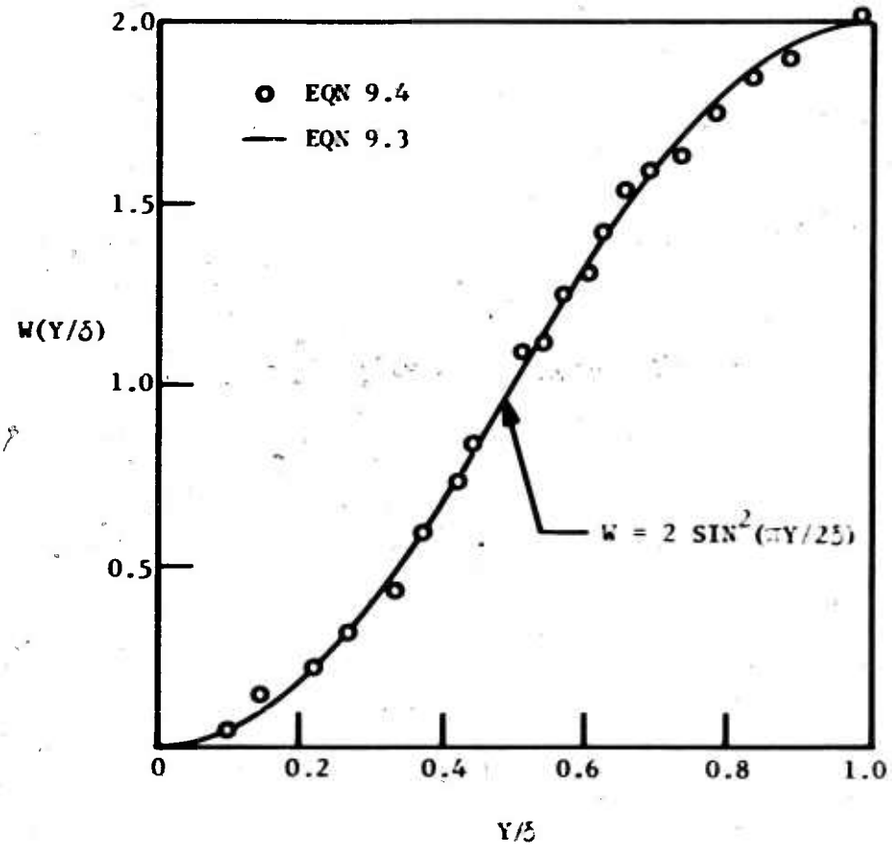


FIGURE 32. COMPARSION OF COMPUTED WAKE FUNCTION, W, WITH ASSUMED VARIATION, EQN (13)

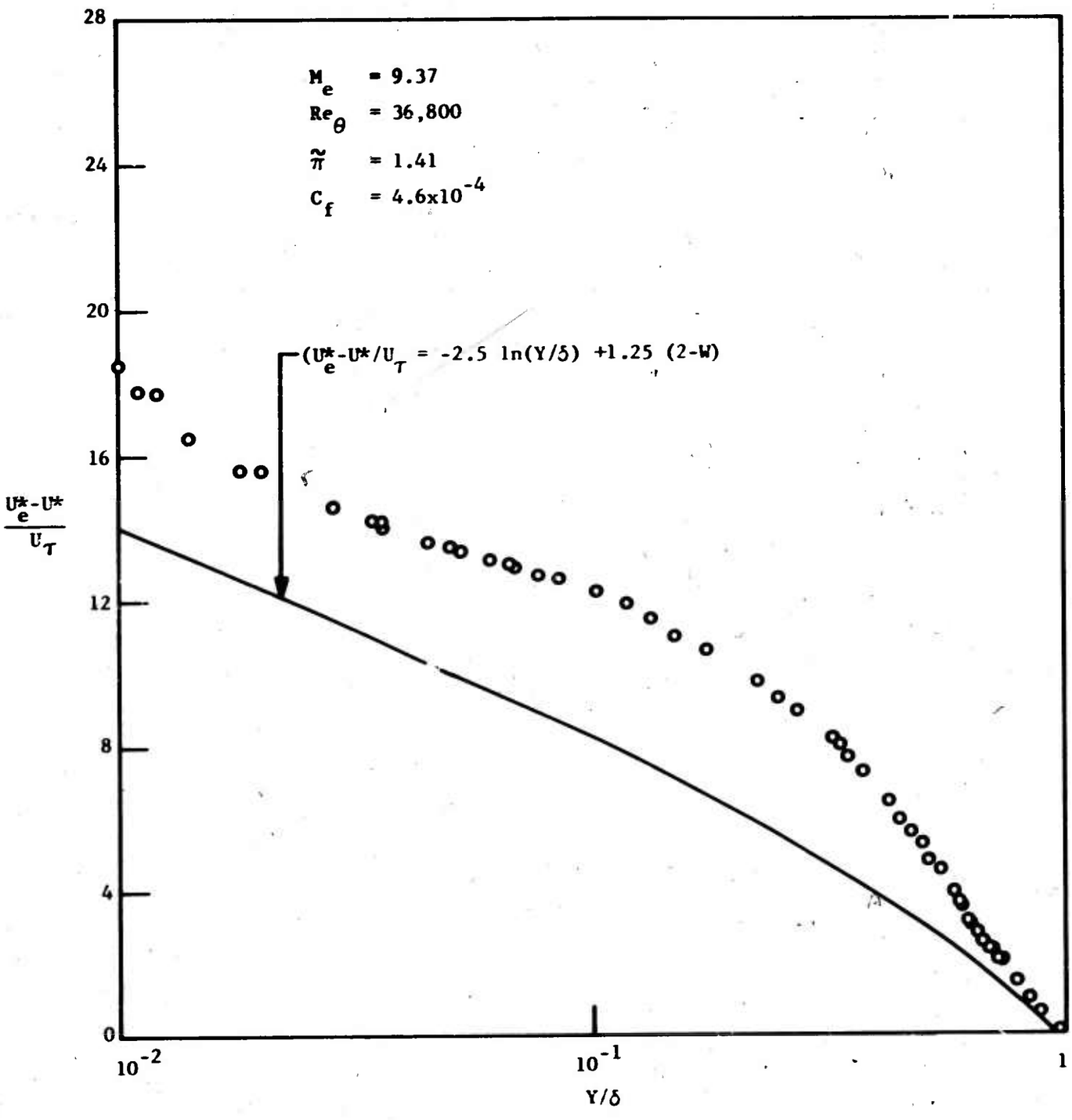


FIGURE 33. CORRELATION OF VELOCITY PROFILE WITH VELOCITY DEFECT LAW

## SECTION X

## SUMMARY AND CONCLUSIONS

The following conclusions can be drawn concerning the measurement of mean flow properties in the hypersonic turbulent boundary layer experiments reported here:

(1) The results of detailed pitot pressure, total temperature, and static pressure surveys carried out at Mach 9.37 in the JPL/HWT demonstrated the two-dimensional, nearly fully developed nature of the ceiling boundary layer. However, the static pressure measurements, which indicated negligible pressure variation in the streamwise direction, also indicated the presence of a significant pressure gradient normal to the wall. Because of the magnitude of the pressure difference, which was approximately 50% of the free-stream pressure, the pressure variation through the boundary layer was taken into account in the reduction of the data. Normal pressure gradients have been observed previously in hypersonic turbulent boundary layers on wind tunnel walls as well as on cones, wedges, and flat plates and, in fact, have been shown to increase with increasing Mach number. Such gradients, however, are frequently ignored either for lack of precise measurements or on the basis that the other flow properties are relatively insensitive to pressure variations. Since the observed pressure gradient may represent a turbulent flow effect which is enhanced at hypersonic speeds, it is clear that further investigation is essential for accurate interpretation of hypersonic boundary layer measurements as well as for the development of improved turbulent boundary layer theories.

(2) The profile of total temperature ratio versus velocity was found to agree with the Crocco theory in the sub-layer region, but followed a quadratic relation between stagnation temperature and velocity in the outer portion of the boundary layer. The quadratic law has been observed to characterize nozzle wall measurements and has been attributed by other investigators to reflect the consequences of the nozzle expansion. Since flat plate data generally agree with the Crocco theory throughout the boundary layer, it has been suggested that the profiles measured on nozzle walls will relax to the Crocco relation at distances far downstream from the throat. It appears, therefore, that the boundary layer in the JPL/HWT is not completely equilibrated in the sense that the observed temperature-velocity variation deviates from what is considered typical of flat plate flows.

(3) Using the Van Driest generalized velocity, the velocity data was correlated to the incompressible law-of-the wake with a rms error of less than 1%. While this implies that the measurements agree with the general form of the incompressible

profile, the strength of the wake component was twice as great as that usually found for flat plate boundary layers. This has been attributed primarily to the effects of the pressure gradient normal to the wall since modification of the correlation procedure to account for the observed quadratic temperature distribution produced essentially the same results. In spite of this anomaly the experimental skin friction coefficient agreed with the theoretical value within several percent.

(4) Although the mean flow measurements extended to 0.010 inches from the wall, no indication of a linear variation of velocity in the sub-layer was found. Possible causes, including the effects of heat transfer, turbulence and instrument errors, were examined without conclusive results. The measurements indicate that the sub-layer is only 0.05 to 0.10 inches thick, which represents 1 to 2% of the total boundary layer thickness. The relatively thin sub-layer has been attributed primarily to the high Reynolds number, $Re_\delta$, of the present study. The sonic line was found to occur at Y = 0.05 inches so that up to 50% of the outer portion of the sub-layer is supersonic.

(5) The stagnation temperature profile calculated from hot-wire anemometer data is in good agreement with that deduced from the mean flow thermocouple measurements. A comparison of the unit stream Reynolds number obtained from the hot-wire and mean flow measurements showed the same trend, but differences as large as 50% were observed. The latter result is not unexpected, however, since it is well known that the hot-wire provides a relatively insensitive measure of Reynolds number.

## APPENDIX A

## CALCULATION OF MEAN FLOW PROPERTIES FROM HOT-WIRE DATA

The procedure for calculating properties of the mean flow in the boundary layer from the hot-wire data was programmed in Basic Language for the Honeywell Model 615 Computer System in time-sharing mode of operation as shown in the flow chart of Figure 34. For eight values of hot-wire current, i, the corresponding resistance was determined from the measured mean voltage across the wire. The method of least squares was used then to provide a linear fit of R versus $i^2$ from which the slope $\partial R/\partial i^2$ and $T_{aw}$ could be found. Using the latter to initially evaluate the thermal conductivity of the fluid, one can obtain the zeroth approximation to $Nu_o$ from Eqn. (6). From $Nu_o$ and the calibration curve $Re_o$ versus $Nu_o$, the zeroth approximation to $Re_o$ is obtained. The calibration curve of $T_r$ versus $Re_o$ is used then to determine the recovery factor which, together with $T_{aw}$, yields the zeroth approximation to the stagnation temperature $T_o$. This, in turn, supplies an improved value of thermal conductivity and the procedure is repeated until the successive approximations to the stagnation temperature converge to the desired accuracy.

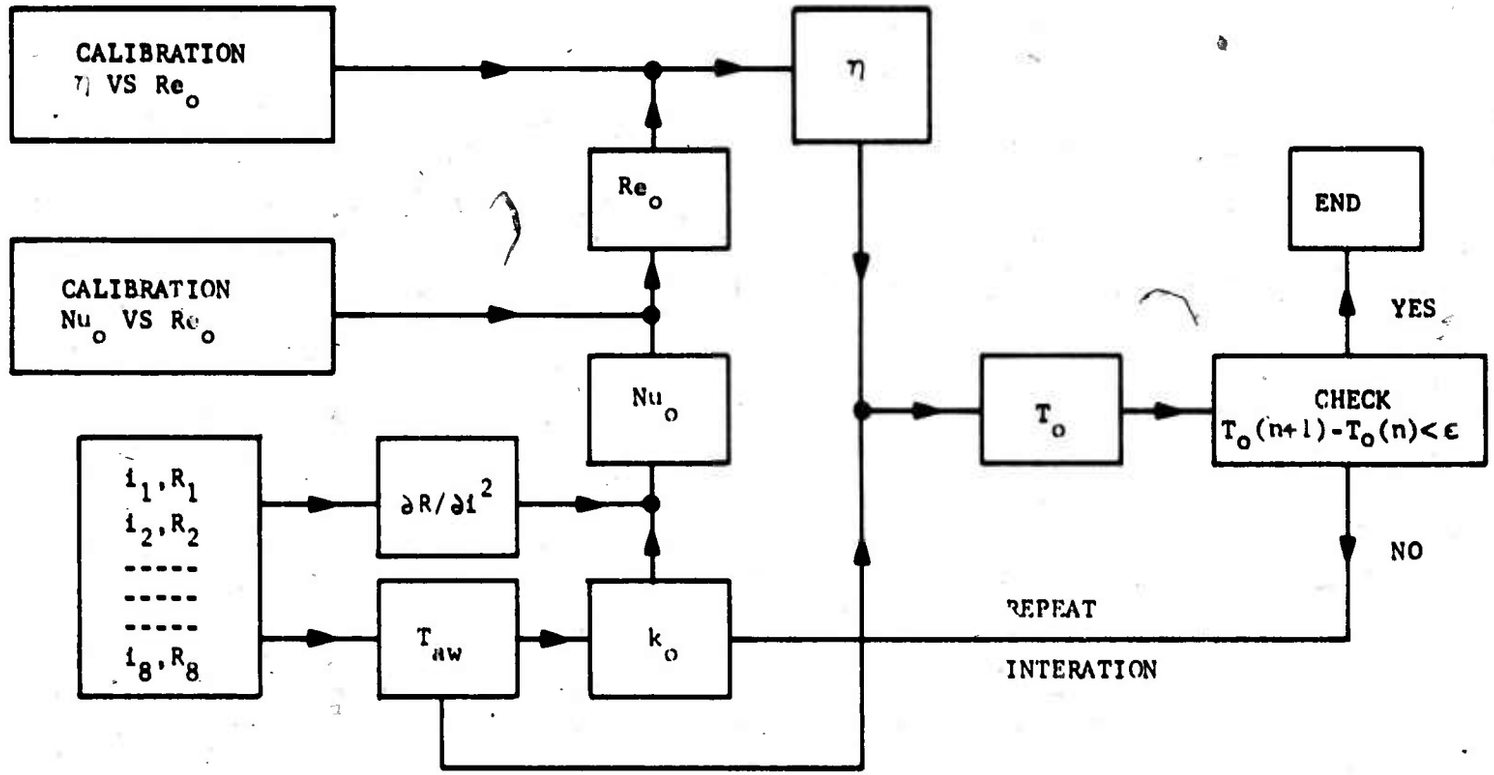


FIGURE 34 . FLOW CHART FOR HOT WIRE COMPUTER PROGRAM

## REFERENCES


1. Kistler, A.L., "Fluctuation Measurements in a Supersonic Turbulent Boundary Layer," Physics of Fluids 2, No. 3, pp 290-296, May-June, 1958.

2. Anon., "Jet Propulsion Laboratory Wind Tunnel Facilities," JPL Tech. Memo 33-335, JPL/CIT Pasadena, Calif., April 1, 1967.

3. J. Laufer, H. Ashkenas and A. Gupta, private communication.

4. Kane, E. D., and Maslach, G. I., "Impact-Pressure Interpretation in a Rarefied Gas at Supersonic Speeds," NACA TN 2210, October, 1950.

5. Mathews, M. L., "An Experimental Investigation of Viscous Effects on Static and Impact Pressure Probes in Hypersonic Flow," Hypersonic Research Memo 44, C.I.T., June, 1958.

6. Rogers, K. W., Wainwright, J.B., and Touryan, K.J., "Impact and Static Pressure Measurements in High Speed Flows with Transitional Knudsen Numbers," pp 151-174, Supplement 3, Vol. 2, Rarefied Gas Dynamics, edited by J. H. deLeeuw, Academic Press, New York, 1966.

7. Behrens, W., "Viscous Interaction Effects on a Static Pressure Probe at M = 6," AIAA Journal 1, No. 12, pp 2864-2866, December 1963.

8. Wagner, R.D., and Watson, R., "Reynolds Number Effects on the Induced Pressures of Cylindrical Bodies with Different Nose Shapes and Nose Drag Coefficients in Helium at a Mach Number of 24," NASA TR-R-182, Nov. 1963.

9. Fiore, A. W., "Turbulent Boundary Layer Measurements at Hypersonic Mach Numbers," ARL 70-0166, Aerospace Research Labs, U. S. Air Force, Aug. 1970.

10. Fisher, M. C., Maddalon, D. V., Weinstein, L. M., and Wagner, R.D., "Boundary-Layer Pitot and Hot-Wire Surveys at $M_\infty \approx 20$," AIAA Journal 9, No. 5, pp 826-834, May 1971.

11. Bertram, M. H., and Neal, L., "Recent Experiments in Hypersonic Turbulent Boundary Layers," NASA TMX-56335, May 1965.

12. Bushnell, D. M., Johnson, C. B., Harvey, W. D., and Feller, W. V., "Comparison of Prediction Methods and Studies of Relaxation in Hypersonic Turbulent Nozzle-Wall Boundary Layers," NASA TND-5433, 1969.

13. Lee, R. E., Yanta, W. J., and Zeonas, A. C., "Velocity Profile, Skin-Friction Balance and Heat Transfer Measurements of the Turbulent Boundary Layers at Mach 5 and Zero-Pressure Gradient," NOL TR 69-106, June 16, 1969.

14. Coles, D., "The Law-of-the-Wake in the Turbulent Boundary Layer," Journal of Fluid Mechanics 1, Part 2, pp 191-226, 1956.

15. Walz, A., "Compressible Turbulent Boundary Layers," pp 300-350, Mecanique de la Turbulence, Centre National de la Recherche Scientifique, Paris, 1962.

16. Lobb, R. K., Winkler, E. M., and Persh, J., "Experimental Investigation of Turbulent Boundary Layers in Hypersonic Flow," NAVORD REP 3880, 1955.

17. Winkler, E.M., and Cha, M. H., "Investigation of Flat Plate Hypersonic Boundary Layers with Heat Transfer at a Mach Number of 5.2," NAVORD REP 6631, 1959.

18. Tetervin, N., "An Analytical Investigation of the Flat Plate Turbulent Boundary Layer in Compressible Flow," NOL TR 67-39, May 1967.

19. Kemp, W. H., and Owens, F. K., "Nozzle Wall Boundary Layers at Mach Numbers 20 to 47," AIAA paper 71-161, 1971.

20. Maise, G., and McDonald, H., "Mixing Length and Kinematic Eddy Viscosity in a Compressible Boundary Layer," AIAA Journal 6, No. 1, pp 73-79, Jan. 1968.

21. R. Gran, private communication.

22. Coles, D., "The Young Persons Guide to the Data," Proceedings AFOSR-IFP-Stanford Conference on Computation of Turbulent Boundary Layers - 1968, Vol. II, compiled data, edited by D. E. Coles and E. A. Hirst, Stanford University, 1969.

23. Van Driest, E. R., "Turbulent Boundary Layer in Compressible Fluids," Journal of Aeronautical Sciences 18, No. 3, pp 145-160, March 1951.

24. Hopkins, E. J., and Inouye, M., "An Evaluation of Theories for Predicting Turbulent Skin Friction and Heat Transfer on Flat Plates at Supersonic and Hypersonic Mach Numbers," AIAA Journal 9, No. 6, pp 993-1003, June 1971.

25. Wallace, J. E., "Hypersonic Turbulent Boundary Layer Measurements Using an Electron Beam," AIAA Journal 1, No. 4, pp 757-759, April 1969, also, TR CAL AN-2112-Y-1, Cornell Aeronautical Lab, August 1968.

26. Clauser, F. H., "The Turbulent Boundary Layer," Advances in Applied Mechanics, Vol. 1, Academic Press, New York, 1956.

 (Page 70 intentionally left blank)

"PRECEDING PAGE BLANK-NOT FILMED".

UNCLASSIFIED
Security Classification

**DOCUMENT CONTROL DATA - R&D**
(Security classification of title, body of abstract and indexing annotation must be entered when the overall report is classified)

1 ORIGINATING ACTIVITY (Corporate author)
Philco-Ford, Aeronutronic Division
Ford Road, Newport Beach, California 92663

2a REPORT SECURITY CLASSIFICATION
UNCLASSIFIED

2b GROUP

3 REPORT TITLE
Mean Flow Measurements in a Hypersonic Boundary Layer

4 DESCRIPTIVE NOTES (Type of report and inclusive dates)
Technical Report October 1970 to July 1971

5 AUTHOR(S) (Last name, first name, initial)
Laderman, Arnold J. and Demetriades, Anthony

| 6 REPORT DATE | 7a TOTAL NO OF PAGES | 7b NO OF REFS |
|---|---|---|
| August 1971 | 82 | 26 |

| 8a CONTRACT OR GRANT NO | 9a ORIGINATOR'S REPORT NUMBER(S) |
|---|---|
| F04701-70-C-0130 | TBD |
| b PROJECT NO | |
| c | 9b OTHER REPORT NO(S) (Any other numbers that may be assigned this report) |
| d | U-4950 |

10 AVAILABILITY/LIMITATION NOTICES Each transmittal of this document outside the Department of Defense must have prior approval of SAMSO (RNSE), Norton Air Force Base, California 92409. The distribution of this report is limited because it contains technology requiring disclosure only within the Department of Defense.

| 11 SUPPLEMENTARY NOTES | 12 SPONSORING MILITARY ACTIVITY |
|---|---|
| | Advanced Research Projects Agency |

13 ABSTRACT

An experimental investigation was carried out to determine the structure of the turbulent boundary layer on the wall of the Jet Propulsion Laboratory Hypersonic Wind Tunnel at a free-stream Mach number of 9.37. Profiles of flow properties were obtained from pitot pressure, static pressure, and total temperature surveys made through the 6 inch thick boundary layer at a station 160 inches from the nozzle throat. Tests were conducted primarily for the following conditions: Unit free-stream Reynolds number of 127,000 per inch, corresponding to a Reynolds number based on momentum thickness of 36,800, and a wall to free-stream total temperature ratio of 0.385. A cursory examination of the boundary layer was also made at a unit stream Reynolds number of 67,000. The static pressure measurements, although indicating negligible streamwise variation, revealed the existence of a significant pressure gradient normal to the wall, with the pressure at the wall approximately 45% greater than its free-stream value. The data indicate that the profile of total temperature ratio versus velocity ratio agrees with the linear Crocco theory in the sub-layer region, but in the outer portion of the boundary layer, closely follows the quadratic relation which has been observed to characterize nozzle wall measurements. The data also indicate that the sub-layer is 0.05 to 0.10 inches thick which corresponds to only several percent of the total boundary layer thickness. Correlation of the velocity profile with the conventional incompressible profile shows poor agreement in the sub-layer and wall-of-the-wake regions, with the latter attributed primarily to the pressure gradient normal to the wall. However, the experimental skin friction coefficient agrees

DD FORM 1 JAN 64 1473

UNCLASSIFIED
Security Classification

| 14 KEY WORDS | LINK A | | LINK B | | LINK C | |
|---|---|---|---|---|---|---|
| | ROLE | WT | ROLE | WT | ROLE | WT |
| Boundary Layer<br>Turbulence<br>Hypersonic Flow<br>Mean Flow Measurements<br>Velocity Profile<br>Compressible Flow | | | | | | |

## INSTRUCTIONS

1. **ORIGINATING ACTIVITY**: Enter the name and address of the contractor, subcontractor, grantee, Department of Defense activity or other organization *(corporate author)* issuing the report.

2a. **REPORT SECURITY CLASSIFICATION**: Enter the overall security classification of the report. Indicate whether "Restricted Data" is included. Marking is to be in accordance with appropriate security regulations.

2b. **GROUP**: Automatic downgrading is specified in DoD Directive 5200.10 and Armed Forces Industrial Manual. Enter the group number. Also, when applicable, show that optional markings have been used for Group 3 and Group 4 as authorized.

3. **REPORT TITLE**: Enter the complete report title in all capital letters. Titles in all cases should be unclassified. If a meaningful title cannot be selected without classification, show title classification in all capitals in parenthesis immediately following the title.

4. **DESCRIPTIVE NOTES**: If appropriate, enter the type of report, e.g., interim, progress, summary, annual, or final. Give the inclusive dates when a specific reporting period is covered.

5. **AUTHOR(S)**: Enter the name(s) of author(s) as shown on or in the report. Enter last name, first name, middle initial. If military, show rank and branch of service. The name of the principal author is an absolute minimum requirement.

6. **REPORT DATE**: Enter the date of the report as day, month, year, or month, year. If more than one date appears on the report, use date of publication.

7a. **TOTAL NUMBER OF PAGES**: The total page count should follow normal pagination procedures, i.e., enter the number of pages containing information.

7b. **NUMBER OF REFERENCES**: Enter the total number of references cited in the report.

8a. **CONTRACT OR GRANT NUMBER**: If appropriate, enter the applicable number of the contract or grant under which the report was written.

8b, 8c, & 8d. **PROJECT NUMBER**: Enter the appropriate military department identification, such as project number, subproject number, system numbers, task number, etc.

9a. **ORIGINATOR'S REPORT NUMBER(S)**: Enter the official report number by which the document will be identified and controlled by the originating activity. This number must be unique to this report.

9b. **OTHER REPORT NUMBER(S)**: If the report has been assigned any other report numbers *(either by the originator or by the sponsor)*, also enter this number(s).

10. **AVAILABILITY/LIMITATION NOTICES**: Enter any limitations on further dissemination of the report, other than those imposed by security classification, using standard statements such as:

(1) "Qualified requesters may obtain copies of this report from DDC."

(2) "Foreign announcement and dissemination of this report by DDC is not authorized."

(3) "U. S. Government agencies may obtain copies of this report directly from DDC. Other qualified DDC users shall request through

_____"

(4) "U. S. military agencies may obtain copies of this report directly from DDC. Other qualified users shall request through

_____"

(5) "All distribution of this report is controlled. Qualified DDC users shall request through

_____"

If the report has been furnished to the Office of Technical Services, Department of Commerce, for sale to the public, indicate this fact and enter the price, if known.

11. **SUPPLEMENTARY NOTES**: Use for additional explanatory notes.

12. **SPONSORING MILITARY ACTIVITY**: Enter the name of the departmental project office or laboratory sponsoring *(paying for)* the research and development. Include address.

13. **ABSTRACT**: Enter an abstract giving a brief and factual summary of the document indicative of the report, even though it may also appear elsewhere in the body of the technical report. If additional space is required, a continuation sheet shall be attached.

It is highly desirable that the abstract of classified reports be unclassified. Each paragraph of the abstract shall end with an indication of the military security classification of the information in the paragraph, represented as (TS), (S), (C), or (U).

There is no limitation on the length of the abstract. However, the suggested length is from 150 to 225 words.

14. **KEY WORDS**: Key words are technically meaningful terms or short phrases that characterize a report and may be used as index entries for cataloging the report. Key words must be selected so that no security classification is required. Identifiers, such as equipment model designation, trade name, military project code name, geographic location, may be used as key words but will be followed by an indication of technical context. The assignment of links, rules, and weights is optional.

DD 1 JAN 64 1473 (BACK)

**ABSTRACT - (Continued)**

with the value predicted by the Van Driest theory within several percent. Finally, the total temperature profile determined from a hot-wire anemometer traverse through the boundary layer is in good agreement with the thermocouple measurements.